Physical results from 2 + 1 flavor domain wall QCD and SU(2) chiral perturbation theory

C. Allton,[1] D. J. Antonio,[2] Y. Aoki,[3] T. Blum,[3,4] P. A. Boyle,[2] N. H. Christ,[5] M. A. Clark,[6] S. D. Cohen,[5,*] C. Dawson,[3,+] M. A. Donnellan,[7] J. M. Flynn,[7] A. Hart,[2] T. Izubuchi,[3,8] C. Jung,[9] A. Jüttner,[7,‡] A. D. Kennedy,[2] R. D. Kenway,[2] M. Li,[5] S. Li,[5] M. F. Lin,[5,§] R. D. Mawhinney,[5] C. M. Maynard,[10] S. Ohta,[11,12,3] B. J. Pendleton,[2] C. T. Sachrajda,[7] S. Sasaki,[3,13] E. E. Scholz,[9] A. Soni,[9] R. J. Tweedie,[2] J. Wennekers,[2] T. Yamazaki,[4] and J. M. Zanotti[2]

(RBC and UKQCD Collaborations)

[1]*Department of Physics, Swansea University, Swansea SA2 8PP, UK*
[2]*SUPA, School of Physics, The University of Edinburgh, Edinburgh EH9 3JZ, UK*
[3]*RIKEN-BNL Research Center, Brookhaven National Laboratory, Upton, New York 11973, USA*
[4]*Physics Department, University of Connecticut, Storrs, Connecticut 06269-3046, USA*
[5]*Physics Department, Columbia University, New York, New York 10027, USA*
[6]*Center for Computational Science, 3 Cummington Street, Boston University, Massachusetts 02215, USA*
[7]*School of Physics and Astronomy, University of Southampton, Southampton SO17 1BJ, UK*
[8]*Institute for Theoretical Physics, Kanazawa University, Kakuma, Kanazawa, 920-1192, Japan*
[9]*Brookhaven National Laboratory, Upton, New York 11973, USA*
[10]*EPCC, School of Physics, The University of Edinburgh, Edinburgh EH9 3JZ, UK*
[11]*Institute of Particle and Nuclear Studies, KEK, Tsukuba, 305-0801, Japan*
[12]*Physics Department, Sokendai Graduate University for Advanced Studies, Hayama, Kanagawa, 240-0193, Japan*
[13]*Department of Physics, University of Tokyo, Tokyo 113-003, Japan*

(Received 16 April 2008; published 30 December 2008)

We have simulated QCD using 2 + 1 flavors of domain wall quarks and the Iwasaki gauge action on a $(2.74\ \mathrm{fm})^3$ volume with an inverse lattice scale of $a^{-1} = 1.729(28)$ GeV. The up and down (light) quarks are degenerate in our calculations and we have used four values for the ratio of light quark masses to the strange (heavy) quark mass in our simulations: 0.217, 0.350, 0.617, and 0.884. We have measured pseudoscalar meson masses and decay constants, the kaon bag parameter B_K, and vector meson couplings. We have used SU(2) chiral perturbation theory, which assumes only the up and down quark masses are small, and SU(3) chiral perturbation theory to extrapolate to the physical values for the light quark masses. While next-to-leading order formulas from both approaches fit our data for light quarks, we find the higher-order corrections for SU(3) very large, making such fits unreliable. We also find that SU(3) does not fit our data when the quark masses are near the physical strange quark mass. Thus, we rely on SU(2) chiral perturbation theory for accurate results. We use the masses of the Ω baryon, and the π and K mesons to set the lattice scale and determine the quark masses. We then find $f_\pi = 124.1(3.6)_{\mathrm{stat}} \times (6.9)_{\mathrm{syst}}$ MeV, $f_K = 149.6(3.6)_{\mathrm{stat}}(6.3)_{\mathrm{syst}}$ MeV, and $f_K/f_\pi = 1.205(0.018)_{\mathrm{stat}}(0.062)_{\mathrm{syst}}$. Using nonperturbative renormalization to relate lattice regularized quark masses to regularization independent momentum scheme masses, and perturbation theory to relate these to $\overline{\mathrm{MS}}$, we find $m_{ud}^{\overline{\mathrm{MS}}}(2\ \mathrm{GeV}) = 3.72(0.16)_{\mathrm{stat}}(0.33)_{\mathrm{ren}}(0.18)_{\mathrm{syst}}$ MeV, $m_s^{\overline{\mathrm{MS}}}(2\ \mathrm{GeV}) = 107.3(4.4)_{\mathrm{stat}}(9.7)_{\mathrm{ren}}(4.9)_{\mathrm{syst}}$ MeV, and $\tilde{m}_{ud}{:}\tilde{m}_s = 1{:}28.8(0.4)_{\mathrm{stat}}(1.6)_{\mathrm{syst}}$. For the kaon bag parameter, we find $B_K^{\overline{\mathrm{MS}}}(2\ \mathrm{GeV}) = 0.524(0.010)_{\mathrm{stat}}(0.013)_{\mathrm{ren}} \times (0.025)_{\mathrm{syst}}$. Finally, for the ratios of the couplings of the vector mesons to the vector and tensor currents (f_V and f_V^T, respectively) in the $\overline{\mathrm{MS}}$ scheme at 2 GeV we obtain $f_\rho^T/f_\rho = 0.687(27)$; $f_{K^*}^T/f_{K^*} = 0.712(12)$, and $f_\phi^T/f_\phi = 0.750(8)$.

DOI: 10.1103/PhysRevD.78.114509 PACS numbers: 11.15.Ha

I. INTRODUCTION

Numerical simulations of quantum chromodynamics (QCD) conventionally discretize four-dimensional spacetime by introducing a lattice scale, a, which yields a well-defined path integral formulation appropriate for study via importance sampling techniques. Measurements of observables at nonzero values of a can then be extrapolated to $a = 0$ to produce continuum results, and if discretization errors are small, the continuum extrapolation is better controlled. An important aspect of simulating QCD is

*Present address: Jefferson Lab, 12000 Jefferson Avenue, Newport News, VA 23606, USA.
+Present address: Department of Physics, University of Virginia, 382 McCormick Road, Charlottesville, VA 22904-4714, USA.
‡Present address: Institut für Kernphysik, Johannes Gutenberg-Universität Mainz, Johann-Hoachim-Becher-Weg 45, D-55099 Mainz, Germany.
§Present address: Center for Theoretical Physics, Massachusetts Institute of Technology, 77 Massachusetts Avenue, 6-319, Cambridge, MA 02139, USA.

choosing a lattice discretization which reduces the a dependence of observables [1]. Here, one is helped by knowing that if an $O(a^2)$ accurate gauge action is used, such as the Wilson action, and a discretization of QCD preserves the continuum chiral symmetries of massless QCD, then the lattice theory can only have errors quadratic in a, in combinations such as $(a\Lambda_{\rm QCD})^2$, and $(ma)^2$, where m is a quark mass. These errors are much smaller than the $O(am)$ discretization errors which can occur if the lattice theory breaks chiral symmetry. Additionally, if chiral symmetry is broken at nonzero lattice spacing, renormalization of the simplest operators, while straightforward, is involved [2]. (For a recent review, see [3].)

Preserving chiral symmetry at nonzero lattice spacing has a large impact on many of the more complicated observables, such as matrix elements of operators, that one wants to determine from lattice QCD. For observables such as hadron masses, which do not require any renormalization, controlling nonzero lattice spacing effects in the discretized theory is helpful. For observables requiring renormalization, such as weak matrix elements in hadronic states, the presence of chiral symmetry at nonzero lattice spacing can be vital to the renormalization and mixing of the relevant operators [4]. The chiral symmetries control the allowed operator mixings, so simplifications take place. Without this control, the number of operators and mixings amongst them can make renormalization very difficult, if not practically impossible. Chiral symmetry can now be preserved at nonzero lattice spacing with a variety of formulations [5–10]. (It is important to point out that some of the benefits of chiral symmetry can be achieved without its presence at nonzero lattice spacing. For example, twisted mass Wilson fermion discretizations [11] make judicious use of chiral transformations to calculate quantities without linear dependence on a and continuum-like renormalization properties, without having full chiral symmetry.)

In addition to taking the limit $a \to 0$, to achieve accurate physical results lattice simulations must reach the large volume ($V \to \infty$) limit and also the limit of physical light quarks. For discretizations which preserve chiral symmetry at nonzero a, simulations with arbitrarily light quarks can be done before taking the continuum limit—without chiral symmetry, lattice artifacts can alter the chiral limit at nonzero a and make the limits noncommuting. Current computer power does not allow simulations with physically light up and down quarks, so an extrapolation from masses used in the simulations to physical light quark masses must be done. Chiral perturbation theory [12,13] provides a theoretical framework for these extrapolations and, for lattice QCD discretizations which preserve chiral symmetry, the chiral perturbation theory is very similar to the continuum theory, since there are only a few lattice alterations to it.

Of long recognized importance, the preservation of the global chiral symmetries in discretized QCD has been achieved by Kaplan's proposal [5] of four-dimensional fermions resulting from a defect in a five-dimensional theory. Further developments led to the domain wall fermions of Shamir and Furman [6,7], which we use here, the overlap formulation of Neuberger and Narayanan [8,9], and the perfect actions of Hasenfratz *et al* [10]. To date, the domain wall formulation has proven to be the most numerically feasible. In this approach, one introduces a fifth dimension (which we label by the index s and which has extent L_s) and only achieves exact chiral symmetry in the $L_s \to \infty$ limit. However, for finite L_s, chiral symmetry breaking effects can be made small enough to be easily controlled, as we will discuss in subsequent sections. The presence of the fifth dimension (we use $L_s = 16$ in this work) increases the number of floating point operations required in a calculation by a factor of $O(L_s)$ over conventional QCD discretizations such as Wilson and staggered fermions, which do not preserve continuum chiral symmetries.

The domain wall fermion formulation has been used extensively in numerical simulations for about a decade. The original works were primarily in the quenched approximation, although some early work did involve QCD with two light quark flavors [14]. More extensive two flavor simulations were done [15], and with recent improvements in algorithms and computers, $2 + 1$ flavor QCD simulations have been completed [16–20]. These previous calculations demonstrated that domain wall fermion QCD shows the expected consequences of having a controlled approximation to the full chiral symmetries of continuum QCD. In particular, the following important features were observed.

(1) A mild dependence on a in the $a \to 0$ limit in the quenched approximation.
(2) For both quenched and unquenched QCD, the residual chiral symmetry breaking at nonzero a, as measured by the additive contribution to the quark mass $m_{\rm res}$, is readily made a small fraction of the input bare quark mass at practical values for L_s.
(3) The operator mixing problem for domain wall fermion QCD is essentially the same as the continuum problem.

These previous calculations were not able to fully exploit one of the main benefits of domain wall fermion QCD—the ability to probe the chiral limit of the theory at nonzero lattice spacing—and hence make accurate contact with the physical quark mass region. With recent advances in computers and algorithms, we have made considerable progress in simulating with light quarks and on large volumes. In this paper, we report on simulations of domain wall fermion QCD, with two light degenerate quarks and a single flavor heavier quark (a $2 + 1$ flavor simulation) and the Iwasaki gauge action. We have used a single lattice size of $24^3 \times 64 \times 16$ and a single inverse lattice spacing of $a^{-1} = 1.729(28)$ GeV, which gives us a

$(2.74\ \mathrm{fm})^3$ spatial volume. We used four different light dynamical quark masses in our simulations and the ratios of these light masses to the physical strange quark mass are 0.217, 0.350, 0.617, and 0.884. A single value for the heavy quark mass was used in all our simulations and its ratio to the physical strange quark mass is 1.150. (An accurate value for the physical strange quark mass was, of course, not known until after our simulation was complete.) For mesons made of degenerate light quarks, the corresponding pseudoscalar meson masses are 331 MeV, 419 MeV, 557 MeV, and 672 MeV. We have also done measurements with a variety of valence quark masses, with a ratio of the smallest mass to the physical strange quark mass of 0.110, corresponding to a pseudoscalar meson with a mass of 242 MeV. In a previous paper [16], we have given results from simulations with the same gauge coupling constant, but on a smaller volume, which gives us some understanding of finite-volume effects.

To extrapolate from our simulation quark masses to the physical values, we use chiral perturbation theory (ChPT), which is an expansion of low-energy QCD observables in powers of the meson masses and momenta over the pseudoscalar decay constant. Within the general framework of ChPT one can consider only the pions to be light particles, yielding an $\mathrm{SU}(2)_L \times \mathrm{SU}(2)_R$ ChPT [which we will call SU(2) ChPT] or one can also consider the kaons as light, yielding an $\mathrm{SU}(3)_L \times \mathrm{SU}(3)_R$ ChPT [which we will call SU(3) ChPT]. In Sec. II, we discuss the domain wall fermion (DWF) corrections to ChPT and develop SU(2) ChPT for the kaon sector, which we will later use to fit our data.

In Sec. III we give details of our simulations, including the rational hybrid Monte Carlo (RHMC algorithm that we use to generate our lattices. Section IV describes the sources and sinks we use for our pseudoscalar observables, our methods of determining desired quantities, and results in lattice units. We will also use the mass of the Ω baryon, which has no corrections from chiral logarithms, as part of our scale setting, and the details of the measurement of m_Ω are given in Sec. V.

In Sec. VI we fit our lattice values for the masses and decay constants of pseudoscalars to partially quenched SU(2) ChPT at next-to-leading order (NLO). We find our data are well described by the theoretical formula from Sec. II, provided the pions have masses below about 420 MeV. We use the fits to SU(2) ChPT as the most accurate way to extrapolate our data to the chiral limit, since SU(2) ChPT does not require the kaon mass to be small, but only requires $m_\pi \ll m_K$. Using the results for pseudoscalar masses from our SU(2) ChPT fits and our lattice values for the Ω baryon mass, we fix the lattice scale and bare quark masses using the known masses of the π, K, and Ω. We find that our inverse lattice spacing is $a^{-1} = 1.729(28)$ GeV. In a separate work [21], we have used nonperturbative renormalization to calculate the multiplicative renormalization factor needed to relate our bare lattice quark masses to continuum $\overline{\mathrm{MS}}$ masses. We find

$$m_{ud}^{\overline{\mathrm{MS}}}(2\,\mathrm{GeV}) = 3.72(0.16)_{\mathrm{stat}}(0.33)_{\mathrm{ren}}(0.18)_{\mathrm{syst}}\ \mathrm{MeV}, \quad (1)$$

$$m_s^{\overline{\mathrm{MS}}}(2\ \mathrm{GeV}) = 107.3(4.4)_{\mathrm{stat}}(9.7)_{\mathrm{ren}}(4.9)_{\mathrm{syst}}\ \mathrm{MeV}, \quad (2)$$

$$\tilde{m}_{ud}{:}\tilde{m}_s = 1{:}28.8(0.4)_{\mathrm{stat}}(1.6)_{\mathrm{syst}}, \quad (3)$$

where $(\cdots)_{\mathrm{stat}}$, $(\cdots)_{\mathrm{ren}}$, and $(\cdots)_{\mathrm{syst}}$ show the statistical error, the error from renormalization, and the systematic error. We assume the light quarks to be degenerate in this work. We now predict values for f_π and f_K and find $f_\pi = 124.1(3.6)_{\mathrm{stat}}(6.9)_{\mathrm{syst}}$ MeV and $f_K = 149.6(3.6)_{\mathrm{stat}} \times (6.3)_{\mathrm{syst}}$ MeV. Our fits to SU(2) ChPT also determine the low-energy constants (LECs) for pseudoscalar masses and decay constants in SU(2) ChPT. Furthermore, implications of our results to Cabibbo-Kobayashi-Maskawa (CKM) matrix elements are discussed.

In Sec. VII we fit our light pseudoscalar data to SU(3) ChPT. Here we also find that our data are well represented by SU(3) ChPT at NLO, provided our pseudoscalars have masses below about 420 MeV. The failure of NLO SU(3) ChPT to fit our data when pseudoscalar masses are near the physical kaon mass rules out using NLO SU(3) ChPT in this mass region. With light masses, we determine values for the SU(3) LECs which agree well with values determined by others. However, we find a small value for the decay constant in the SU(3) chiral limit, which we denote by f_0 (a complete description of our notation is given in the Appendix A). Our fits give $f_0 = 94$ MeV, with conventions such that the physical value is $f_\pi = 131$ MeV, and this value is smaller than generally found phenomenologically, which we discuss further in Sec. VII. Along with this we find that the size of the NLO corrections to SU(3) ChPT, relative to the leading order term, is in the range of 50% or more. This makes the convergence of SU(3) ChPT for these quark masses unreliable. Thus, although it represents our data well and the parameters we find generally agree with others, we find the systematic errors in SU(2) ChPT substantially smaller and use it as our most accurate means of extrapolating our data to the chiral limit.

In Sec. VIII, we discuss our determination of the kaon bag parameter, B_K, which is needed to relate indirect CP violation in the standard model to experimental measurements. This section expands upon the data and analysis presented in [19]. Here we also find extrapolations to the physical quark masses to be under much better control with SU(2) than with SU(3) ChPT. We present our estimates of systematic errors, including finite size effects. We find $B_K^{\overline{\mathrm{MS}}}(2\ \mathrm{GeV}) = 0.524(0.010)_{\mathrm{stat}}(0.013)_{\mathrm{ren}}(0.025)_{\mathrm{syst}}$.

In Sec. IX we present results for the couplings of light vector mesons to vector and tensor currents. The results for the ratios of the couplings of the vector mesons to the vector and tensor currents (f_V and f_V^T, respectively) in the $\overline{\mathrm{MS}}$ scheme at 2 GeV are $f_\rho^T/f_\rho = 0.687(27)$; $f_{K^*}^T/f_{K^*} = 0.712(12)$, and $f_\phi^T/f_\phi = 0.750(8)$.

II. CHIRAL PERTURBATION THEORY

In this section, we discuss chiral perturbation theory for domain wall fermions in subsection II A. We develop SU (2) ChPT for kaons in II B. Our notation and an extensive list of the formulas from SU(2) and SU(3) ChPT that we use in this work are given in the appendixes.

A. Chiral perturbation theory for domain wall fermions

Our simulations are done with domain wall fermions, which have explicit chiral symmetry breaking effects at nonzero lattice spacing. These effects are controlled by the extent of the lattice in the fifth dimension, denoted by L_s, whose value is chosen to make such terms small, consistent with current computer power. The small chiral symmetry breaking that remains can be measured and its effects taken into account, as has been discussed extensively in the literature. A recent review of this topic is available in [22].

As previously discussed in [4,23], for a theory with N quarks these explicit symmetry breaking effects can be easily included by introducing an $N \times N$ matrix parameter Ω into the domain wall fermion action. This parameter connects four-dimensional planes at the midpoint of the fifth dimension and is included into the action by adding

$$S_\Omega = -\sum_x \{\bar{\Psi}_{x,L_s/2-1} P_L (\Omega^\dagger - 1)\Psi_{x,L_s/2} + \bar{\Psi}_{x,L_s/2} P_R (\Omega - 1)\Psi_{x,L_s/2-1}\} \quad (4)$$

to the conventional action for domain wall fermions [24]. Here, $\Psi_{x,s}$ represents a five-dimensional fermion field with four spin components and suppressed flavor indices. We recover the conventional domain wall fermion action when we set $\Omega = 1$.

If we let Ω transform as

$$\Omega \to V_R \Omega V_L^\dagger \quad (5)$$

under $\mathrm{SU}(N)_L \times \mathrm{SU}(N)_R$, then the domain wall fermion Dirac operator possesses exact chiral symmetry. Thus we can use Ω to track the explicit chiral symmetry breaking from domain wall fermions, in both the Symanzik style effective Lagrangian for domain wall fermion QCD and in Green functions. However, we note that Ω itself is not a small quantity, since a general Green function involving the five-dimensional fermion fields does not have any approximate chiral symmetry. However, for the effective action and low-momentum limit of Green functions made from the four-dimensional fields at the boundaries of the fifth dimension, each power of Ω that enters should come with a suppression related to the ratio of amplitudes of the low-energy fermion modes between the boundaries and the midpoint in the fifth dimension.

Consider a nonzero a effective Lagrangian description of QCD with domain wall fermions at finite L_s. The presence of the parameter Ω implies that the terms containing fermions, up to operators of dimension five, are

$$\frac{Z_m m_f}{a}\bar{\psi}\psi + \frac{c_3}{a}\{\bar{\psi}\Omega^\dagger P_R \psi + \bar{\psi}\Omega P_L \psi\} + a c_5 \{\bar{\psi}\sigma_{\mu\nu}F_{\mu\nu}\Omega^\dagger P_R\psi + \bar{\psi}\sigma_{\mu\nu}F_{\mu\nu}\Omega P_L\psi\}. \quad (6)$$

Here m_f is the dimensionless input bare quark mass in the domain wall fermion formulation, and c_3 and c_5 are dimensionless parameters that represent the mixing of left- and right-handed quarks between the five-dimensional boundaries. These parameters are of $O(e^{-\alpha L_s})$ at weak coupling; for coarse lattices where there are localized dislocations in the gauge fields corresponding to changes in the topology, they are generically $O(a_1 e^{-\alpha L_s} + a_2)/L_s$, where $a_2 \neq 0$ is due to the density of localized topological dislocations [17].

Setting $\Omega = 1$, we have

$$\frac{Z_m m_f}{a}\bar{\psi}\psi + \frac{c_3}{a}\bar{\psi}\psi + a c_5 \bar{\psi}\sigma_{\mu\nu}F_{\mu\nu}\psi. \quad (7)$$

The combination $Z_m m_f + c_3$ is the total (dimensionless) quark mass and we choose L_s to control the contribution of the second term, by changing the size of c_3. Equation (7) is identical to the result for Wilson fermions, except that the coefficients c_3 and c_5 are expected to be small, $O(10^{-3})$, for realistic domain wall fermion simulations, compared to being $O(1)$ as for Wilson fermions.

We can now discuss the application of chiral perturbation theory to our domain wall fermion simulations at a fixed lattice spacing. Our discussion will be for SU(3), but the results are easily generalized. We start from the conventional QCD SU(3) chiral Lagrangian in the continuum and make use of the presence of the Ω spurion field to add all additional terms to it. Initially we power count only in Ω and defer, for the moment, the additional question of power counting in a. We choose $\Sigma(x) = \mathrm{e}^{2i\phi(x)/f_0}$, where Σ transforms as $\Sigma \to V_L \Sigma V_R^\dagger$, V_L, $V_R \in \mathrm{SU}(3)$. We define $\hat{\chi} = 2B_0 \mathrm{diag}(m_u, m_d, m_s)$, where B_0 is one of the LECs that enters in chiral perturbation theory. To $O(p^4)$ the continuum Lagrangian is

$$\begin{aligned}\mathcal{L} =& \frac{f_0^2}{8}\mathrm{Tr}[\partial_\mu\Sigma\partial^\mu\Sigma^\dagger] + \frac{f_0^2}{8}\mathrm{Tr}[\hat{\chi}\Sigma + (\hat{\chi}\Sigma)^\dagger] \\ &+ L_1^{(3)}\{\mathrm{Tr}[\partial_\mu\Sigma(\partial^\mu\Sigma)^\dagger]\}^2 \\ &+ L_2^{(3)}\mathrm{Tr}[\partial_\mu\Sigma(\partial_\nu\Sigma)^\dagger]\mathrm{Tr}[\partial^\mu\Sigma(\partial^\nu\Sigma)^\dagger] \\ &+ L_3^{(3)}\mathrm{Tr}[\partial_\mu\Sigma(\partial^\mu\Sigma)^\dagger\partial_\nu\Sigma(\partial^\nu\Sigma)^\dagger] \\ &+ L_4^{(3)}\mathrm{Tr}[\partial_\mu\Sigma(\partial^\mu\Sigma)^\dagger]\mathrm{Tr}(\hat{\chi}\Sigma + (\hat{\chi}\Sigma)^\dagger) \\ &+ L_5^{(3)}\mathrm{Tr}[\partial_\mu\Sigma(\partial^\mu\Sigma)^\dagger(\hat{\chi}\Sigma + (\hat{\chi}\Sigma)^\dagger)] \\ &+ L_6^{(3)}[\mathrm{Tr}(\hat{\chi}\Sigma + (\hat{\chi}\Sigma)^\dagger)]^2 + L_7^{(3)}[\mathrm{Tr}(\hat{\chi}\Sigma \\ &- (\hat{\chi}\Sigma)^\dagger)]^2 + L_8^{(3)}\mathrm{Tr}(\hat{\chi}\Sigma\hat{\chi}\Sigma + (\hat{\chi}\Sigma\hat{\chi}\Sigma)^\dagger). \quad (8)\end{aligned}$$

For the domain wall fermion case, we can generate the new terms that arise by starting from the Lagrangian in Eq. (8).

Since Ω transforms as $\hat{\chi}$ or $\Sigma^\dagger$ does, new terms can be created by substituting Ω for $\hat{\chi}$ and $\Sigma^\dagger$ in Eq. (8), remembering that derivatives acting on Ω vanish. Since the dominant contribution of explicit chiral symmetry breaking in Eq. (7) is an additive contribution to the quark mass, we power count Ω as $O(p^2)$. Keeping terms of $O(p^4)$ and using D_i, $\tilde{D}_i$ for the LECs for these terms, we have additional contributions to Eq. (8) of

$$\begin{aligned}
&\frac{f^2}{8} D_0 \,\mathrm{Tr}[\Omega\Sigma + (\Omega\Sigma)^\dagger] + \frac{f^2}{8}\tilde{D}_0 \,\mathrm{Tr}[\Omega\hat{\chi}^\dagger \\
&\quad + \Omega^\dagger\hat{\chi}] D_4 \,\mathrm{Tr}[\partial_\mu\Sigma(\partial^\mu\Sigma)^\dagger]\,\mathrm{Tr}(\Omega\Sigma + (\Omega\Sigma)^\dagger) \\
&\quad + D_5 \,\mathrm{Tr}[\partial_\mu\Sigma(\partial^\mu\Sigma)^\dagger(\Omega\Sigma + (\Omega\Sigma)^\dagger)] \\
&\quad + D_6[\mathrm{Tr}(\Omega\Sigma + (\Omega\Sigma)^\dagger)][\mathrm{Tr}(\hat{\chi}\Sigma + (\hat{\chi}\Sigma)^\dagger)] \\
&\quad + \tilde{D}_6[\mathrm{Tr}(\Omega\Sigma + (\Omega\Sigma)^\dagger)]^2 + D_7[\mathrm{Tr}(\Omega\Sigma \\
&\quad - (\Omega\Sigma)^\dagger)][\mathrm{Tr}(\hat{\chi}\Sigma - (\hat{\chi}\Sigma)^\dagger)] + \tilde{D}_7[\mathrm{Tr}(\Omega\Sigma \\
&\quad - (\Omega\Sigma)^\dagger)]^2 + D_8 \,\mathrm{Tr}(\hat{\chi}\Sigma\Omega\Sigma + (\hat{\chi}\Sigma\Omega\Sigma)^\dagger) \\
&\quad + \tilde{D}_8 \,\mathrm{Tr}(\Omega\Sigma\Omega\Sigma + (\Omega\Sigma\Omega\Sigma)^\dagger). \qquad (9)
\end{aligned}$$

Terms which involve two derivatives, a factor of $\hat{\chi}$ and a factor of Ω, will be $O(p^6)$ and will have been neglected. Note that we have kept the term involving $\tilde{D}_0$, even though it does not involve any Σ fields. Such a term does play a role in determining the value for the chiral condensate through the variation of the partition function with respect to the quark mass.

We would seem to have many new low-energy constants to determine with domain wall fermions at nonzero a. However, the form of the Symanzik effective Lagrangian for DWF QCD shows that the leading order (in a) chiral symmetry breaking effect is a universal shift in the quark mass, i.e., c_3/a multiplies the dimension three operator $\bar{\psi}\psi$. Thus, there is no difference in ChPT between m_f and c_3, and we can rewrite the terms in Eq. (9) in terms of the original LECs of QCD, with a shifted quark mass, plus higher-order corrections. Letting $\chi = 2B_0[\mathrm{diag}(m_u, m_d, m_s) + c_3\,\mathrm{diag}(1,1,1)]$ and looking at the D_4 term as an example, we have

$$\begin{aligned}
&D_4 \,\mathrm{Tr}[\partial_\mu\Sigma(\partial^\mu\Sigma)^\dagger]\,\mathrm{Tr}(\Omega\Sigma + (\Omega\Sigma)^\dagger) \\
&\quad = L_4^{(3)} \,\mathrm{Tr}[\partial_\mu\Sigma(\partial^\mu\Sigma)^\dagger]\,\mathrm{Tr}(\chi\Sigma + (\chi\Sigma)^\dagger) \\
&\qquad + O(ac_5) L_4^{(3)} \,\mathrm{Tr}[\partial_\mu\Sigma(\partial^\mu\Sigma)^\dagger]\,\mathrm{Tr}(\Sigma + \Sigma^\dagger). \qquad (10)
\end{aligned}$$

The last term is $O(a) \times O(c_5) \times O(p^2)$. It is customary to power count $O(a)$ and $O(p^2)$ terms as the same size for unimproved Wilson fermions, and this same term appears there [25], except that c_5^{Wilson} is $O(1)$. While for Wilson fermions, this term must be kept at NLO in the chiral Lagrangian, for domain wall fermions, where c_5 is very small, it can be neglected.

Examining all the terms in Eq. (9), we see that the complete NLO chiral Lagrangian for domain wall fermions is given by Eq. (8), with $\hat{\chi} \to \chi$, where χ is proportional to the sum of the input bare quark mass, m_f, and the additive quark mass contribution which comes from c_3. Since we will be working to NLO order of ChPT in this work, domain wall fermions at nonzero lattice spacing should be described by the chiral Lagrangian given in Eq. (8). When we fit our data for specific quantities to the chiral formula following from Eq. (8), the LECs L_i will differ at $O(a^2)$ from their continuum values. Since we work at a single lattice spacing, we will not be able to correct for these deviations from continuum QCD.

The size of the residual symmetry breaking terms represented by c_3 and c_5 in Eq. (6) is most easily studied by examining the five-dimentional current $\mathcal{A}_\mu^a$ which can be easily defined for domain wall fermions and is exactly conserved in the limit $m_f \to 0$ and $L_s \to \infty$ [7]. The DWF equations of motion imply that this current obeys the divergence condition

$$\Delta_\mu \mathcal{A}_\mu^a(x) = 2m_f J_5^a(x) + 2J_{5q}^a(x), \qquad (11)$$

where J_5^a is a pseudoscalar density made up of quark fields on the boundary of the fifth dimension and J_{5q}^a is a pseudoscalar density containing quark fields at $L_s/2 - 1$ and $L_s/2$. While the J_5^a term is the result of the usual chiral noninvariance of the mass term, the J_{5q}^a operator is expected to have vanishing matrix elements at low energy as $L_s \to \infty$. It represents the effects of residual, finite-L_s, chiral symmetry breaking. For low-energy Green functions, the midpoint term in Eq. (11) can be expanded as

$$J_{5q}^a \sim m_{\mathrm{res}} J_5^a - \frac{(Z_{\mathcal{A}} - 1)}{2} \Delta_\mu \mathcal{A}_\mu^a + c_5' O_5^a. \qquad (12)$$

Here we have introduced the m_f-independent parameter m_{res}, related to the constant c_3 in Eq. (6). We also have a new lattice operator, O_5^a, similar to the axial transform of the c_5 term in Eq. (6), which is carefully subtracted so that its matrix elements are of order a^2 smaller than those of the operator J_5^a at long distances. Since the low-energy matrix elements of the midpoint operator on the left-hand side of Eq. (12) will be suppressed by a factor $\exp(-\alpha L_s)$, we expect the quantities m_{res}, $(Z_{\mathcal{A}} - 1)$, and c_5' to all be of this order (at least in the perturbative regime).

While an expansion such as that written in Eq. (12) is typically written in terms of the operators of the effective theory, the present form of this equation is useful because it can be combined with Eq. (11) to yield

$$Z_{\mathcal{A}} \Delta_\mu \mathcal{A}_\mu^a(x) = 2(m_f + m_{\mathrm{res}}) J_5^a(x) + c_5' O_5^a. \qquad (13)$$

As is well known from the classic analysis of the case of Wilson fermions [2], the conservation of the vector current and the vector Ward identities implies that product $m_f J_5^a(x)$ in Eq. (13) approaches its continuum counterpart without multiplicative renormalization. This equation then implies that the product $Z_{\mathcal{A}} \mathcal{A}_\mu^a(x)$ will reproduce the standard

continuum axial current when evaluated in low-energy Green functions.

The appearance of the $(Z_{\mathcal{A}} - 1)$ term on the right-hand side of Eq. (12) and the consequent renormalization of the five-dimensional DWF axial current is an effect that was not recognized in earlier RBC or RBC-UKQCD work. Such a possibility was raised by Steve Sharpe [22]. However, in this paper, Sharpe argues that $(Z_{\mathcal{A}} - 1)$ is expected to be of order $m_{\rm res}^2$, not the order $m_{\rm res}$ scale suggested by the above argument. Sharpe's argument relies on the chiral character of the operators $V_\mu \pm A_\mu$, defined in terms of fields on the boundaries of the fifth dimension. The mixing between these operators implied by $Z_{\mathcal{A}} \neq 1$ can arise only if a fermion and an antifermion move from one wall to the other, a situation suppressed as $m_{\rm res}^2$. We believe that this generally very useful argument does not apply in the present case because the right- and left-handed currents under consideration each span one-half of the entire five dimensions and are not localized on the left and right walls. For example, two fermions can propagate from the midpoint operator J_{5q} to the same wall with only a suppression of $[\exp(-\alpha L_s/2)]^2 = \exp(-\alpha L_s)$. Note, this argument only applies to the perturbative piece. For tunneling caused by near-zero modes of the four-dimension Wilson operator, two such modes are needed implying a suppression more like $m_{\rm res}^2$.

Finally it is informative to consider the implications of this more complete analysis on the conventional calculation of the residual mass from a ratio of low-energy pion to vacuum matrix elements. We measure a quantitiy commonly called $m'_{\rm res}(m_f)$ and given by

$$m'_{\rm res}(m_f) = \frac{\langle 0|J^a_{5q}|\pi\rangle}{\langle 0|J^a_5|\pi\rangle} \tag{14}$$

$$= \frac{\langle 0|(m_{\rm res}J^a_5 - \frac{(Z_{\mathcal{A}}-1)}{2}\Delta_\mu \mathcal{A}^a_\mu + c'_5 O^a_5)|\pi\rangle}{\langle 0|J^a_5|\pi\rangle}. \tag{15}$$

We can then use the lattice equations of motion to evaluate the $\Delta_\mu \mathcal{A}^a_\mu$ term so that Eq. (15) takes the form

$$m'_{\rm res}(m_f) = m_{\rm res} + \left(\frac{1}{Z_{\mathcal{A}}} - 1\right)(m_f + m_{\rm res}) + \frac{c'_5}{2}\left(1 + \frac{1}{Z_{\mathcal{A}}}\right)\frac{\langle 0|O^a_5|\pi\rangle}{\langle 0|J^a_5|\pi\rangle}. \tag{16}$$

This equation governs the m_f dependence of $m'_{\rm res}(m_f)$. Since, by construction, the third term on the right-hand side is of order a^2, we might be tempted to neglect it and use Eq. (16) to relate the m_f dependence of $m'_{\rm res}(m_f)$ to the difference $(1/Z_{\mathcal{A}} - 1)$. However, we can distinguish the dependence of $m'_{\rm res}(m_f)$ on the valence and sea masses, $m_f^{\rm val}$ and $m_f^{\rm sea}$ (m_x and m_l in the general notation of the rest of this paper). We see that there is valence quark mass dependence in both the $1/Z_{\mathcal{A}} - 1$ term and in the term containing c'_5, while the sea quark mass dependence is only in the c'_5 term. As will be shown in Sec. IV B, $m'_{\rm res}$ depends to a roughly equal degree on both $m_f^{\rm val}$ and $m_f^{\rm sea}$. In particular, we find that $d\ln(m'_{\rm res})/dm_f^{\rm val} \approx -4$ and $d\ln(m'_{\rm res})/dm_f^{\rm sea} \approx 6$. This implies that the third term in Eq. (16), which can depend on both the valence and sea quark masses, must be of an equal size to the second. In fact, if we introduce physical dimensions, we expect the ratio $\langle 0|O^a_5|\pi\rangle/\langle 0|J^a_5|\pi\rangle$ to be of $O((a\Lambda_{\rm QCD})^2)$. The effect of the quark masses on this ratio will be to replace one of the factors of $\Lambda_{\rm QCD}$ by the dimensioned factor $m_f^{\rm val}/a$ or $m_f^{\rm sea}/a$. Thus, the quark-mass-dependent terms coming from the third term in Eq. (16) are suppressed by only $O(a\Lambda_{\rm QCD})$ relative to the second term, which is apparently insufficient to permit them to be neglected, a fact already pointed out by Sharpe [22].

The arguments above show that we expect $Z_{\mathcal{A}} - 1$ to be $O(m_{\rm res})$. If all of the unitary mass dependence of $m'_{\rm res}(m_f)$ came from the $1/Z_{\mathcal{A}} - 1$ term, this would give $Z_{\mathcal{A}} - 1 = -0.003$. Similarly, the valence mass dependence would give $Z_{\mathcal{A}} - 1 = 0.01$. At present, we do not have sufficient data to measure $Z_{\mathcal{A}} - 1$ without contamination from the c'_5 term. Thus, for the remainder of this work, we take $Z_{\mathcal{A}} = 1$ and we expect this to introduce an error of 1% or less in our axial current normalization.

We also work with a local, four-dimensional axial current A^a_μ, which we renormalize so that $Z_A A^a_\mu = \mathcal{A}^a_\mu$, so that

$$Z_A \Delta_\mu A^a_\mu(x) = 2\tilde{m} J^a_5(x). \tag{17}$$

B. $SU(2)_L \times SU(2)_R$ chiral perturbation theory for kaon physics

1. Introduction

An important goal of this paper is the comparison of the mass dependence of our lattice results with both $SU(3)_L \times SU(3)_R$ and $SU(2)_L \times SU(2)_R$ ChPT at NLO (i.e., at one-loop order). For compactness of notation, throughout the remainder of this section we will simply refer to SU(3) and SU(2) ChPT. We will see that our data for pseudoscalar masses and decay constants only agree with NLO SU(3) ChPT with good precision when the quark masses are small. This will be quantified in detail in Sec. VII, where we will see that NLO SU(3) ChPT provides a good description of our data when the average, dimensionless, input valence mass satisfies $m_{\rm avg} < 0.01$ (all our results will be obtained using data for valence u and d quark masses below this value). In order to attempt to extend the range of agreement to heavier masses (to include the strange quark, for example), one possible approach is to use next-to-next-to-leading order (NNLO) (or even higher-order) ChPT. This introduces many additional LECs and

we find that we have insufficient data to determine all of these with sufficient precision.

Instead of attempting to fit our data using NNLO (or even higher-order) ChPT, we propose to use SU(2) ChPT at NLO. For pion physics, where it is possible to satisfy the condition, $m_{\rm avg} < 0.01$ for the valence quarks, both SU(2) and SU(3) ChPT provide a good description of our data. Moreover, we will see in Secs. VI and VII that the SU(2) LECs obtained directly are consistent with those obtained by ''converting'' the SU(3) LECs to SU(2) [13,26] (conversion formulas appear in Appendix B 2 c). For kaons on the other hand, the presence of the valence strange quark means that we do not satisfy the condition $m_{\rm avg} < 0.01$ and so we propose to use SU(2) ChPT at NLO. The effects of the strange quark mass are now absorbed into the LECs of the SU(2) ChPT. This eliminates the errors due to neglected higher powers of $\chi_s/\Lambda^2_{\rm CSB}$ present when using SU(3) ChPT, but now one has to ensure that the u and d quark masses are sufficiently small to be able to neglect higher-order terms in χ_{ud}/χ_s. Here $\Lambda_{\rm CSB} \sim 4\pi f_\pi$ is the chiral symmetry breaking scale, while χ_{ud} and χ_s are tree-level masses of pseudoscalars made of ud and s quarks (see Appendix A).

In this section we derive the NLO formulas for the behavior of the kaon's leptonic decay constant f_K, its mass m_K, and the bag parameter B_K as a function of the light quark masses in SU(2) ChPT. At each stage, we start by presenting the arguments and calculations in the unitary theory, with valence and sea quark masses equal, and then proceed to the partially quenched theory. In the partially quenched theory in general the valence and sea strange quark masses, m_y and m_h respectively, are also different and the SU(2) LECs depend on both these masses. For compactness of notation, we write these LECs with a single argument m_h, but it should be remembered that if $m_y \neq m_h$, then m_h should be replaced by the pair of variables m_y, m_h. We note that in this subsection quark masses written without a tilde have their usual interpretation as Lagrangian mass parameters in continuum ChPT or partially quenched chiral perturbation theory (PQChPT) (a change from the notation defined in Appendix A and used elsewhere in this paper).

We start by introducing our notation. In the unitary effective theory, the pion matrix, quark mass matrix, and kaon fields are written in the form

$$\phi = \begin{pmatrix} \pi^0/\sqrt{2} & \pi^+ \\ \pi^- & -\pi^0/\sqrt{2} \end{pmatrix}, \quad M = \begin{pmatrix} m_l & 0 \\ 0 & m_l \end{pmatrix}, \quad K = \begin{pmatrix} K^+ \\ K^0 \end{pmatrix}. \tag{18}$$

We work in the isospin limit in which the two light quarks are degenerate with mass m_l. The pion matrices ξ and Σ are defined in the standard way:

$$\xi = \exp(i\phi/f) \quad \text{and} \quad \Sigma = \xi^2, \tag{19}$$

where the constant f is the pion decay constant (f_π) at lowest order in the chiral expansion (we use the convention in which $f_\pi = 132$ MeV). Under global left- and right-handed transformations, L and R, respectively, these quantities transform as follows:

$$\Sigma \to L\Sigma R^\dagger, \qquad \xi \to L\xi U^\dagger = U\xi R^\dagger, \quad \text{and} \quad K \to UK, \tag{20}$$

where U is a function of L, R, and the meson fields, but reduces to a global vector transformation when $L = R$. The pion Lagrangian at lowest order is

$$L^{(2)}_{\pi\pi} = \frac{f^2}{8}\,\mathrm{tr}\partial_\mu\Sigma\partial^\mu\Sigma^\dagger + \frac{f^2 B}{4}\,\mathrm{tr}(M^\dagger\Sigma + M\Sigma^\dagger), \tag{21}$$

where f and B are the usual leading order LECs and, to this order, $m_\pi^2 = 2Bm_l$.

The results for m_π^2 and f_π at NLO in the chiral expansion are well known [12] and are presented in Eqs. (B34) and (B38) in Appendix B. We now turn our attention to kaon physics using ''Kaon ChPT'' (KChPT). The corresponding chiral Lagrangian has already been introduced by Roessl [27] in order to study πK scattering close to threshold. At leading order the interaction of kaons with soft pions is described by the Lagrangian

$$L^{(1)}_{\pi K} = D_\mu K^\dagger D^\mu K - M_K^2 K^\dagger K, \tag{22}$$

where the covariant derivative D_μ is constructed using the vector field V_μ so that $D_\mu K$ transforms like K under chiral transformations:

$$D_\mu K = \partial_\mu K + V_\mu K \to U D_\mu K. \tag{23}$$

V_μ itself is constructed from the pion fields and transforms as

$$V_\mu = \frac{1}{2}(\xi^\dagger\partial_\mu\xi + \xi\partial_\mu\xi^\dagger) \to UV_\mu U^\dagger + U\partial_\mu U^\dagger. \tag{24}$$

We refer the reader to Eq. (11) of [27] for the higher-order terms in the $K\pi$ Lagrangian [terms up to $O(m_l^4)$ are explicitly listed]. For completeness we also present the axial field:

$$A_\mu = \frac{i}{2}(\xi^\dagger\partial_\mu\xi - \xi\partial_\mu\xi^\dagger) \to UA_\mu U^\dagger. \tag{25}$$

In the following, when constructing Feynman diagrams from the $K\pi$ Lagrangian and the effective theory local operators, we expand the vector and axial fields in terms of pion fields:

$$V_\mu = [\phi, \partial_\mu\phi]/2f^2 + \cdots \quad \text{and}$$
$$A_\mu = -\partial_\mu\phi/f + \cdots. \tag{26}$$

The use of PQChPT, in which we vary the valence quark masses independently of those of the sea quarks, gives us more scope to determine the low-energy constants of the unitary chiral theory and in this paper we will profit from

this opportunity. We consider the case with two degenerate light sea quarks, two degenerate light valence quarks, and two "ghost" degenerate light commuting quarks to cancel the loop effects of the valence quarks. Thus we are using the graded symmetry method [28,29], based on Morel's ghost-quark trick [30]. See the lectures by Sharpe [31] for a recent review of PQChPT and references to the original literature (as well as many other applications of chiral perturbation theory to lattice QCD). We let the sea quarks have mass m_l, while the valence and ghost quarks have mass m_x. Thus we build an $\mathrm{SU}(4|2)_L \times \mathrm{SU}(4|2)_R$ effective theory. We identify the quark flavors using the ordered list

$$u_v, d_v, u_s, d_s, \tilde{u}_v, \tilde{d}_v, \tag{27}$$

where subscripts v and s are for valence and sea, respectively, while the tilde denotes a ghost quark. We remind the reader that the strange quark mass does not appear explicitly here; rather, the LECs are functions of the strange quark mass.

The matrix of Goldstone fields is written in block form

$$\Phi = \begin{pmatrix} \phi & \eta_1 \\ \eta_2 & \tilde{\phi} \end{pmatrix}, \tag{28}$$

where ϕ is a 4×4 block containing normal mesons, $\eta_1 = \eta_2^\dagger$ is a 4×2 block of normal-ghost mesons, and $\tilde{\phi}$ is a 2×2 block of ghost-ghost mesons. The QCD pions are present in the central 2×2 block of Φ. As before, we work with the quantities ξ and Σ,

$$\xi = \exp(i\Phi/f) \quad \text{and} \quad \Sigma = \xi^2, \tag{29}$$

in terms of which the leading order PQ chiral Lagrangian is

$$\mathcal{L}_{\mathrm{PQ}}^{(2)} = \frac{f^2}{8} \operatorname{str}(D_\mu \Sigma)^\dagger D^\mu \Sigma + \frac{f^2 B}{4} \operatorname{str}(\mathcal{M}\Sigma^\dagger + \Sigma \mathcal{M}^\dagger), \tag{30}$$

where $\mathcal{M}$ is the mass matrix

$$\mathcal{M} = \operatorname{diag}(M_v, M_s, M_v), \quad \text{with } M_v = \operatorname{diag}(m_x, m_x) \quad \text{and} \quad M_s = \operatorname{diag}(m_l, m_l). \tag{31}$$

The quadratic terms in $\mathcal{L}_{\mathrm{PQ}}^{(2)}$ are

$$\begin{aligned} \mathcal{L}_{\mathrm{PQ,quad}}^{(2)} &= \frac{1}{2} \operatorname{str}(\partial_\mu \Phi \partial^\mu \Phi) - B \operatorname{str}(\mathcal{M}\Phi^2) \\ &= \frac{1}{2} \operatorname{tr}(\partial_\mu \phi \partial^\mu \phi + \partial_\mu \eta_1 \partial^\mu \eta_2 - \partial_\mu \eta_2 \partial^\mu \eta_1 \\ &\quad - \partial_\mu \tilde{\phi} \partial^\mu \tilde{\phi}) - B \operatorname{tr}\Big((\phi\phi + \eta_1 \eta_2) \\ &\quad \times \begin{pmatrix} M_v & 0 \\ 0 & M_s \end{pmatrix} - \eta_2 \eta_1 M_s - \tilde{\phi}\,\tilde{\phi}\, M_s \Big). \end{aligned} \tag{32}$$

The Lagrangian in Eq. (32) leads to a number of propagators which appear in the Feynman diagrams in the following sections. We distinguish the propagators for the following mesons:

(I) Normal "charged" (off-diagonal) mesons ($\sim q_1 \bar{q}_2$):

$$\frac{i}{p^2 - m_{12}^2}, \qquad m_{12}^2 = B(m_1 + m_2) = (\chi_1 + \chi_2)/2, \tag{33}$$

where $m_{1,2}$ are valence or sea masses.

(II) "Charged" ghost mesons ($\sim \tilde{q}_1 \bar{\tilde{q}}_2$):

$$\frac{-i}{p^2 - m_{12}^2}, \qquad m_{12}^2 = B(m_1 + m_2) = (\chi_1 + \chi_2)/2. \tag{34}$$

Here $m_{1,2}$ are valence masses.

(III) "Charged" quark/ghost-quark mesons ($\sim q_1 \bar{\tilde{q}}_2$ or $\sim \tilde{q}_1 \bar{q}_2$):

$$\frac{i}{p^2 - m_{12}^2}, \qquad m_{12}^2 = B(m_1 + m_2) = (\chi_1 + \chi_2)/2, \tag{35}$$

where $m_{1,2}$ are a valence mass from the ghost and a valence or sea mass from the quark.

(IV) "Neutral" mesons from diagonal parts of ϕ and $\tilde{\phi}$:

$$\langle \Phi_{ii} \Phi_{jj} \rangle = i \frac{\epsilon_i \delta_{ij}}{p^2 - \chi_i} - \frac{i}{N} \frac{p^2 - \chi_l}{(p^2 - \chi_i)(p^2 - \chi_j)}, \tag{36}$$

for N sea quarks which are all degenerate with mass m_l, with $N = 2$ here and

$$\epsilon_i = \begin{cases} +1 & \text{valence or sea} \\ -1 & \text{ghost.} \end{cases} \tag{37}$$

Note that the neutral propagators are determined after implementing the constraint $\operatorname{str}[\Phi] = 0$, which has the effect that neutral valence-valence meson propagators can have contributions from neutral sea quark states (see [31], for example).

We now add a kaon matter field

$$K = \begin{pmatrix} K_v^+ \\ K_v^0 \\ K^+ \\ K^0 \\ \tilde{K}^+ \\ \tilde{K}^0 \end{pmatrix} \sim \begin{pmatrix} \bar{s} u_v \\ \bar{s} d_v \\ \bar{s} u_s \\ \bar{s} d_s \\ \bar{s} \tilde{u}_v \\ \bar{s} \tilde{d}_v \end{pmatrix}. \tag{38}$$

The partially quenched $K\pi$ Lagrangian is the generalization of Eq. (22) written in terms of the partially quenched fields.

In the following three subsections we derive the mass dependence of f_K, m_K^2, and B_K respectively.

2. Chiral behavior of f_K

The kaon decay constant, f_K, is defined by the matrix element of the axial vector current:

$$\langle 0|\bar{u}\gamma_\mu\gamma_5 s|K^-(p)\rangle \equiv -if_K p_\mu. \tag{39}$$

We now need to match the QCD axial vector current to operators in KChPT. We start by doing this for left- and right-handed currents and then build the axial vector current. The left-handed QCD current for kaon decay is

$$\frac{1}{2}\bar{q}\gamma_\mu(1-\gamma_5)s, \tag{40}$$

where $q = u$ or d. It is convenient to promote q to be a 2-component vector with components u and d and to introduce a constant 2-component spurion vector h in order to be able to project u or d as required; specifically we write the left-handed current as

$$\frac{1}{2}\bar{q}h\gamma_\mu(1-\gamma_5)s. \tag{41}$$

The current in Eq. (41) would be invariant under $SU(2)_L$ transformations if h transformed as $h \to Lh$.

We match to the effective theory by building quantities linear in h and with a single Lorentz index, which would also be invariant if h transformed as above. At lowest order, we identify two terms:

$$(D_\mu K)^\dagger \xi^\dagger h, \quad \text{and} \quad K^\dagger A_\mu \xi^\dagger h. \tag{42}$$

By using equations of motion, operators with more covariant derivatives acting on the kaon field (which transform in the same way under chiral transformations) can be reduced to ones of higher-order in the chiral expansion.

For a right-handed current we simply take the h transformation to be $h \to Rh$ and obtain the two operators

$$(D_\mu K)^\dagger \xi h, \quad \text{and} \quad K^\dagger A_\mu \xi h, \tag{43}$$

which transform in the same way as $\bar{q}h\gamma_\mu(1+\gamma_5)s$.

Under a parity transformation, the quantities in the effective theory transform as

$$K \to -K, \qquad \xi \to \xi^\dagger, \qquad A_\mu \to -A_\mu. \tag{44}$$

Noting that parity transforms the left-handed current into the right-handed current and vice versa, we deduce that the currents are of the form

$$J^L_\mu = -L_{A1}(D_\mu K)^\dagger \xi^\dagger h + iL_{A2}K^\dagger A_\mu \xi^\dagger h, \tag{45}$$

$$J^R_\mu = L_{A1}(D_\mu K)^\dagger \xi h + iL_{A2}K^\dagger A_\mu \xi h, \tag{46}$$

where L_{A1} and L_{A2} are low-energy constants. To the extent that the kaon is regarded as heavy, the L_{A2} term is subleading (and in any case does not contribute to f_K at the tree or one-loop level). The axial vector current $J^R_\mu - J^L_\mu$ is therefore

$$J^5_\mu = L_{A1}(D_\mu K)^\dagger(\xi+\xi^\dagger)h + iL_{A2}K^\dagger A_\mu(\xi-\xi^\dagger)h. \tag{47}$$

We have introduced a factor of i in the L_{A2} term to make the low-energy constants real. This can be seen by considering charge conjugation $\mathcal{C}$. For the quark current (taking h to be real), we have

$$J^5_\mu = \bar{q}h\gamma_\mu\gamma_5 s \xrightarrow{\mathcal{C}} \bar{s}\,\gamma_\mu\gamma_5 h^{\mathrm{T}} q = (J^5_\mu)^\dagger. \tag{48}$$

In the effective theory, the charge conjugation transformations are

$$\xi \to \xi^{\mathrm{T}}, \qquad A_\mu \to A^{\mathrm{T}}_\mu, \qquad V_\mu \to -V^{\mathrm{T}}_\mu, \tag{49}$$

together with

$$\begin{aligned} &K_a \to K_a^\dagger, \\ &(D_\mu K)_a = \partial_\mu K_a + (V_\mu K)_a \to \partial_\mu K_a^\dagger - (K^\dagger V_\mu)_a \\ &\qquad = (D_\mu K)^\dagger_a, \end{aligned} \tag{50}$$

where a is a flavor label. Using these transformations, the current in the effective theory is transformed into its Hermitian conjugate under charge conjugation provided L_{A1} and L_{A2} are both real.

The leading contribution to f_K in the chiral expansion can be readily deduced. The first term in the axial current has a $\partial_\mu K$ factor with no pion fields, so that at tree level f_K is fixed by L_{A1}, specifically

$$f^{(K)}(m_h) = 2L_{A1}, \tag{51}$$

where m_h is the mass of the strange quark (we are using the notation defined in Appendix A).

The NLO contribution to f_K is obtained from the tadpole diagram in Fig. 1(a). From the $K\pi\pi$ vertex in the L_{A1} term in the axial current we obtain the contribution

$$\begin{aligned} &2L_{A1}(-ip_\mu)\frac{-iC_F}{f^2}\int\frac{d^4k}{(2\pi)^4}\frac{1}{k^2-m_\pi^2} \\ &\quad = 2L_{A1}(-ip_\mu)\frac{-iC_F}{(4\pi f)^2}m_\pi^2\left(\log\frac{m_\pi^2}{\Lambda_\chi^2} + \text{constant}\right), \end{aligned} \tag{52}$$

where $C_F = 3/4$ is the eigenvalue of the quadratic Casimir operator for SU(2) in the fundamental representation and

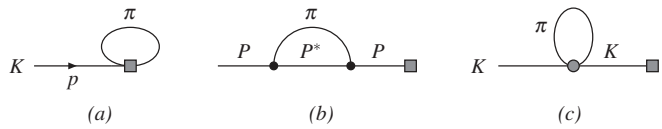

FIG. 1. (a) One-loop correction to f_K, (b) one-loop wave-function-like contribution proportional to g^2, (c) diagram contributing to the one-loop wave function (and mass) renormalization. The gray square denotes a flavor-changing axial vector current operator, the black bullets in (b) represent the $PP^*\pi$ vertex, and the gray circle in (c) denotes a $KK\pi\pi$ vertex from $L^{(1)}_{\pi K}$ in Eq. (22).

Λ_χ is an arbitrary renormalization scale. There is no contribution at one-loop order from the term in the axial current proportional to L_{A2} and so we have shown that the chiral behavior of f_K is of the form

$$f_K = f^{(K)}(m_h)\left\{1 + c(m_h)\frac{m_\pi^2}{f^2} - \frac{m_\pi^2}{(4\pi f)^2}\frac{3}{4}\log\frac{m_\pi^2}{\Lambda_\chi^2}\right\}, \quad (53)$$

where $c(m_h)$ is a low-energy constant and $m_\pi^2 = \chi_l$.

Before proceeding to discuss the chiral behavior of f_K in partially quenched SU(2) ChPT, we compare the above calculation with that of f_B in heavy meson ChPT [32]. In that case the NLO contribution has the corresponding contribution to Eq. (53), but in addition it has a second contribution from the self-energy diagram in Fig. 1(b). To discuss this for both f_B and f_K simultaneously, let P and P^* be pseudoscalar and vector mesons containing a light quark (u or d) and a heavier antiquark (e.g., s or b). Let the masses of the P and P^* mesons be M and M_*, respectively. The interaction of pions with pseudoscalar and vector mesons, P and P^*, takes the form $Mg\partial^\mu \pi P P^*_\mu/f$, where the $1/f$ arises because there is one pion and the Mg is put in for compatibility with heavy meson chiral perturbation theory (where the fields are usually normalized with an implicit factor of $\sqrt{M}$) so that the coupling constant g is dimensionless. The diagram in Fig. 1(b), for a P meson with momentum p, is proportional to $(Mg/f)^2 I$ where I is the Feynman integral:

$$I = \int \frac{d^4l}{(2\pi)^4}\frac{l^\mu l^\nu[g_{\mu\nu} - (p-l)_\mu(p-l)_\nu/M_*^2]}{(l^2 - m_\pi^2)((p-l)^2 - M_*^2)}. \quad (54)$$

We now compare the behavior of this integral with m_π^2 in the cases: (i) the heavy quark limit in which $M \to \infty$ with $M_*^2 - M^2 = O(\Lambda_{\rm QCD}^2)$ which is an approximation for B physics and (ii) M and M_* both of $O(\Lambda_{\rm QCD})$ and not degenerate, a situation which is appropriate for kaon physics.

In the heavy quark limit, we write $p = Mv + k$, where v is the meson's four-velocity ($v^2 = 1$) and the leading term in I in the $1/M$ expansion is

$$I \simeq \frac{1}{2M}\int \frac{d^4l}{(2\pi)^4}\frac{l^\mu l^\nu[g_{\mu\nu} - v_\mu v_\nu]}{(l^2 - m^2)(v\cdot(k-l) - \Delta)}, \quad (55)$$

where $\Delta = (M_*^2 - M^2)/2M$ which is of $O(\Lambda_{\rm QCD}^2/M)$ and hence negligible compared to m_π in the heavy quark limit. We stress that in this analysis we take the heavy quark limit before the chiral limit; i.e., we keep $\Lambda_{\rm QCD}/M \ll m_\pi/\Lambda_{\rm QCD}$. By power counting we see that the component of I contributing to the wave function renormalization can have a term proportional to

$$\frac{v\cdot k}{M} m_\pi^2 \log\frac{m_\pi^2}{\Lambda_\chi^2} \quad (56)$$

and so can lead to terms proportional to $(g^2/f^2)m_\pi^2 \ln(m_\pi^2/\Lambda_\chi^2)$ in the behavior of f_B. An explicit evaluation of the diagram confirms that such terms are indeed present [32].

In contrast, there is no contribution of the form $m_\pi^2 \log m_\pi^2$ in KChPT, i.e., when we take the chiral limit of small m_π^2 while keeping M and M_* fixed, nondegenerate, and neither especially large or small. To see this we combine the denominators in I using Feynman parametrization and write

$$I = \int_0^1 d\alpha \int \frac{d^4l}{(2\pi)^4}\frac{N(\alpha)}{D^2(\alpha)}, \quad (57)$$

where α is the Feynman parameter,

$$N(\alpha) = (l+\alpha p)^2 - \frac{((l+\alpha p)\cdot(l-(1-\alpha)p))^2}{M_*^2} \quad (58)$$

and

$$D(\alpha) = l^2 + \alpha(1-\alpha)p^2 - (1-\alpha)m_\pi^2 - \alpha M_*^2. \quad (59)$$

The question we are addressing is whether there is a contribution to I of the form $m_\pi^2 \log m_\pi^2$. If there is such a term, then we can isolate it by differentiating with respect to m_π^2, setting $m_\pi^2 \to 0$ and searching for a logarithmic (infrared) divergence in

$$\left.\frac{dI}{dm_\pi^2}\right|_{m_\pi^2=0} = -2\int_0^1 d\alpha(1-\alpha)\int \frac{d^4l}{(2\pi)^4} \times \frac{N(\alpha)}{D^3(\alpha, m_\pi^2 = 0)}. \quad (60)$$

We use dimensional regularization in $D = 4 + 2\varepsilon$ dimensions. The contribution from the first term in N in Eq. (58) is

$$\begin{aligned}\left.\frac{dI_1}{dm_\pi^2}\right|_{m_\pi^2=0} &= -2\int_0^1 d\alpha(1-\alpha)\int \frac{d^Dl}{(2\pi)^D} \times \frac{l^2 + \alpha^2 p^2}{[l^2 + \alpha(1-\alpha)p^2 - \alpha M_*^2]^3} \\ &= \frac{-i}{(4\pi)^{2+\varepsilon}}\int_0^1 d\alpha(1-\alpha)\alpha^\varepsilon \times [M_*^2 - (1-\alpha)p^2]^\varepsilon\left\{(2+\varepsilon)\Gamma(-\varepsilon) - \frac{\alpha p^2}{M_*^2 - (1-\alpha)p^2}\right\}. \end{aligned} \quad (61)$$

The contribution to the self-energy is the coefficient of p^2 at $p^2 = M^2$, which we can isolate by differentiating with respect to p^2 and setting $p^2 = M^2$. By inspection we can readily verify that there are no infrared singular terms and hence no term proportional to $m_\pi^2 \log m_\pi^2$ in I. Note that $M_* > M$ and hence $M_*^2 - (1-\alpha)p^2 > 0$ for $p^2 = M^2$ throughout the integration region in α. A parallel argument shows that there is also no contribution to I of the form

$m_\pi^2 \log m_\pi^2$ from the second term in $N(\alpha)$ on the right-hand side of Eq. (58).

Note also that I does contain a term proportional to $m_\pi^4 \log m_\pi^2$. In this case we seek an infrared divergence after differentiating I twice with respect to m_π^2 and setting $m_\pi^2 \to 0$. The power of $l^2 + \alpha(1-\alpha)p^2 - \alpha M_*^2$ in the integrand is -4 as compared to -3 in Eq. (61). After performing the l integration, we find that for small α the integrand behaves as $\alpha^{-1+\varepsilon}$, which diverges in four dimensions and is a signature of the presence of a $\log m_\pi^2$ term (i.e., a $m_\pi^4 \log m_\pi^2$ term in I).

There are also no chiral logarithms from the tadpole diagram in Fig. 1(c). The $KK\pi\pi$ term in $L_{\pi K}^{(1)}$ in Eq. (22) is proportional to $K(\partial_\mu K)[\phi, \partial^\mu \phi]$ and so the integrand is an odd function of the pion's momentum and the integral vanishes.

Finally in this section we derive the behavior of f_K in the partially quenched case, i.e., in PQKChPT. The axial vector current is of the form of that in Eq. (47), but uses the PQ K and ξ fields. As before, the spurion h is chosen to pull out the appropriate flavor. The tree and quadratic terms from this current are

$$J_\mu^{5a} = 2L_{A1}\partial_\mu K_b^\dagger \left(1 - \frac{\Phi^2}{2f^2}\right)_{ba} + \cdots, \tag{62}$$

where we have dropped terms with a single derivative acting on a Goldstone field.

To calculate the decay constant for a kaon containing a valence light quark, we take the flavor index $a = 1$ or 2. Choosing, for illustration, $a = 1$ we find

$$2L_{A1}\partial_\mu K_1^\dagger \Big[1 - \frac{1}{2f^2}(\eta_{1,11}\eta_{2,11} + \eta_{1,12}\eta_{2,21} + \phi_{11}^2 + \phi_{12}\phi_{21} + \phi_{13}\phi_{31} + \phi_{14}\phi_{41})\Big]. \tag{63}$$

There are also terms containing $\partial_\mu K_2^\dagger$, but these have Goldstone field pairings which cannot be contracted to give a one-loop tadpole contribution and thus are not listed above. The one-loop tadpole contribution to $f_{K_v^+}$ is

$$-L_{A1}\frac{1}{f^2}\int \frac{d^4l}{(2\pi)^4}\left\{-\frac{2i}{l^2-\chi_x} + \frac{i}{l^2-\chi_x} + \frac{2i}{l^2-(\chi_x+\chi_l)/2} + \frac{i}{l^2-\chi_x} - \frac{1}{2}\frac{l^2-\chi_l}{(l^2-\chi_x)^2}\right\}. \tag{64}$$

The five terms in the integrand of Eq. (64) have the following origin:

(i) The first term comes from the quark/ghost-quark mesons in the tadpole loop. These have valence-valence quark masses and the minus sign arises from the closed loop of anticommuting fields.

(ii) The second term has the $\phi_{12}\phi_{21}$ propagator with both quarks having valence masses.

(iii) The third term has the $\phi_{13}\phi_{31} + \phi_{14}\phi_{41}$ propagators with one quark having the valence quark mass and the other the sea quark mass.

(iv) and

(v) The final two terms have a neutral propagator in the tadpole diagram from the ϕ_{11}^2 term on the right-hand side of Eq. (63). Both quarks have valence quark masses.

We observe, as expected, that the tadpole contribution with the valence-ghost propagator cancels that with the valence-valence one. Extracting the chiral logarithms from the loop integrals we arrive at the expression

$$f_{xh} = 2L_{A1}\left\{1 - \frac{1}{(4\pi f)^2}\left[\frac{\chi_l+\chi_x}{2}\log\frac{\chi_l+\chi_x}{2\Lambda_\chi^2} + \frac{\chi_l-2\chi_x}{4}\log\frac{\chi_x}{\Lambda_\chi^2}\right]\right\} + \cdots. \tag{65}$$

The analytic terms can be proportional to χ_l and χ_x and so we obtain the final result for the mass behavior of a meson with a light valence quark x and a heavier (strange) valence quark h:

$$f_{xh} = f^K(m_h)\left\{1 + \frac{\lambda_3(m_h)}{f^2}\chi_l + \frac{\lambda_4(m_h)}{f^2}\chi_x - \frac{1}{(4\pi f)^2} \times \left[\frac{\chi_x+\chi_l}{2}\log\frac{\chi_x+\chi_l}{2\Lambda_\chi^2} + \frac{\chi_l-2\chi_x}{4}\log\frac{\chi_x}{\Lambda_\chi^2}\right]\right\}, \tag{66}$$

where $\lambda_{3,4}$ are LECs and we remind the reader that if the valence and sea strange quark masses are different, then the LECs $f^{(K)}$ and $\lambda_{3,4}$ depend on both these masses. Equation (66) agrees with the corresponding calculation of the chiral behavior of f_B [32], when the terms proportional to the square of the $BB^*\pi$ coupling are neglected. The right-hand side of Eq. (66) reduces to Eq. (53) in the unitary limit $\chi_x = \chi_l$.

3. Chiral behavior of m_K^2

We now consider the chiral behavior of m_K^2, starting in the unitary theory in which the valence and sea masses are equal. In principle the chiral logarithms could come from the tadpole diagram in Fig. 1(c). However, just as for the wave function renormalization, there is no such contribution at one-loop order. The $KK\pi\pi$ term in $L_{\pi K}^{(1)}$ in Eq. (22) is proportional to $K(\partial_\mu K)[\phi, \partial^\mu \phi]$ and so the integrand is an odd function of the pion's momentum and the integral vanishes. This is also the case in the partially quenched theory, and so at NLO in the chiral expansion, the mass dependence of m_K^2 comes from the analytical terms coming from the higher-order terms in the $K\pi$ Lagrangian. For the partially quenched theory at NLO

$$m_{xh}^2 = B^{(K)}(m_h)\tilde{m}_h\left\{1 + \frac{\lambda_1(m_h)}{f^2}\chi_l + \frac{\lambda_2(m_h)}{f^2}\chi_x\right\}. \tag{67}$$

In the unitary theory we have the natural simplification of only a single low-energy constant.

4. Chiral behavior of B_K

The nonperturbative strong interaction effects in neutral kaon mixing are contained in the matrix elements of the QCD operator

$$\bar{s}_L \gamma_\mu d_L \bar{s}_L \gamma^\mu d_L, \tag{68}$$

between K^0 and $\bar{K}^0$ states. This operator is part of a multiplet transforming under $\mathrm{SU}(2)_L$ on the two down quarks and is symmetric under the interchange of the two d_L's. Hence it transforms as a triplet under $\mathrm{SU}(2)_L$ and is a singlet under $\mathrm{SU}(2)_R$ [the analogous situation for neutral B-meson mixing is that the corresponding operator is part of a 6 representation of $\mathrm{SU}(3)_L$ [33]].

In our effective kaon theory the combination ξK transforms as $\xi K \to L \xi K$ under $\mathrm{SU}(2)_L$, and we can use it to build the leading $\Delta S = 2$ operator,

$$\mathcal{O}_{ab} = 2\beta (\xi K)_{\{a} (\xi K)_{b\}}, \tag{69}$$

which is symmetrized in the flavor indices a and b and has a LEC β [the analogous construction for neutral B-meson mixing in $\mathrm{SU}(3)_L \times \mathrm{SU}(3)_R$ heavy meson chiral perturbation theory leads to an operator $4\beta_Q (\xi P^{(Q)\dagger})_{\{a} (\xi P^{(\bar{Q})})_{b\}}$ [33], where $P^{(Q)}$ and $P^{(\bar{Q})}$ destroy mesons containing heavy Q and $\bar{Q}$ quarks, respectively]. As in the discussion of the axial current, operators with one or both of the kaon fields on the right-hand side of Eq. (69) replaced by $D^n K$, where D is the covariant derivative (the Lorentz indices have been suppressed) transform in the same way as $\mathcal{O}_{ab}$. Again, by using the equations of motion, the leading component of these operators can be reduced to $\mathcal{O}_{ab}$.

In order to evaluate B_K we will need the matrix element $\langle \bar{K}^0 | \mathcal{O}_{22} | K^0 \rangle$ and thus need to use the $K^0 K^0$ piece of $\mathcal{O}_{22}$. At tree level we find

$$4\beta = \frac{8}{3} m_K^2 f_K^2 B_K. \tag{70}$$

In order to evaluate the one-loop contributions to the matrix element (see Fig. 2) we expand $\mathcal{O}_{22}$ up to second order in the pion fields:

$$\mathcal{O}_{ab} = 2\beta K_a K_b - \frac{2\beta}{f^2}\Big\{(\phi K)_a (\phi K)_b + \frac{1}{2}[(\phi^2 K)_a K_b + K_a (\phi^2 K)_b]\Big\} + \cdots. \tag{71}$$

We observe, by comparing to the expansion of the axial vector current in Eq. (47), that the two terms containing ϕ^2 lead to relative one-loop corrections, each of which is the same as the relative one-loop correction for f_K. Since we are calculating a matrix element proportional to $f_K^2 B_K$, these two corrections will not affect B_K and we need only calculate the one-loop correction from the $(\phi K)_a \times (\phi K)_b$ term. Thus the relevant component of $\mathcal{O}_{22}$ is the $K^0 K^0$ term in

$$-\frac{2\beta}{f^2}(\phi K)_2 (\phi K)_2 = -\frac{2\beta}{f^2}\frac{\pi^0 \pi^0}{2} K^0 K^0 + \cdots. \tag{72}$$

Contracting the two pions into a loop leads to a contribution:

$$-\frac{2\beta}{f^2}\int \frac{d^4k}{(2\pi)^4}\frac{i}{k^2 - m_\pi^2} = -\frac{2\beta}{f^2}\frac{1}{(4\pi f)^2} m_\pi^2 \log\frac{m_\pi^2}{\Lambda_\chi^2} + \text{analytic terms}. \tag{73}$$

Hence we find that

$$B_K = B_K^{\text{tree}}\left\{1 - \frac{1}{2}\frac{1}{(4\pi f)^2} m_\pi^2 \log\frac{m_\pi^2}{\Lambda_\chi^2}\right\} + \cdots. \tag{74}$$

This agrees with the result for B_B in Eq. (3.8) of Sharpe and Zhang [32] when the $BB^*\pi$ coupling $g \to 0$.

We now promote the above discussion to the partially quenched case. The effective theory operator is still of the form of Eq. (69), but now the flavor labels take 6 values and ξ is expanded in terms of Φ in Eq. (28). This echoes the discussion for partially quenched neutral B-meson mixing in Sharpe and Zhang [32], starting from the QCD discussion in [33].

To obtain the mixing matrix element for neutral kaons with valence down quarks, we look at the $K_2 K_2$ piece of the $\mathcal{O}_{22}$ operator, expanded up to second order in the Goldstone fields:

$$\mathcal{O}_{22} = 2\beta K_2 K_2 - \frac{2\beta}{f^2}\Big\{(\Phi K)_2 (\Phi K)_2 + \frac{1}{2}[(\Phi^2 K)_2 K_2 + K_2 (\Phi^2 K)_2]\Big\} + \cdots. \tag{75}$$

As in the unquenched calculation above, the $(\Phi^2 K)_2 K_2$ terms lead to chiral logarithms which are canceled by those from f_K^2 when extracting B_K from the $\Delta S = 2$ matrix element. Hence the pieces of the partially quenched operator we need are

$$2\beta\left(1 - \frac{1}{f^2}\phi_{22}^2\right) K_2 K_2. \tag{76}$$

The ϕ_{22} field is a valence-valence neutral meson, so we find a one-loop correction:

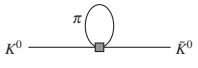

FIG. 2. One-loop contribution to B_K. The gray box denotes the insertion of the $KK\pi\pi$ operator $\mathcal{O}_{22}$ as defined in the text.

$$-\frac{4\beta i}{f^2}\int\frac{d^4l}{(2\pi)^4}\left\{\frac{1}{l^2-\chi_x}-\frac{1}{2}\frac{l^2-\chi_l}{(l^2-\chi_x)^2}\right\}$$
$$=-\frac{2\beta}{(4\pi f)^2}\chi_l\log\frac{\chi_x}{\Lambda_\chi^2}+\cdots. \quad (77)$$

For B_K the result is

$$B_{xh}=B_{\rm PS}^{(K)}\left\{1-\frac{1}{2}\frac{1}{(4\pi f)^2}\chi_l\log\frac{\chi_x}{\Lambda_\chi^2}\right\}+\cdots$$

This agrees with Eq. (3.9) in Sharpe and Zhang [32] with $g\to 0$ and $N_f=2$. It also reduces to the QCD result above, Eq. (74), when $\chi_x=\chi_l=m_\pi^2$. Noting that there are analytic terms proportional to both χ_l and χ_x, the final result for the mass dependence of B_K is that in Eq. (B48) of Appendix B

$$B_{xh}=B_{\rm PS}^{(K)}(m_h)\left\{1+\frac{b_1(m_h)}{f^2}\chi_l+\frac{b_2(m_h)}{f^2}\chi_x-\frac{\chi_l}{32\pi^2f^2}\log\frac{\chi_x}{\Lambda_\chi^2}\right\}, \quad (78)$$

where $b_{1,2}$ are LECs.

5. Comments

We conclude this section with the observation that for all the physical quantities considered in this section the chiral logarithms in the SU(2) theory can be simply deduced from those in the SU(3) theory. In all these cases the chiral behavior is of the generic form

$$O=O_{\rm LO}(1+\text{chiral logarithms}+\text{analytic terms}), \quad (79)$$

where O is the physical quantity (pseudoscalar mass squared, decay constant, or bag parameter) and there is a single LEC at lowest order ($O_{\rm LO}$). The generic form in Eq. (79) holds in both the SU(2) and SU(3) theories. As an example consider the pseudoscalar decay constant f_{xh}, with a degenerate heavy (strange) valence and sea quark with mass m_h and partially quenched up and down quarks. In the partially quenched SU(3) theory at NLO we have from Eq. (B18)

$$f_{xh}=f_0\left\{1-\frac{1}{8\pi^2f_0^2}\left[\frac{\chi_x+\chi_l}{4}\log\frac{\chi_x+\chi_l}{2\Lambda_\chi^2}+\frac{\chi_h+\chi_l}{4}\times\log\frac{\chi_h+\chi_l}{2\Lambda_\chi^2}+\frac{\chi_x+\chi_h}{8}\log\frac{\chi_x+\chi_h}{2\Lambda_\chi^2}+\frac{\chi_h}{4}\log\frac{\chi_h}{\Lambda_\chi^2}\right]\right.$$
$$+\frac{1}{96\pi^2f_0^2}\left[\left(\chi_x-\chi_h-\chi_x\frac{\chi_l-\chi_x}{\chi_\eta-\chi_x}\right)\log\frac{\chi_x}{\chi_h}+\chi_\eta(\chi_h-\chi_x)\frac{\chi_\eta-\chi_l}{\chi_\eta-\chi_x}\left(\frac{\log\frac{\chi_\eta}{\chi_x}}{\chi_x-\chi_\eta}-\frac{\log\frac{\chi_\eta}{\chi_h}}{\chi_h-\chi_\eta}\right)\right]$$
$$\left.+\text{analytic terms}\right\}. \quad (80)$$

"Converting" to the SU(2) theory, we can expand in m_x/m_h and m_l/m_h obtaining

$$f_{xh}=f_0\left\{1-\frac{1}{8\pi^2f_0^2}\frac{\chi_x+\chi_l}{4}\log\frac{\chi_x+\chi_l}{2\Lambda_\chi^2}+\frac{1}{64\pi^2f_0^2}\times(2\chi_x-\chi_l)\log\frac{\chi_x}{\Lambda_\chi^2}+\text{analytic and higher-order terms}\right\}. \quad (81)$$

The analytic terms now include contributions proportional to χ_h which do not vanish in the SU(2) chiral limit. They are absorbed into the lowest-order SU(2) LEC f, which now depends on m_h. Whether or not the relation between f and f_0 is well approximated by one-loop SU(3) ChPT or whether higher-order (χ_h^2 and higher powers) terms must be included depends on m_h and on the convergence of the series. In any case, if f_{xh} is to satisfy the generic form dictated by SU(2) ChPT given in Eq. (79), the chiral logs are fixed from Eq. (81):

$$f_{xh}=f\left\{1-\frac{1}{8\pi^2f^2}\frac{\chi_x+\chi_l}{4}\log\frac{\chi_x+\chi_l}{2\Lambda_\chi^2}+\frac{1}{64\pi^2f^2}(2\chi_x-\chi_l)\log\frac{\chi_x}{\Lambda_\chi^2}+\text{analytic and higher-order terms}\right\}, \quad (82)$$

which agrees with the result from the direct evaluation in the SU(2) theory [see Eq. (66)]. The same is true for the other quantities being studied here. Of course, in general there may be more than one operator in the effective theory with the same quantum numbers as the QCD operator whose matrix element is to be evaluated. In such cases there are more than one LEC at leading order, Eq. (79) does not apply, and the simple arguments presented here have to be generalized.

III. SIMULATION DETAILS AND ENSEMBLE PROPERTIES

Following the work in [16,34] we have used the Iwasaki gauge action and the domain wall fermion action. By producing smoother gauge fields at the lattice scale, for a fixed lattice spacing in physical units, the Iwasaki action removes some of the gauge field dislocations that contribute to the residual chiral symmetry breaking for domain wall fermions at finite L_s. While suppressing such dislocations improves residual chiral symmetry breaking, it also suppresses topology change in the evolution [17]. Since we want our ensembles to sample topological sectors of the theory as well as possible, we have found the Iwasaki gauge action to provide a reasonable balance between these two, contradictory goals.

We generate ensembles with two degenerate light quarks, whose bare input mass is given by m_l, and one heavy-strange quark of mass m_h. We use the exact RHMC

algorithm to generate ensembles. During the course of this work, we made improvements to the RHMC algorithm, as detailed in [34], yielding three variants of the RHMC algorithm, 0, I, and II. The original RHMC 0 algorithm [35,36] was used for the $2+1$ flavor simulations in [16] and the RHMC I was used for most of the simulations in [34]. We also compared the RHMC I and II algorithms in [34]. We find the RHMC II algorithm to be the best version to date. It uses a single stochastic noise source to estimate ratios of determinants, which reduces the size of the forces in the molecular-dynamics integration [15]. It produces ensembles that change topology more rapidly than RHMC I, likely due to this decrease in the fermionic force. It uses a multiple time scale Omelyan integrator and light quark preconditioning [37,38], which has the effect of making the time spent solving the light quark Dirac equation less than the time spent solving for heavier quarks.

We can briefly define the RHMC II algorithm. Letting $\mathcal{D}(m_i) = D^{\dagger}_{\mathrm{DWF}}(M_5, m_i) D_{\mathrm{DWF}}(M_5, m_i)$, where $D_{\mathrm{DWF}}(M_5, m_i)$ is the domain wall fermion Dirac operator, M_5 is the domain wall height, and m_i is the mass of the quark we wish to simulate, we write the fermionic contribution to the path integral as

$$\det\left\{\frac{\mathcal{D}(m_l)}{\mathcal{D}(1)}\right\}\det\left\{\frac{\mathcal{D}(m_h)}{\mathcal{D}(1)}\right\}^{1/2} = \det\left\{\frac{\mathcal{D}(m_l)}{\mathcal{D}(m_h)}\right\} \times\left[\det\left\{\frac{\mathcal{D}(m_h)}{\mathcal{D}(1)}\right\}^{1/2}\right]^3. \tag{83}$$

[Recall that for domain wall fermions, a regulator must be added to remove the bulk infinity that would arise as $L_s \to \infty$. The $\mathcal{D}(1)$ terms in Eq. (83) are this regulator.] Each ratio of determinants on the right-hand side of Eq. (83) is represented by a single stochastic estimator; i.e., a single estimator is used for the ratio involving m_l and m_h and three estimators are used for the three, fractional power determinants involving m_h and 1. The light quark ratio is integrated on the coarsest time scale, using a conventional hybrid Monte Carlo algorithm. The three $1/2$ powers of ratios involving the heavy dynamical quark are integrated on a 2 times finer time scale using the RHMC algorithm. For each integration step of the RHMC and for each field, a single solution of the Dirac equation is required with mass m_h and two solutions with the regulator mass of 1. (The solutions are found with the conjugate gradient algorithm.) The regulator mass solutions take roughly half as many conjugate gradient iterations in the RHMC as the m_h solutions, but there are twice as many required. Thus the time spent solving the Dirac equation in the two cases is comparable. Because of the three different stochastic estimators needed in the RHMC, and the coarser time step for the HMC, the number of conjugate gradient iterations in the RHMC is larger than in the HMC part of the algorithm for the quark masses currently used. This has made simulating at lighter quark masses much less expensive. The gauge field is integrated on an even finer time scale than the RHMC. For a further review of the RHMC, see [39].

As mentioned, we had already begun evolving configurations with the RHMC 0 algorithm as improved versions were being developed. Table I gives the molecular-dynamics time when we changed from one algorithm to the next, for each of our ensembles. Since the RHMC II gives more decorrelated lattices than earlier versions, all of the observables in this paper have been measured only on configurations generated by the RHMC II algorithm. The configurations generated with the earlier algorithms are being used only for equilibration.

As one indicator of how well the RHMC II algorithm is decorrelating our ensembles, we have measured the global topological charge. Of course, for infinite volumes, the global topological charge is not relevant to local physics. However, in finite volume knowing that global topology is changing gives us evidence that there are local topological fluctuations. To calculate the topological charge the configurations are first cooled by applying 30 updates with a quenched, five-loop improved gauge action with zero coupling strength, $\beta = \infty$. After cooling, the topological charge is measured using a five-loop improved gluonic topological charge operator, the 5Li method of [40], and the results are shown in Fig. 3. This figure shows that the RHMC algorithm is sampling different topological sectors for each of our ensembles and the histograms indicate, by their symmetry and shape, that the topological landscape has been sampled reasonably well.

Figures 4 and 5 show the integrated autocorrelation time for the pion correlator at a separation of 12 lattice spacings for the $m_l = 0.005$ ensemble. Both show an integrated autocorrelation time for this quantity of 10 to 15 molecular-dynamics time units. Figure 6 shows the evolution of the plaquette for the $m_l = 0.02$ ensemble. For this short-distance observable, equilibration took a few hundred molecular-dynamics time units.

TABLE I. Improvements to the RHMC algorithm were implemented as the ensemble generation progressed. The table details the algorithms used for each ensemble and the range, in molecular-dynamics (MD) time, where measurements were made.

m_l	RHMC	MD range	Measurement range
0.005	II	0–4435	900–4460
0.01	0	0–549	
	I	550–1454	
	II	1455–5020	1460–5020
0.02	0	0–1519	
	I	1520–1884	
	II	1885–3610	1800–3560
0.03	0	0–492	
	I	493–929	
	II	930–3060	1260–3040

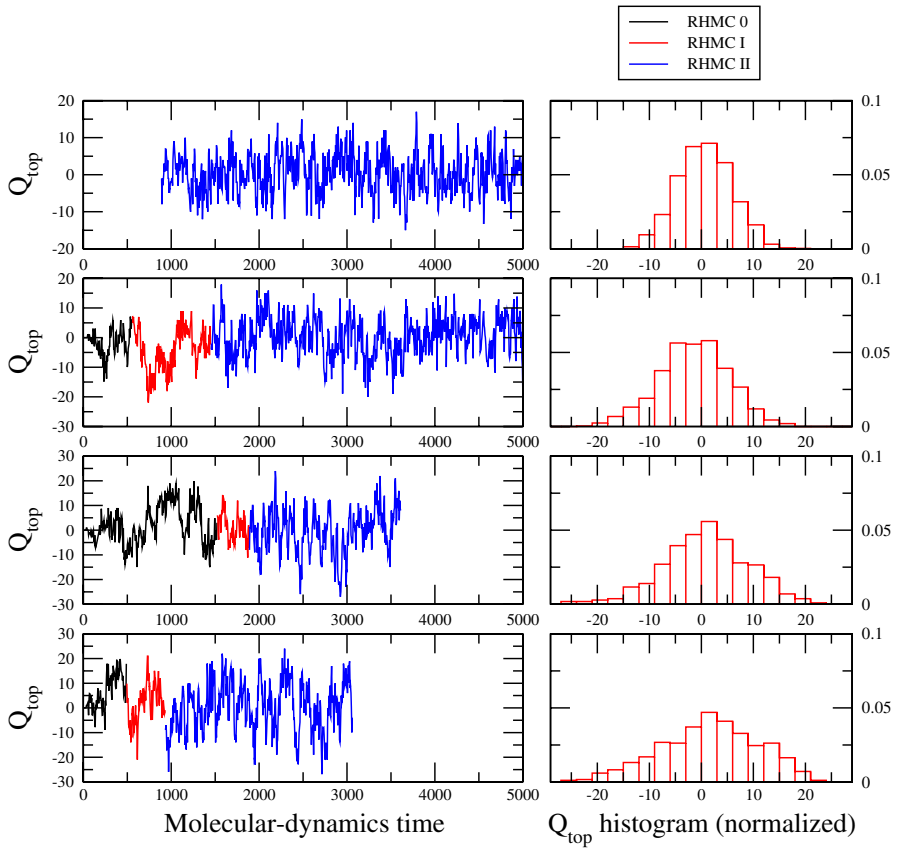

FIG. 3 (color online). The left graphs show topological charge, as measured on each ensemble every 5th unit of molecular-dynamics time. The right panels show normalized histograms of toplogical charge. Notice the width of the histograms decreases as the light quark mass is reduced. For both the left and right graphs, the light dynamical quark mass is $m_l = 0.005, 0.01, 0.02, 0.03$, from top to bottom.

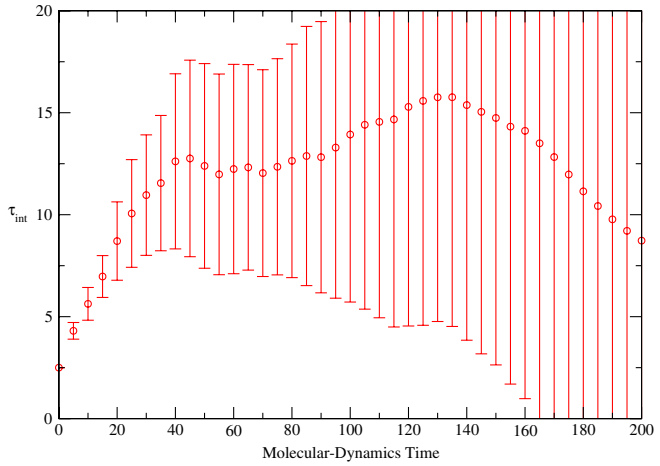

FIG. 4 (color online). Integrated autocorrelation time for 12th time slice of the unitary degenerate pseudoscalar correlator with local sources and sinks $\langle P^{LL}, P^{LL}\rangle$ measured on the $m_l = 0.005$ ensemble. Measurements were done every fifth trajectory in the range 900–1530 and a bin factor of 2 was used in the analysis.

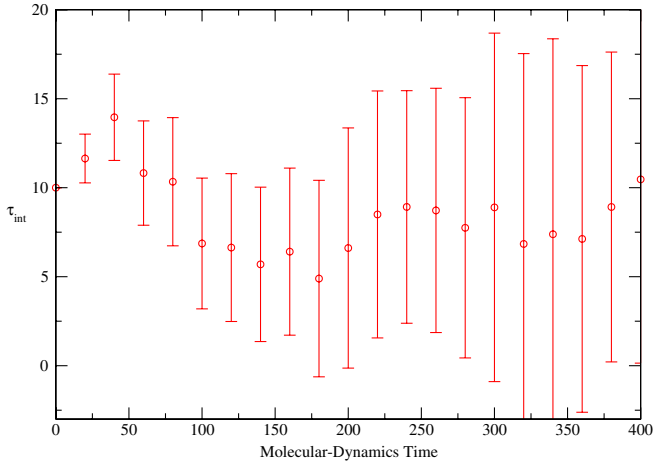

FIG. 5 (color online). Integrated autocorrelation time for 12th time slice of the unitary degenerate pseudoscalar correlator with a local sink and a Gaussian source $\langle P^{LL}, P^{HH}\rangle$ measured on the $m_l = 0.005$ ensemble. Measurements were done every twentieth trajectory in the range 500–4500 and a bin factor of 4 was used in the analysis.

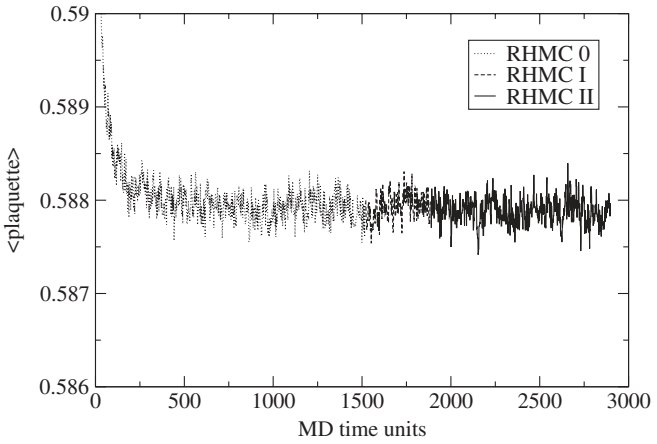

FIG. 6. Evolution history of the plaquette for the ensemble $m_l = 0.02$.

TABLE II. Calculation parameters for the three separate data sets FPQ, DEG, and UNI. The range and measurement separation Δ are specified in molecular-dynamics time units. N_{meas} is the number of measurements for each source position t_{src}. The total number of measurements is therefore $N_{\text{meas}} \times N_{\text{src}}$, where N_{src} is the number of different values for t_{src}.

m_l	Data set	Range	Δ	N_{meas}	$t_{\text{src locations}}$
0.005	FPQ	900–4460	40	90	5, 59
	DEG	900–4460	40	90	0, 32
	UNI	900–4480	20	180	0, 32, 16
0.01	FPQ	1460–5020	40	90	5, 59
	DEG	1460–5020	40	90	0, 32
	UNI	800–3940	10	315	0, 32
0.02	DEG	1800–3560	40	45	0, 32
	UNI	1800–3580	20	90	0, 32
0.03	DEG	1260–3020	40	45	0, 32
	UNI	1260–3040	20	90	0, 32

IV. LATTICE RESULTS FOR PSEUDOSCALAR MASSES AND DECAY CONSTANTS

A. Measurements

Since we are most interested in the light quark limit where pion masses are close to the physical values, we put significant computational effort into the measurements on the two lightest ensembles with $m_l = 0.005$ and $m_l = 0.01$. On these two ensembles, three separate measurements have been done, which we shall refer to as full partially quenched (FPQ), degenerate (DEG), and unitary (UNI). In the FPQ measurement we computed hadron two-point correlators for all the combinations with valence quark masses m_x, $m_y \in \{0.001, 0.005, 0.01, 0.02, 0.03, 0.04\}$. The DEG data set consists of hadron correlators with *degenerate* quarks with the same list of masses. In the UNI data set only quark propagators with masses equal to the light and strange sea quark masses were calculated, and the light-light, light-strange, and strange-strange meson correlators were then constructed. On the $m_l = 0.02$ and $m_l = 0.03$ ensembles, only the DEG and UNI calculations were performed. Details of the measurements, including the gauge configurations used, separation of each measurement, and the total number of measurements, can be found in Table II. For the $m_l = 0.005$ and $m_l = 0.01$ ensembles, we blocked the data so that each block contains measurements from every 80 molecular-dynamics time unit, while for the $m_l = 0.02$ and 0.03 ensembles the block size was chosen to be 40 time units to yield a reasonable number of jackknife blocks to perform the analysis.

In each of the FPQ measurements, we used Coulomb gauge fixed wall (W) sources of size 24^3, which were placed at $t = 5$ and $t = 59$. For each source, two quark propagators were calculated, one with the periodic, and the other antiperiodic, boundary condition in the temporal direction. The sum of these two quark propagators (as a single quark propagator) was then used to construct the meson correlators. The resulting cancellation of backward propagating states has the effect of doubling the temporal extent of the lattice, so over much of the lattice volume, there is no excited state contribution to the hadron propagator. We find this works well with our Coulomb gauge fixed wall sources, which generally have small statistical errors but are not tuned to remove excited state contaminations. The long plateaus and small statistical errors allow us to work far enough from the source that excited states are not a worry.

The DEG measurements used a Coulomb gauge fixed box source (B) of size 16^3 which we have found to give the optimal early onset of the plateaus for pseudoscalar mesons. The sources were placed at two time slices, $t = 0$ and 32.

In the UNI measurements, the propagators were calculated from Coulomb gauge fixed hydrogen S-wave function (H) sources [41], with radius $r = 3.5$, in lattice units, or gauge invariant gaussian (G) sources and sinks with radius $r = 4$. Again the sources were placed at multiple time slices for a better sampling over the gauge fields.

We also used two different interpolating operators for the pseudoscalar state, namely, the pseudoscalar operator $P^a(x) = \bar{q}(x)\gamma_5(\tau^a/2)q(x)$, which we refer to using a shorthand notation P, and the axial vector operator $A^a_\mu(x) = \bar{q}(x)\gamma_\mu\gamma_5(\tau^a/2)q(x)$, which we refer to as A. Here τ^a is a flavor symmetry generator. Unless otherwise specified, we only consider the time component of $A^a_\mu(x)$, i.e., $A^a_4(x)$. Together with the different source/sink smearings described above, this allows us to construct several different pseudoscalar meson correlators, which are tabulated in Table III. (Table IV has similar information for vector and tensor correlators, which are discussed in detail in Sec. IX.) The notation in Table III follows Ref. [16], where quark propagators are specified by the smearings applied in the source and sink. For example, WL means a quark propagator calculated with a wall (W) source and a local (L) sink. Meson correlators are then denoted by the

TABLE III. Combinations of quark source and sink smearings used for correlation functions for each of the data sets FPQ, DEG, and UNI. A is the time component of the axial current density operator and P is the pseudoscalar density operator. XY-XY denotes the contraction of two quark propagators with X-type smearing at source and a Y-type smearing at sink. W = wall source, B = box source, H = hydrogen S-wave, and L = local.

Operator type $\langle \mathcal{O}_{\rm snk}\mathcal{O}_{\rm src}\rangle$	Data set FPQ	DEG	UNI
$\langle A, A\rangle$	WL-WL	BL-BL	HL-HL
			LL-LL
$\langle P, A\rangle$			HL-HL
			LL-LL
$\langle A, P\rangle$	WL-WL	BL-BL	HL-HL
	WW-WW	BB-BB	LL-LL
$\langle P, P\rangle$	WL-WL	BL-BL	HL-HL
	WW-WW		LL-LL

type of quark propagators used in the contraction; e.g., WL-WL refers to a meson correlator with two WL quark propagators. In this case we may also use WL to refer to the meson correlator unless ambiguities arise.

In this paper we only consider meson correlators with zero-momentum projection. Our meson states are normalized such that the time dependence of the correlators in the large t limit can be expressed as

$$\mathcal{C}^{s_1 s_2}_{O_1 O_2}(t) = \frac{\langle 0|O_1^{s_1}|\pi\rangle\langle\pi|O_2^{s_2}|0\rangle}{2m_{xy}V}\left[e^{-m_{xy}t} + (-1)^p e^{-m_{xy}(T-t)}\right], \tag{84}$$

where the superscripts specify the smearings for the quark propagators, and the subscripts specify the interpolating operators used. m_{xy} is the ground-state mass of a pseudoscalar meson composed of two valence quarks with masses m_x and m_y. For convenience the amplitude of the correlator will be denoted as

$$\mathcal{N}^{s_1 s_2}_{O_1 O_2} \equiv \frac{\langle 0|O_1^{s_1}|\pi\rangle\langle\pi|O_2^{s_2}|0\rangle}{2m_{xy}V}. \tag{85}$$

TABLE IV. The different source and sink contraction of the quark propagators for the UNI data set. $V = \gamma_i$ (i = 1, 2, 3) is one of the spatial components of the vector current and $T = \sigma_{4i}$ are the calculated components of the tensor current. XY-XY denotes contraction of two quark propagators with an X-type smearing at source and a Y-type smearing at sink. H = hydrogen S-wave, G = Gaussian wave function (cf. [16]), and L = point.

Contraction $\langle \mathcal{O}_{\rm snk}\mathcal{O}_{\rm src}\rangle$	UNI data set m = 0.005, 0.02, 0.03	m = 0.01
$\langle V, V\rangle$	HL-HL	GL-GL
	LL-HL	LL-GL
	HL-LL	GL-LL
$\langle T, V\rangle$	HL-HL	GL-GL
	LL-HL	LL-GL
	HL-LL	GL-LL

B. Residual chiral symmetry breaking

As discussed in Sec. II A, the finite size in the fifth dimension of the domain wall fermion formulation in our current simulations permits the mixing between the two light quark states bound to the boundary walls, resulting in a residual chiral symmetry breaking [7,14,17]. Close to the continuum limit, this effect can be quantified as a residual mass term (denoted as $m_{\rm res}$), which, up to $O(a^2)$, behaves as a regular quark mass, making the total quark mass effectively the sum of the bare input quark mass and the residual mass. We determine the residual mass by computing the ratio [14,16]

$$R(t) = \frac{\langle \sum_{\vec{x}} J^a_{5q}(\vec{x}, t)P^a(\vec{0}, 0)\rangle}{\langle \sum_{\vec{x}} P^a(\vec{x}, t)P^a(\vec{0}, 0)\rangle}, \tag{86}$$

where J^a_{5q} is the "midpoint" operator which mixes the quark states from the left and right walls [7,14], and P^a is the pseudoscalar operator defined earlier. For t large enough that only pions contribute to the correlators in Eq. (86), $R(t) \to m'_{\rm res}(m_f)$. From the DEG data sets, we obtained the residual mass for each pair of valence quark masses by averaging the plateaus of $R(t)$ from $t = 10$ to $t = 32$. Figure 7 shows the residual mass as a function of the valence quark mass. We can see that the residual mass has a linear dependence on the input quark masses, and the magnitude of the slope is larger in the valence sector than the sea sector. The slopes have opposite signs, as was also observed in our previous simulations on smaller volumes [16,34]. In particular, $d\ln(m'_{\rm res})/dm_f^{\rm val} = -4.1$ for the ensemble with $m_l = 0.005$ and -4.5 for the $m_l = 0.03$ ensemble. We also find $d\ln(m'_{\rm res})/dm_f^{\rm sea} = 6$, and for the dynamical quark mass dependence in the unitary case, the result is $d\ln(m'_{\rm res}))/dm_l = 1.1$. In terms of the discussion at the end of Sec. II A, it appears that the $Z_{\mathcal{A}} - 1$ and dimension five terms are comparable in magnitude. We define a mass-independent residual mass for our simulations by evaluating $m_{\rm res}(m_l)$ at the $m_l = 0$ limit. The straight line in Fig. 7 shows a linear fit to the four unitary points with $m_x = m_y = m_l$. And the star is the resulting residual mass at $m_l = 0$, which we determined to be

$$m_{\rm res} = 0.003\,15(2). \tag{87}$$

It is worth noting that this result is in decent agreement with that obtained from earlier simulations at the same gauge coupling but with a smaller lattice volume [34], indicating that the finite-volume effect for the residual mass is small.

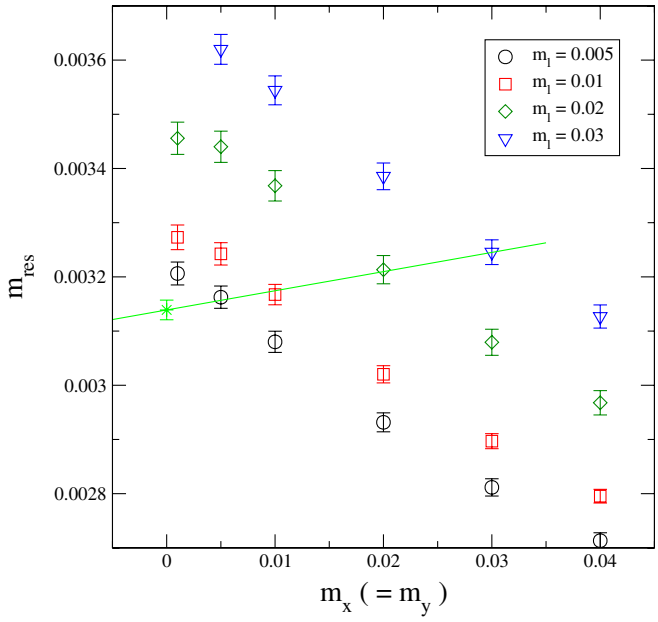

FIG. 7 (color online). The residual mass as a function of the valence quark mass. The solid line is a linear fit to the four unitary points with $m_l = 0.005$, 0.01, 0.02, and 0.03. The star is the extrapolation to $m_l = 0$, which we quote as the residual mass in our simulations.

C. Pseudoscalar meson masses and decay constants

1. Results from the $m_l = 0.005$ and 0.01 ensembles

To obtain the masses and decay constants for the pseudoscalar mesons from the $m_l = 0.005$ and $m_l = 0.01$ ensembles, we focus on the FPQ data sets, since the long plateaus of the FPQ data sets lessen the uncertainty in choosing the fit ranges. In fact, including the UNI and DEG measurements in the simultaneous fits (described below) does not change significantly either the central values or statistical errors of the final results. Thus here we only quote results from the FPQ data sets.

For each mass combination in the FPQ data sets, we performed a simultaneous fit to the five correlators as specified in the second column of Table III to determine a common mass and a different amplitude for each correlator. This approach has the advantage of averaging out the systematic uncertainties due to different characteristics of the interpolating operators (P or A), and reducing the uncertainty of fit range choices. One drawback is that, as the number of data points included in the fit (~ 220) is greater than the number of independent measurements we have in hand, the covariance matrix is poorly resolved, and we lean on uncorrelated fits to obtain results. The resulting pseudoscalar meson masses for all the mass combinations of the $m_l = 0.005$ and 0.01 ensembles are given in Table V. Note that the quoted χ^2/dof only give a qualitative indication of how different fits compare to each other. They are not meaningful quantitative indications of the goodness of the fits.

TABLE V. Lattice values for the pseudoscalar meson mass and χ^2/dof calculated from an *uncorrelated* simultaneous fit to five correlators of the FPQ data set on $m_l = 0.005$ and $m_l = 0.01$ ensembles.

		$m_l = 0.005$		$m_l = 0.01$	
m_x	m_y	m_{xy}	χ^2/dof	m_{xy}	χ^2/dof
0.001	0.001	0.1402(9)	0.36(7)	0.1432(10)	0.18(6)
0.001	0.005	0.1680(8)	0.38(8)	0.1706(9)	0.21(6)
0.005	0.005	0.1915(8)	0.39(9)	0.1938(8)	0.25(6)
0.001	0.010	0.1971(8)	0.38(8)	0.1994(9)	0.26(7)
0.005	0.010	0.2172(8)	0.38(9)	0.2194(8)	0.25(7)
0.010	0.010	0.2400(7)	0.36(9)	0.2421(7)	0.24(7)
0.001	0.020	0.2449(9)	0.36(9)	0.2473(9)	0.30(8)
0.005	0.020	0.2611(8)	0.34(9)	0.2635(8)	0.24(8)
0.010	0.020	0.2802(7)	0.31(8)	0.2825(7)	0.22(7)
0.020	0.020	0.3155(7)	0.26(8)	0.3178(6)	0.23(8)
0.001	0.030	0.2850(10)	0.33(10)	0.2877(10)	0.33(10)
0.005	0.030	0.2990(8)	0.32(9)	0.3016(8)	0.26(9)
0.010	0.030	0.3158(7)	0.28(8)	0.3183(7)	0.24(8)
0.020	0.030	0.3477(6)	0.23(7)	0.3500(6)	0.26(10)
0.030	0.030	0.3775(6)	0.21(8)	0.3797(6)	0.29(11)
0.001	0.040	0.3204(11)	0.34(13)	0.3234(11)	0.36(12)
0.005	0.040	0.3329(8)	0.31(10)	0.3358(8)	0.31(11)
0.010	0.040	0.3482(7)	0.26(8)	0.3508(7)	0.29(11)
0.020	0.040	0.3776(6)	0.22(8)	0.3800(6)	0.30(12)
0.030	0.040	0.4055(6)	0.21(8)	0.4077(5)	0.32(13)
0.040	0.040	0.4320(6)	0.21(9)	0.4341(5)	0.34(13)

Besides a common mass for each valence mass combination, we also obtained an amplitude for each correlator included in the simultaneous fit, namely,

$$\mathcal{N}_{AA}^{LW}, \mathcal{N}_{PP}^{LW}, \mathcal{N}_{AP}^{LW}, \mathcal{N}_{PP}^{WW}, \quad \text{and} \quad \mathcal{N}_{AP}^{WW}. \tag{88}$$

Combinations of these amplitudes can be used to determine the pseudoscalar decay constant, which we will describe in the following.

The pseudoscalar decay constant can be determined by

$$f_{xy} = \frac{Z_A |\langle \pi | A_4 | 0 \rangle|}{m_{xy}}, \tag{89}$$

where Z_A is the axial vector current renormalization constant which relates the (partially) conserved axial vector current in the original five-dimensional theory of domain wall fermions to the local four-dimensional axial vector current [4]. Alternatively, the axial Ward identity in Eq. (11) connects the divergence of the partially conserved axial vector current to the pseudoscalar density, allowing us to determine the pseudosclar decay constant through

$$f_{xy} = \frac{(\tilde{m}_x + \tilde{m}_y) |\langle \pi | P | 0 \rangle|}{m_{xy}^2}, \tag{90}$$

where $\tilde{m}_{x,y} = m_{x,y} + m_{\rm res}$.

We determined Z_A from the DEG data sets using the improved ratio [24] of $\langle \mathcal{A}_4(t) P(0) \rangle$ to $\langle A_4(t) P(0) \rangle$, where

$\mathcal{A}_\mu(x)$ is the partially conserved axial vector current for domain wall fermions [4,7]. Similar to the residual mass, we computed the value of Z_A at each unitary quark mass, and extrapolated it to the chiral limit at $m_l = -m_{\rm res}$, finding

$$Z_A = 0.7161(1), \tag{91}$$

which agrees very well with the result of our smaller volume simulations [34].

There are in principle five methods [42] to determine the matrix element necessary for the f_{xy} calculation in Eq. (89) or (90). These use jackknife ratios of different amplitudes in Eq. (88). We found that different methods give statistically consistent results for all quark masses except for the lightest or heaviest quark masses, where systematic deviations for results obtained using Eqs. (89) and (90) are observed. The methods where the pseudoscalar density is used make use of the equation of motion for the conserved axial current and are more indirect, since we have not systematically controlled higher-order renormalization effects here. As was discussed in Sec. II A, the renormalization of the conserved axial current is known to $O(m_{\rm res})$, and we know the renormalization between the local and conserved current to high accuracy. Therefore, we have chosen as our preferred result a determination of f_{xy} using axial current matrix elements and postpone further investigation of the differences we are seeing for future work. We also find that the statisical errors are the smallest when only the axial vector current matrix elements are used in the analysis. Thus, we determine f_{xy} by

$$f_{xy} = Z_A \sqrt{\frac{2}{m_{xy}} \frac{\mathcal{N}_{AP}^{LW2}}{\mathcal{N}_{PP}^{WW}}}. \tag{92}$$

The final results for the $m_l = 0.005$ and 0.01 ensembles are shown in Table VI.

Comparing the results from the $m_l = 0.01$ ensemble with those obtained from a smaller volume reported in Ref. [34], we find that there is a statistically significant 4% difference at the unitary point of $m_x = m_y = m_l = 0.01$, as shown in Fig. 8. As we shall see in Sect. VI A, such a difference is about twice as large as predicted by finite-volume chiral perturbation theory. While it is possible that ChPT still underestimates the finite-volume effect for f_{xy}, we want to point out that the $16^3 \times 32$ gauge configurations were generated using RHMC I which could intrinsically induce long-range autocorrelations. Another difference is that there we determined f_{xy} using correlators with much shorter plateaus compared to the $24^3 \times 64$ ensembles discussed here, which means the smaller volume results may suffer from larger systematic errors. Although we tried our best to estimate uncertainties on the physical quantities of the $16^3 \times 32$ simulations, the errors might still be underestimated. With these factors taken into account, the discrepancy between the lattice data and the predictions of the finite-volume ChPT may not be as significant as it appears.

TABLE VI. Lattice values for the pseudoscalar decay constant calculated using the method described in Eq. (92).

m_x	m_y	$f_{xy}(m_l = 0.005)$	$f_{xy}(m_l = 0.01)$
0.001	0.001	0.0829(7)	0.0860(7)
0.001	0.005	0.0846(7)	0.0878(6)
0.005	0.005	0.0860(6)	0.0891(6)
0.001	0.010	0.0867(7)	0.0900(6)
0.005	0.010	0.0880(6)	0.0910(6)
0.010	0.010	0.0898(6)	0.0928(6)
0.001	0.020	0.0904(7)	0.0928(7)
0.005	0.020	0.0915(6)	0.0946(6)
0.010	0.020	0.0934(6)	0.0962(6)
0.020	0.020	0.0969(6)	0.0995(5)
0.001	0.030	0.0936(8)	0.0972(8)
0.005	0.030	0.0947(6)	0.0979(6)
0.010	0.030	0.0965(6)	0.0994(6)
0.020	0.030	0.1001(6)	0.1025(5)
0.030	0.030	0.1033(6)	0.1056(5)
0.001	0.040	0.0965(8)	0.1003(8)
0.005	0.040	0.0975(7)	0.1008(7)
0.010	0.040	0.0993(6)	0.1022(6)
0.020	0.040	0.1029(6)	0.1053(5)
0.030	0.040	0.1062(6)	0.1083(5)
0.040	0.040	0.1091(7)	0.1111(5)

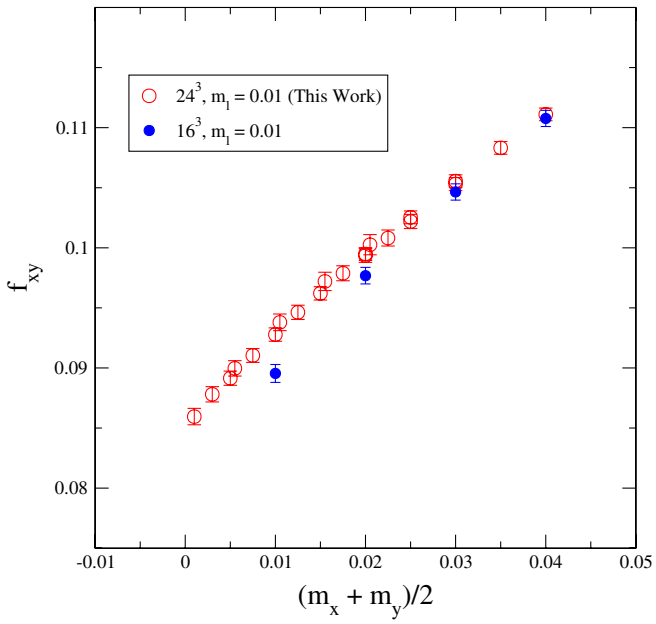

FIG. 8 (color online). Comparison of the lattice results for the pseudoscalar decay constants on the $16^3 \times 32$ and $24^3 \times 64$ lattices with $m_l = 0.01$.

TABLE VII. Lattice values for the pseudoscalar meson mass and χ^2/dof calculated from an *uncorrelated* simultaneous fit to four correlators of the DEG data set on $m_l = 0.02$ and $m_l = 0.03$ ensembles.

	$m_l = 0.02$		$m_l = 0.03$	
m_x	m_{xx}	χ^2/dof	m_{xx}	χ^2/dof
0.001	0.1493(11)	0.7(4)	...	...
0.005	0.1993(9)	0.5(3)	0.2016(11)	0.4(1)
0.010	0.2471(8)	0.4(2)	0.2500(10)	0.3(1)
0.020	0.3227(7)	0.3(2)	0.3261(9)	0.3(1)
0.030	0.3849(6)	0.4(2)	0.3884(9)	0.2(1)
0.040	0.4396(6)	0.4(2)	0.4429(8)	0.2(1)

TABLE VIII. Lattice values for the pseudoscalar decay constant calculated using the method described in Eq. (93).

m_x	$f_{xx}(m_l = 0.02)$	$f_{xx}(m_l = 0.03)$
0.001	0.0926(18)	...
0.005	0.0947(15)	0.0961(14)
0.010	0.0969(13)	0.0985(13)
0.020	0.1021(11)	0.1038(12)
0.030	0.1077(10)	0.1092(11)
0.040	0.1133(9)	0.1145(10)

2. *Results from the* $m_l = 0.02$ *and 0.03 ensembles*

For the two heavy ensembles with $m_l = 0.02$ and 0.03 we performed uncorrelated simultaneous fits to four correlators from the DEG data sets: $C_{AA}^{LB}(t)$, $C_{PP}^{LB}(t)$, $C_{AP}^{LB}(t)$, and $C_{AP}^{BB}(t)$. The time slices included in the fits are from $t = 10$ to 32 for each correlator. The pseudoscalar meson masses obtained this way are presented in Table VII. The corresponding amplitudes of these correlators can be used to determine the pseudoscalar meson decay constants by the following relation:

$$f_{xy} = Z_A \sqrt{\frac{2}{m_{xy}} \frac{\mathcal{N}_{AA}^{LB} \mathcal{N}_{AP}^{LB}}{\mathcal{N}_{AP}^{BB}}}, \tag{93}$$

the results of which are given in Table VIII.

V. RESULTS FOR THE OMEGA BARYON MASS

We have chosen to set the lattice scale using the Ω^- baryon mass because it is made of three strange valence quarks and so does not have nonanalytic light quark mass terms at NLO in chiral perturbation theory [43,44]. Thus, it is justified to linearly extrapolate in m_l to obtain the physical value of 1672.25(0.29) MeV [45].

The interpolating field for the decuplet baryons is

$$\chi_{\text{dec}} = \varepsilon_{abc}[q_a^T C \gamma_\mu q_b] q_c, \tag{94}$$

which couples to both spin 3/2 and 1/2 states, the former being the ground state [46]. For $q = s$, the strange quark, the operator destroys an Ω^- baryon.

The correlation function is constructed using the BL quark propagator described in Sec. IV computed from sources set at time slices 0 and 32 for every twentieth trajectory, starting from a thermalized one. Results are averaged over these sources and blocked in bins of size 80 trajectories to reduce autocorrelations. The total number of measurements made varies between about 100 and 200, depending on the light sea quark mass (see Table IX). To avail ourselves of all possible statistics, we average over forward propagating particle states, and backward propagating antiparticle states, as well as all three spatial directions for the interpolating operator.

The average correlation function is fit using a jackknife procedure where the covariance matrix is estimated for each jackknife block. The minimum time slice used in the fit was varied in the range $4 \leq t_{\text{min}} \leq 10$; the maximum was fixed to 14. Though the mass values do not depend sensitively on the choice of t_{min}, we chose to take as central values the masses obtained from $t_{\text{min}} = 8$ to minimize excited state contamination without losing control of the statistical error and because χ^2 is acceptable for this t_{min} value. The baryon mass values for valence quark masses $m_x = 0.03$ and 0.04 are summarized in Table IX and plotted in Fig. 9.

Also shown in the figure is a linear extrapolation, for each degenerate valence mass, to the physical value of the light sea quark mass (solid lines). The linear fit to the $m_x = 0.03$ data has a χ^2/dof of 1.2 and that of the $m_s = 0.04$

TABLE IX. Decuplet baryon masses for degenerate valence quarks. "Trajectories" refers to the Monte Carlo trajectories used for measurements. Numbers in parentheses give the total number of measurements, separated by 40 trajectories in each case. To reduce effects of autocorrelations, the measurements were block averaged into bins of size 80 trajectories before fitting.

m_l	m_x	Trajectories (no. meas.)	χ^2/dof	Mass
0.005	0.03	900-4460 (90), 920-4480 (90)	0.5(7)	0.9647(65)
0.005	0.04		0.6(8)	1.016(51)
0.01	0.03	1460-5020 (90), 1480-4040 (65)	1.1(1.1)	0.9809(88)
0.01	0.04		1.2(1.2)	1.033(60)
0.02	0.03	1600-3600 (50), 1900-3580 (43)	1.7(1.6)	1.030(11)
0.02	0.04		2.0(1.8)	1.074(10)
0.03	0.03	1020-3060 (52), 1320-3040 (44)	1.4(1.7)	1.040(10)
0.03	0.04		1.8(2.2)	1.082(6)

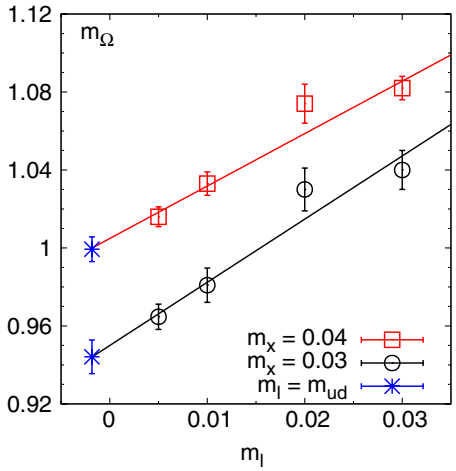

FIG. 9 (color online). Sea quark mass dependence of the decuplet baryon masses for degenerate valence quarks $m_x = 0.03$ (circles) and 0.04 (squares). Linear fits are shown by solid lines. Asterisks denote masses extrapolated to the physical value of the bare, light sea quark mass m_{ud}.

data has a χ^2/dof of 1.4. In the next section we use these values to interpolate to the physical strange quark mass in order to set the lattice scale using the Ω^- baryon mass.

A systematic error in the Ω^- mass, and hence in the lattice spacing, results from the fixed unphysical value of the strange sea quark mass in the simulation. This effect can be estimated from the slope of the baryon mass with respect to the light sea quark mass (see Fig. 9). The effect, which is similar for both valence quark masses, is about 2%–3% for a (required) shift in sea quark mass of about 0.008. Since this results from varying both light quarks together, it should be divided by two for the single strange quark in the simulation. This is about a 1% downward shift in the mass, which is smaller than the statistical errors, as shown in the next section, so we ignore it.

VI. LATTICE SCALE, QUARK MASSES, AND DECAY CONSTANTS USING SU(2) CHPT

A. SU(2) × SU(2) chiral fits

In this subsection we present a brief overview of the techniques we use to perform the chiral extrapolations for pseudoscalar masses and decay constants. For our simulations with 2 + 1 flavors of dynamical fermions, the traditional approach would be to use the SU(3) chiral perturbation theory to guide the extrapolations. However, as we shall see in Sec. VII A, NLO SU(3) ChPT does not describe our data for the pseudoscalar mesons which contain a quark as heavy as the strange quark. In order to extrapolate our results reliably to the physical quark masses (and, in particular, to the physical strange quark mass) we therefore use a different approach and impose only SU(2) chiral symmetry in the light quark sector, as has been discussed in Sec. II. We divide our discussion into two parts. In Sec. VI A 1 we discuss the chiral extrapolations in the pion sector and in Sec. VI A 2 we extend the discussion to kaons. We present physical results for the quark masses and pseudoscalar decay constants using the SU(2) chiral fits in Sec. VI B below.

1. The pion sector

In the pion sector, the chiral dynamics of $SU(2)_L \times SU(2)_R$ symmetry is sufficient to describe the physics we are interested in. The effects of the dynamical strange quark are fully contained in the low-energy constants of $SU(2)_L \times SU(2)_R$ ChPT [12]. There is a caveat. *A posteriori* we learn that the dynamical strange quark mass used in our simulations is a little larger than the physical one. Ideally, we would need to perform the simulations with several different dynamical strange quark masses and interpolate the results to the physical strange quark mass. In the absence of such simulations, the dynamical strange quark mass is fixed to $m_h = 0.04$, and we need to be aware that the corresponding LECs will have a corresponding small systematic error (see Sec. VI C 3).

The next-to-leading order partially quenched SU(2) formulas for the squared masses, m_{xy}^2, and decay constants, f_{xy}, of the light pseudoscalar mesons composed of two valence quarks with masses m_x and m_y can be derived from [47], as has been done, for instance, in [48]. For reference, we summarize these formulas in Appendix B 2. As discussed in Sec. II, for domain wall fermions the effective quark mass is the sum of the input quark parameters $m_{x,y,l,h}$ and the residual mass, which we denote as $\tilde{m}_{x,y,l,h} \equiv m_{x,y,l,h} + m_{\rm res}$ (here l and h denote the light and heavy sea quarks, respectively). To next-to-leading order, this is the only correction to the continuum chiral formulas. Since f_{xy} and m_{xy}^2 share two unknown low-energy constants B and f, we perform combined fits to both of them, using the two ensembles with dynamical light quark masses of $m_l = 0.005$ and 0.01. Such combined fits with valence quark masses m_x, $m_y = 0.001$, 0.005, and 0.01 [which therefore satisfy the cut $m_{\rm avg} \equiv (m_x + m_y)/2 \leq 0.01$] are shown in Fig. 10. The values of the fit parameters are given in Table X, where we quote the scale-dependent low-energy constants at two commonly used renormalization scales $\Lambda_\chi = 770$ MeV and 1.0 GeV. These partially quenched LECs [of SU(4|2) PQChPT] can be related to those in the physical unitary theory [SU(2)], l_3^r and l_4^r, by Eqs. (B35) and (B39). In Table X we also quote the values of $\bar{l}_3$ and $\bar{l}_4$, which are conventionally defined at the scale of the pion mass; see Eq. (B44).

Using partially quenched NLO SU(2) chiral perturbation theory we are able to describe the data with the mass cut $m_{\rm avg} \equiv (m_x + m_y)/2 \leq m_{\rm cut} = 0.01$. It is not possible, however, to extend the range of masses significantly. For example, the quality of the fit degrades significantly if instead we impose a mass cut of $m_{\rm avg} \leq 0.02$: the

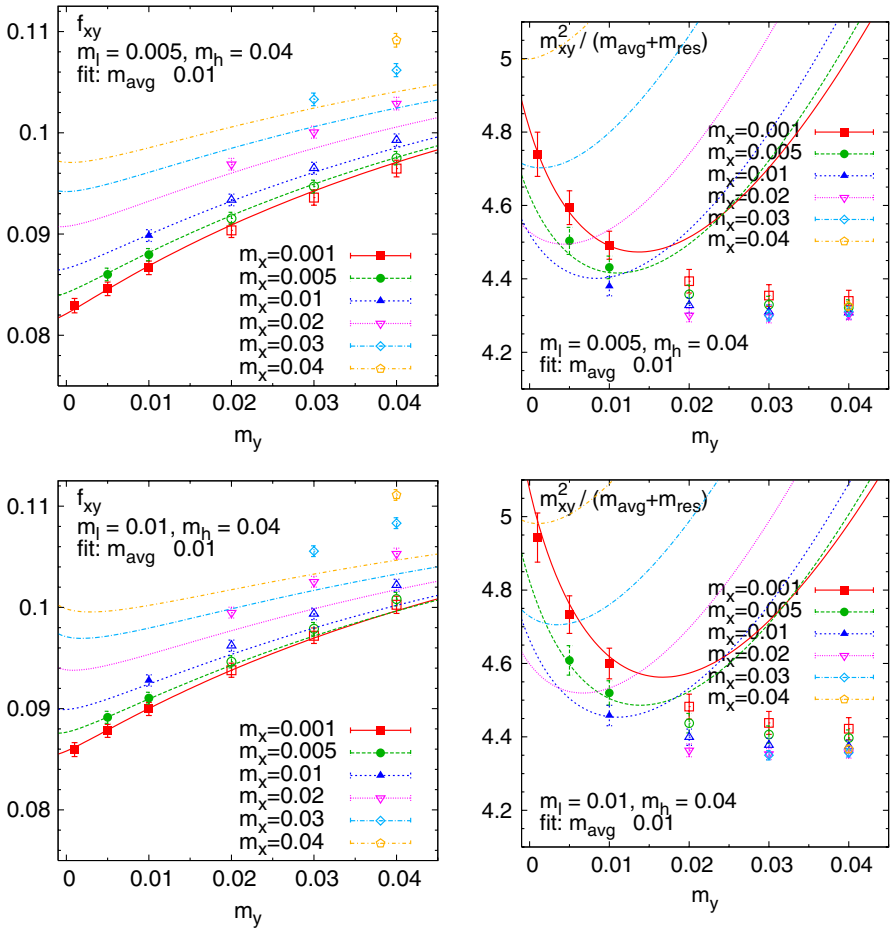

FIG. 10 (color online). Combined SU(2) × SU(2) fits for the meson decay constants (left panels) and masses (right panels) at two different values for the light sea quark mass, and with a cut on the valence masses $m_{\rm avg} \leq 0.01$. Points marked by filled symbols were included in the fit, while those with open symbols were excluded.

χ^2/dof increases from 0.3 ($m_{\rm cut} = 0.01$) to 1.2 ($m_{\rm cut} = 0.015$) and even 3.6 for $m_{\rm cut} = 0.02$. (We only report the uncorrelated χ^2/dof since we could not reliably determine the correlations, so these numbers most likely underestimate the "true" deviation from the fit.) This suggests that higher orders of chiral perturbation theory (NNLO or even more) are needed in this mass range. (See also the discussion in Sec. VI C 1 regarding the inclusion of analytic NNLO terms.)

TABLE X. Low-energy constants obtained from SU(2) × SU(2) fits with a valence mass cut $m_{\rm avg} \leq 0.01$. For convenience the LECs $L_i^{(2)}$ are quoted in units of 10^{-4} at two different chiral scales, $\Lambda_\chi = 770$ MeV and 1 GeV. The definitions of the low-energy constants are given in the appendixes. (Only statistical errors are quoted.)

B	f	$\bar{l}_3$	$\bar{l}_4$
2.414(61)	0.0665(21)	3.13(0.33)	4.43(0.14)

Λ_χ	$L_4^{(2)}$	$L_5^{(2)}$	$(2L_6^{(2)} - L_4^{(2)})$	$(2L_8^{(2)} - L_5^{(2)})$
770 MeV	3.3(1.3)	9.30(0.73)	0.32(0.62)	0.50(0.43)
1 GeV	1.3(1.3)	5.16(0.73)	−0.71(0.62)	4.64(0.43)

2. The kaon sector

In order to incorporate the valence strange quark mass in the chiral extrapolations, we need to extend the SU(2) ChPT to the kaon sector. As has been discussed in Sec. II, this can be done by considering the kaon as a heavy meson under the assumption that $\tilde{m}_l \ll \tilde{m}_s$, in analogy to the heavy-light meson (or heavy baryon) chiral perturbation theory [32,49]. In this framework the chiral expansions are ordered in powers of $\tilde{m}_l/\tilde{m}_h$ or equivalently m_π^2/m_K^2, as well as m_π^2/Λ_χ^2. We present the NLO chiral formulas for m_{xy}^2 and f_{xy}, the masses and decay constants of pseudoscalar mesons composed of a light valence quark with mass m_x and a heavy valence quark with mass m_y in Eqs. (66) and (67) (see also Appendix B 3 for the complete set of formulas at NLO).

For kaons a new set of low-energy constants $f^{(K)}$, $B^{(K)}$, and $\lambda_{1,2,3,4}$ are introduced. These LECs depend on the

valence and dynamical strange quark masses and we have made this explicit by assigning a functional dependence, writing for instance, $f^{(K)}(m_h)$. Here m_h represents both the masses of the heavy (strange) dynamical and valence quarks. The parameters B and f are the usual LECs in the (pionic) SU(2) theory, and their values are determined from the quantities in the pion sector; i.e., their values are fixed to the ones given in Table X.

The strange quark mass dependence in the formulas for the meson masses and decay constants, Eqs. (66) and (67), is contained in the low-energy constants. Since it is not possible to tune the dynamical heavy quark mass m_h perfectly to the mass m_s of the physical strange quark, in principle we would wish to perform the calculations at several values of m_h and interpolate the results to m_s. Since we only have results at a single value of m_h ($m_h = 0.04$), we rely as far as possible on using the behavior of our results with the valence strange quark masses, m_y, to extrapolate to the physical kaon.

Finally, we briefly summarize our fitting procedure. We start by fitting the mass dependence of m_{xy}^2 and f_{xy} using Eqs. (66) and (67) for $m_x \in [0.001, 0.01]$ and $m_y = 0.04$, with B and f fixed to the values in Table X. Since these two formulas do not have any unknown parameters in common, the fits can be done independently. We then extrapolate to the physical value of the light quark mass to obtain $m_K(m_y = 0.04)$ and $f_K(m_y = 0.04)$. (The physical light quark mass m_{ud} is determined from the SU(2) pion sector fits; see VI B 1 for a detailed description.) This step is shown in Fig. 11, where the circles give the extrapolated values $m_K(m_y = 0.04)$ (right) and $f_K(m_y = 0.04)$ (left). Then similar fits are performed with $m_y = 0.03$, giving values for $m_K(m_y = 0.03)$ and $f_K(m_y = 0.03)$. Eventually, we take the results at $m_y = 0.03$ and 0.04 and interpolate linearly between them. As discussed in Sec. VI B, we define the physical strange quark mass from the interpolation of m_{xy}^2 to the physical value of m_K^2. Having determined

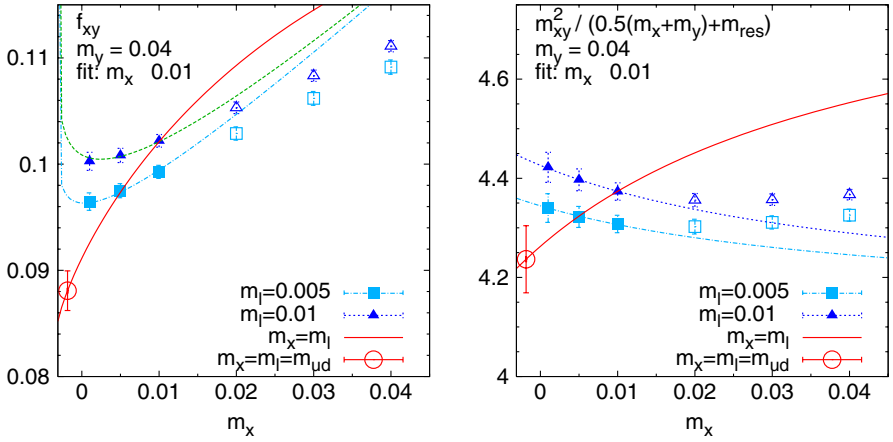

FIG. 11 (color online). SU(2) × SU(2) fits for the kaon sector. Left panel: Kaon decay constant. Right panel: Kaon mass squared for $m_y = 0.04$. Points with filled symbols were included in the fit, while those with open symbols were excluded.

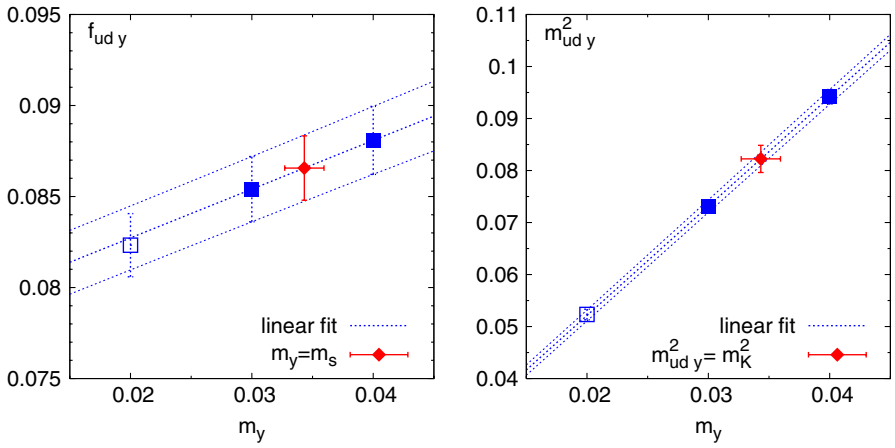

FIG. 12 (color online). Interpolation to the physical strange quark mass (diamond) for m_K^2 and f_K. Square symbols denote measured values and open symbols are not included in the interpolations. Left panel: Kaon decay constant. Right panel: Squared kaon mass.

the physical value of the strange quark mass, we extract the kaon decay constant from the interpolation of f_{xy} to this mass. The linear fits are shown in Fig. 12. In the same figure we also include the points obtained with $m_y = 0.02$. Although at such a low mass the use of SU(2) chiral perturbation theory is questionable, we see that nevertheless the points lie very close to the line obtained from the interpolation between $m_y = 0.04$ and $m_y = 0.03$, suggesting that the higher-order corrections of $O(\tilde{m}_l/\tilde{m}_h)^2$ may be small.

B. Lattice scale, physical quark masses, and decay constants

Having established the procedure for the chiral extrapolations, we now turn to obtaining the physical results. In this subsection we start by explaining how the lattice scale and physical bare quark masses were determined. We then use the renormalization constant for the quark masses which was determined nonperturbatively in [21] to obtain the physical quark masses in the $\overline{\text{MS}}$ scheme at $\mu = 2$ GeV. Finally we present the results for f_π, f_K, and the CKM matrix element $|V_{us}|$ determined from our measured ratio f_K/f_π together with experimental inputs.

1. Determination of m_{ud}, m_s, and a^{-1}

In order to determine the quark masses m_{ud}, m_s, and the lattice spacing a, we need to compare our lattice results for three quantities to their physical values. We take the pseudoscalar masses m_π and m_K as two of these. Natural choices for the third would be the ρ mass or the Sommer scale. However, since the ρ meson is a resonance with a finite width and there is an uncertainty of order 10% in the value of the Sommer scale, we choose instead to use the mass of the Ω baryon. This is a state composed of three valence strange quarks. One advantage of using this baryon mass is that up to NLO in χPT it is free of logarithms containing the light quark masses [43,44]. Therefore the extrapolation of the measured masses to the light physical mass can be readily performed using a linear ansatz without an uncertainty due to chiral logarithms.

The physical quark masses were obtained from the SU(2) $\times$ SU(2) fits described in Sec. VI A. For the average light quark mass, $m_{ud} \equiv (m_u + m_d)/2$, we solved for a pion mass of $m_\pi = 135.0$ MeV, corresponding to the physical neutral pion mass, while for the strange quark mass m_s the fit to the kaon mass was solved at $m_K = 495.7$ MeV, which is the quadratically averaged neutral and charged kaon mass.

The determination of the three parameters is a coupled problem. The lattice scale is needed to convert masses between lattice units and physical ones, whereas the quark masses are needed for the extrapolation and interpolation in the light and strange quark masses to obtain the mass of the Ω baryon. We performed the determination iteratively, starting with an initial ''guess'' for the quark masses, fixing the lattice spacing by requiring that m_Ω take its physical value, then using this value of a to adjust the quark masses by requiring that m_π and m_K take their physical values and so on until no further changes in the parameters were observed. The final values for $1/a$, a, m_{ud}, m_s can be found in Table XI, with only the statistical errors shown. (We will discuss the systematic errors in Sec. VI C.) We also find the quark mass ratio to be $\tilde{m}_{ud}$:$\tilde{m}_s = 1$:28.8(4).

An independent check of the lattice scale has been done from the spectrum of heavy-heavy and heavy-strange quark states using the nonperturbatively determined relativistic heavy quark action [50,51]. The preliminary analysis [52] gave $1/a = 1.749(14)$ GeV, where the error is statistical only. The agreement of this result with that obtained from the m_{Ω^-} shown in Table XI suggests that the associated systematic errors are small.

2. Quark masses in $\overline{\text{MS}}$ scheme

In this section we present the results for the quark masses in the $\overline{\text{MS}}$ renormalization scheme. The renormalization factor $Z_m = 1/Z_S$ (where S represents the scalar density) needed to convert the bare quark masses to the commonly used $\overline{\text{MS}}$ scheme at a scale of 2 GeV has been calculated with the same action on a $16^3 \times 32 \times 16$ lattice [21]. (For details about this ensemble of configurations, see [34].) We first matched the bare lattice operators to the regularization independent momentum (RI-MOM) scheme using the nonperturbative Rome-Southampton technique [53], and then performed a perturbative matching to the $\overline{\text{MS}}$ scheme. The relation between the renormalized and bare quark masses is given by

$$m_X^{\overline{\text{MS}}}(2\text{ GeV}) = Z_m^{\overline{\text{MS}}}(2\text{ GeV})a^{-1}(a\tilde{m}_X), \qquad (95)$$

where $X = ud$, s and for clarity we made explicit the factors of the lattice spacing a. In Ref. [21] it was found that $Z_m^{\overline{\text{MS}}}(2\text{ GeV}) = 1.656(48)(150)$, where the first error is statistical, while the second is the combined systematic uncertainty due to residual chiral symmetry breaking, the use of a three-loop matching factor between the RI-MOM and $\overline{\text{MS}}$ schemes and mass effects. With this renormalization constant, the results for the average light quark mass

TABLE XI. Lattice scale and unrenormalized quark masses in lattice units. Note $\tilde{m}_X \equiv m_X + m_{\text{res}}$. Only the statistical errors are given here.

a^{-1} [GeV]	a [fm]	m_{ud}	$\tilde{m}_{ud}$	m_s	$\tilde{m}_s$	$\tilde{m}_{ud}$:$\tilde{m}_s$
1.729(28)	0.1141(18)	−0.001847(58)	0.001300(58)	0.0343(16)	0.0375(16)	1:28.8(4)

and the strange quark mass are determined to be

$$m_{ud}^{\overline{\rm MS}}(2\ {\rm GeV}) = 3.72(16)(33)\ {\rm MeV}, \quad (96)$$

$$m_{s}^{\overline{\rm MS}}(2\ {\rm GeV}) = 107.3(4.4)(9.7)\ {\rm MeV}, \quad (97)$$

where the first error is the combined statistical error from the bare lattice quark masses, the lattice spacing, and $Z_m^{\overline{\rm MS}}$ and the second error is the systematic error in $Z_m^{\overline{\rm MS}}$.

Related to the renormalization of the quark masses is the renormalization of the lowest-order LEC B, which is proportional to the quark condensate and therefore is renormalized by $Z_S = 1/Z_m$, ensuring that the product of B and a quark mass does not depend on the renormalization scheme or scale. We have

$$B^{\overline{\rm MS}}(2\ {\rm GeV}) = (Z_m^{\overline{\rm MS}}(2\ {\rm GeV}))^{-1} \cdot (1/a) \cdot aB \quad (98)$$

$$= 2.52(11)(23)\ {\rm GeV}, \quad (99)$$

where the first error is statistical and the second is the systematic uncertainty from renormalization. The renormalized value for the chiral condensate, $\Sigma = f^2 B/2$, reads

$$\Sigma^{\overline{\rm MS}}(2\ {\rm GeV}) = (255(8)(8)\ {\rm MeV})^3. \quad (100)$$

3. f_π, f_K, and $|V_{us}|$

The chiral fits described in Sec. VI A also allow us to determine the decay constants f_π and f_K. Extrapolation to the physical light quark mass m_{ud} using the SU(2) × SU(2) fits in the pion sector gives $f_\pi = 124.1(3.6)$ MeV, while interpolation to the physical strange quark mass m_s, as described in Sec. VI A, gives $f_K = 149.6(3.6)$ MeV. In both cases only the statistical errors are given. Systematic errors will be discussed in Sec. VI C. These results can be compared to the physical values [54], $f_\pi = 130.7(0.1) \times (0.36)$ and $f_K = 159.8(1.4)(0.44)$ MeV. For the ratio of the decay constants we find $f_K/f_\pi = 1.205(18)$ compared to the experimental value of 1.223(12). See [55] for possible implications of an updated result for the measured value of the CKM matrix element V_{ud} [57].

An important application of the result for f_K/f_π is the determination of the CKM matrix element $|V_{us}|$, as has been pointed out in [58]. Using the experimentally determined branching ratios $\Gamma(K \to \mu\nu(\gamma))$ and $\Gamma(\pi \to \mu\nu(\gamma))$, together with the radiative electroweak corrections from [54], we obtain

$$|V_{us}|/|V_{ud}| = 0.2292(034)_{\rm stat}(118)_{\rm syst}(005)_{\rm other}, \quad (101)$$

where the first two errors are statistical and systematic (as discussed in Sec. VI C below), while the third error is the combined uncertainty from the measurement of the branching ratios and the radiative electroweak corrections [54]. Taking $|V_{ud}| = 0.973\,77(27)$ from superallowed nuclear β decays [54], we obtain

$$|V_{us}| = 0.2232(033)_{\rm stat}(115)_{\rm syst}(005)_{\rm other} \quad (102)$$

(the third error now also contains the uncertainty in $|V_{ud}|$). This implies

$$|V_{us}|^2 + |V_{ud}|^2 = 0.9980(15)_{\rm stat}(51)_{\rm syst}(06)_{\rm other} \equiv 0.9980(54)_{\rm total}. \quad (103)$$

Since $|V_{ub}|$ is negligible, our result implies that the unitarity relation is satisfied within the uncertainties, constraining the possible breaking of quark-lepton universality in models of new physics. For completeness we now present the corresponding results obtained using the recently published value $|V_{ud}| = 0.974\,18(26)$ [57] [instead of the PDG value of $|V_{ud}| = 0.973\,77(27)$ which was used in obtaining the results in Eqs. (102) and (103) above]:

$$|V_{us}| = 0.2232(033)_{\rm stat}(115)_{\rm syst}(005)_{\rm other}, \quad (104)$$

$$|V_{us}|^2 + |V_{ud}|^2 = 0.9989(15)_{\rm stat}(51)_{\rm syst}(06)_{\rm other} \equiv 0.9989(54)_{\rm total}. \quad (105)$$

We have also determined V_{us} (with a smaller error) from the experimentally measured rates of semileptonic K_{l3} decays by computing the form factor $f^+(q^2 = 0)$, where q is the momentum transfer. The results [in particular $|V_{us}| = 0.2249(14)$] and an outline of the calculation are presented in [18].

C. Systematic errors

In this section we will discuss the systematic errors resulting from various sources: (1) chiral extrapolations, (2) finite-volume effects, (3) the unphysical dynamical strange quark mass, and (4) scaling errors.

1. Errors arising from the chiral extrapolations

As explained above, we obtain our results by using NLO chiral perturbation theory to fit the measured values of the meson masses and decay constants in the range of valence quark masses satisfying $m_{\rm avg} \leq 0.01$ and with $m_l = 0.005$ and 0.01. We do not have enough data to extend the analysis fully to NNLO where the chiral logarithms depend on the Gasser-Leutwyler coefficients and there are too many parameters to make the fits meaningful. In order to estimate the effects of the (neglected) higher-order terms in the chiral expansion, we have therefore extended the range of quark masses to $m_{\rm avg} \leq 0.02$ but included only the analytic NNLO terms in the fit functions. In the pion sector, the analytic terms at NNLO are quadratic in the χ's and symmetric under $\chi_x \leftrightarrow \chi_y$; there are four such terms:

$$(\chi_x + \chi_y)^2, (\chi_x - \chi_y)^2, (\chi_x + \chi_y)\chi_l, \quad \text{and} \quad \chi_l^2. \quad (106)$$

We therefore have four new parameters for the behavior of the mass of the pseudoscalar mesons and four for the decay constants. Unfortunately, with only two values for the

dynamical sea quark mass (which is proportional to χ_l), we were not able to resolve the complete sea quark mass dependence up to NNLO in our fits. We therefore dropped the term proportional to χ_l^2 and were then able to obtain stable fits with a good χ^2/dof (about 0.1). We stress that the NNLO analytic terms are necessary in order to obtain good fits; NLO chiral perturbation theory does not represent our data in the extended range of masses $m_{\rm avg} \leq 0.02$. With the NNLO analytic terms included, not only do we obtain good fits to our data but the behavior of the chiral expansion is sensible; i.e., the relative importance of successive terms in the series is as expected. We illustrate this point in Fig. 13, where, in the top two graphs, we plot the size of LO, NLO, and NNLO contributions (normalized such that the LO contribution equals one) for the masses squared and decay constants of mesons with $m_x = m_y = m_l$ (i.e., for mesons in the unitary theory). Up to a quark mass of 0.01 (the 3rd vertical dashed line in the plots, counting from the left) the NLO contributions are much larger than the NNLO terms, which are negligible in this region. As expected, the NNLO corrections become more important for larger quark masses, and in particular, for masses close to 0.02 (rightmost vertical dashed line) they represent a significant fraction of the decay constant. This study is reassuring, but since we have neglected the chiral logarithms at NNLO terms, it is only a phenomenological estimate of the likely contributions from higher-order terms in the chiral expansion.

As our final estimate of the errors due to the chiral extrapolation we take *twice* the difference between the results from our standard NLO SU(2)-ChPT fit in the mass range $m_{\rm avg} \leq 0.01$ and those from including the analytic NNLO terms in the range $m_{\rm avg} \leq 0.02$. The factor of 2 was included, rather cautiously, because of the phenomenological nature of the NNLO analysis, and, in particular, because we were unable to study the sea quark mass dependence. The systematic error is reported in Table XII.

The systematic error due to the extrapolation in the mass of the light quark in the kaon quantities, m_s and f_K, was also estimated as twice the difference between our standard results and those obtained using kaon SU(2) PQChPT in the mass range $m_x \leq 0.02$ with the values of f and B obtained from the NNLO fit described above. The errors are also tabulated in Table XII. For this case we get a good description of our data up to $m_x = 0.02$ without the necessity of adding NNLO analytic terms (χ_x^2, χ_l^2, and $\chi_x\chi_l$). Therefore one expects those terms to have a negligible effect even in the mass range $m_x \leq 0.02$. The lower panels in Fig. 13 show the LO and NLO contributions, normalized so that the LO contribution equals one, to m_{lh}^2 and f_{lh}. The horizontal axis is χ_l, which is proportional to the total light sea quark mass. We see that the size of the NLO contributions is at most 35% for the range of masses where we have data.

2. Finite-volume effects

In this section we estimate the errors due to the fact that the simulations are performed on a finite volume, $(aL)^3 \approx (2.74\ \text{fm})^3$. We do this by following the procedure proposed by Gasser and Leutwyler [59–61] in which one compares results obtained in ChPT using meson propagators in finite volume, $G^{(L)}(x)$, to those obtained with the

TABLE XII. Central value and statistical error (stat) for the fit parameters from SU(2) ChPT and systematic error estimates from four sources. These are finite-volume effects (FV), lattice artefacts (a^2), the chiral extrapolation in the light quark masses (ChPT), and the unphysical value of the dynamical strange quark mass (m_s). For details we refer to Sec. VI C. The LECs are quoted here only at a scale $\Lambda_\chi = 1$ GeV, but the absolute value of the error is independent of Λ_χ. The total systematic error is obtained by adding the separate errors in quadrature, neglecting any possible correlations between them.

			Systematic errors				
	Value	Stat	FV	a^2	ChPT	m_s	Total
B	2.414	(0.061)	(0.049)	(0.097)	(0.034)	(0.017)	(0.115)
f	0.0665	(21)	(13)	(27)	(36)	(01)	(47)
$(2L_6^{(2)} - L_4^{(2)}) \cdot 10^4$	−0.7	(0.6)	(0.1)	$(\cdots)$	(1.8)	$(\cdots)$	(1.8)
$(2L_8^{(2)} - L_5^{(2)}) \cdot 10^4$	4.64	(0.43)	(0.95)	$(\cdots)$	(3.20)	$(\cdots)$	(3.34)
$L_4^{(2)} \cdot 10^4$	1.3	(1.3)	(0.3)	$(\cdots)$	(1.8)	$(\cdots)$	(1.8)
$L_5^{(2)} \cdot 10^4$	5.16	(0.73)	(0.16)	$(\cdots)$	(8.20)	$(\cdots)$	(8.20)
$\bar{l}_3$	3.13	(0.33)	(0.20)	(0.08)	(0.10)	(0.02)	(0.24)
$\bar{l}_4$	4.43	(0.14)	(0.05)	(0.08)	(0.76)	(0.04)	(0.77)
$\tilde{m}_{ud}$	0.001 300	(58)	(23)	(52)	(22)	(09)	(62)
$\tilde{m}_s$	0.0375	(16)	(00)	(15)	(04)	(08)	(17)
$\tilde{m}_{ud}$:$\tilde{m}_s$	1:28.8	(0.4)	(0.5)	(1.2)	(0.6)	(0.6)	(1.6)
f_π [MeV]	124.1	(3.6)	(1.9)	(5.0)	(4.4)	(0.2)	(6.9)
f_K [MeV]	149.6	(3.6)	(0.4)	(6.0)	(1.0)	(1.5)	(6.3)
f_K/f_π	1.205	(18)	(14)	(48)	(34)	(12)	(62)

infinite-volume propagators, $G(x)$. The finite-volume and infinite-volume propagators are related by

$$G^{(L)}(x) = G(x) + \sum_{\vec{n}\neq 0} G(x + L\vec{n}), \tag{107}$$

with the 3-vector $\vec{n} \in \mathbb{Z}^3$. This allows one to calculate the corrections in the PQChPT formulas for the meson masses and decay constants directly. We list the expressions in Appendix C, where details of the numerical implementation can also be found. (See also Refs. [62–64] for the analogous discussion with staggered PQChPT.) We now repeat the chiral fits using PQChPT with the finite-volume propagators and obtain a new set of fit parameters. For each physical quantity, we assign the difference between the results obtained using the finite-volume and infinite-volume formulas as the systematic error and tabulate these finite-volume errors in Table XII for both the pion and the kaon sectors. In the latter case we find that the finite-volume corrections in m_s and f_K are actually negligible. In Fig. 14 we plot the correction factor for the decay constants and squared masses, $(1 - \Delta_{xy}^{Lf})$ and $(1 - \Delta_{xy}^{Lm^2})$ (cf. App. C for their definition), respectively, for our two values of the dynamical light quark mass ($m_l = 0.01$ and 0.005). Since the volume is reasonably large, these corrections are found to be below 1%, except for the very light valence masses.

We now compare our results for the finite-volume corrections obtained using ChPT (as described above) to the theoretical predictions by Colangelo, Dürr, and Haefeli [65], who use a resummed Lüscher formula. The results in Ref. [65] are presented for the unitary theory ($m_x = m_y = m_l$ in our notation) and so we restrict the comparison to this case. We take the results in Tables 3 and 4 of [65] which we interpolate to the volume and pion masses used in our simulation. In Table XIII we present the finite-volume corrections for the pion mass and decay constant estimated using 3 methods, SU(2) and SU(3) ChPT and that of Ref. [65]. The quantities R_m and R_f are defined by

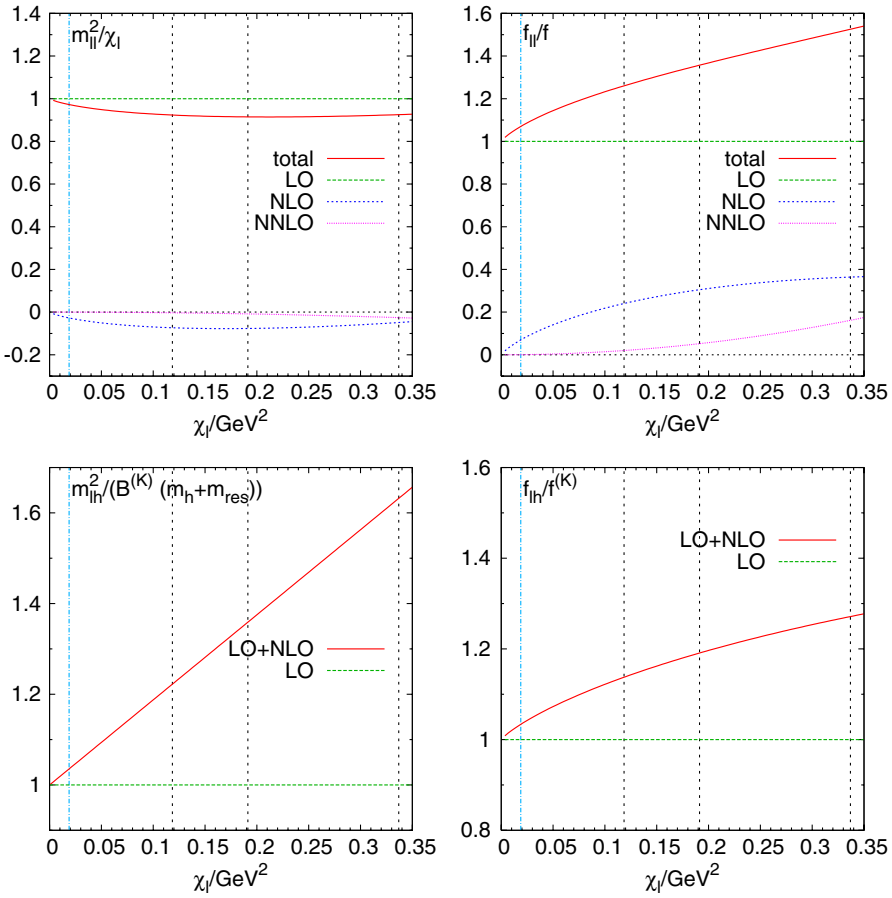

FIG. 13 (color online). Comparison of the size of the LO, NLO, and NNLO contributions in the SU(2) × SU(2) fits for unitary degenerate meson masses squared m_{ll}^2 (upper left panel) and decay constants f_{ll} (upper right panel) as a function of the light sea quark mass parameter χ_l (for details see Sec. VI C 1). The LO contribution is normalized to one. Vertical dashed lines indicate quark masses of $m_l = m_{ud}$, 0.005, 0.01, and 0.02 (from left to right). The lower panels give a comparison of the size of the LO and NLO contributions in kaon ChPT for the kaon mass squared m_{lh}^2 (lower left panel) and kaon decay constant f_{lh} (lower right panel) as a function of the light sea quark mass.

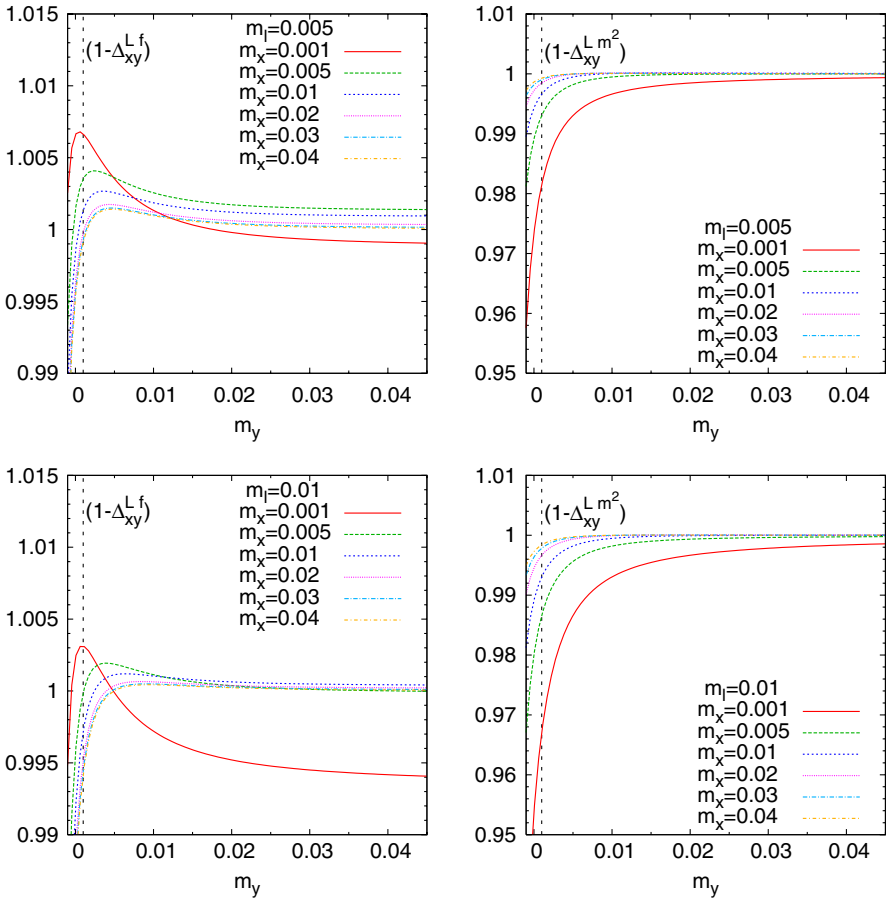

FIG. 14 (color online). Finite-volume correction factor obtained from the SU(2) fits for the decay constants (left panels) and squared meson masses (right panels) at sea quark masses $m_l = 0.005$ (top panels) and 0.01 (bottom panels). The vertical dashed line denotes the lightest (valence) mass used in this analysis ($m_y = 0.001$).

$$R_m = \frac{m_{ll}(L) - m_{ll}(\infty)}{m_{ll}(\infty)} = \frac{1}{2}\Delta_{ll}^{Lm^2},$$
$$R_f = \frac{f_{ll}(L) - f_{ll}(\infty)}{f_{ll}(\infty)} = \Delta_{ll}^{Lf}. \tag{108}$$

Within the uncertainties, we see a reasonable agreement between the estimates obtained with the different methods.

In an earlier publication [34], we presented results for the masses and decay constants obtained with the same action and coupling as in this paper, but on a smaller volume, about $(1.83\ \text{fm})^3$ compared to $(2.74\ \text{fm})^3$ used here. (In [34] a different method was used to extract the lattice scale. Since the gauge action and coupling are identical, for consistency we quote here the volume obtained with the value for a^{-1} used throughout this work.)

Specifically the lattice in [34] has 16 points in each spatial direction as compared to 24 in this paper. We are therefore able to compare the theoretical estimates of the finite-volume corrections described above, with the difference of our results on the two lattices with different volumes. We compare the measured pion mass and decay constant at the common unitary point at $m_x = m_y = m_l = 0.01$, $m_h = 0.04$ for which the pion mass is ≈ 427 MeV (this is the smallest mass for which we have results on both

TABLE XIII. Finite-volume correction factors obtained from the SU(2) and SU(3) PQChPT fits compared to the prediction by Colangelo, Dürr, and Haefeli (CDH) [65] at the unitary pion masses of 331 MeV ($m_x = m_y = m_l = 0.005$) and 419 MeV ($m_x = m_y = m_l = 0.01$).

	R_m [%]			$-R_f$ [%]		
m_π [MeV]	SU(2)	SU(3)	CDH	SU(2)	SU(3)	CDH
331	0.09(0.01)	0.14(0.04)	0.13(0.04)	0.36(0.03)	0.56(0.16)	0.32(0.00)
419	0.03(0.00)	0.04(0.01)	0.04(0.01)	0.10(0.01)	0.17(0.05)	0.09(0.00)

TABLE XIV. The measured pion mass and decay constant at $m_x = m_y = m_l = 0.01$, $m_h = 0.04$ at two different volumes (for 16^3 data see [34]). We compare directly the measured ratio to the predictions from SU(2) and SU(3) ChPT and the value interpolated from Colangelo, Dürr, and Haefeli (CDH) [65]. For explanation see Eq. (109) and text.

	Measured			$\frac{1-R^{(16c)}}{1-R^{(24c)}}$		
	24^3	16^3	Ratio	SU(2)	SU(3)	CDH
m_π	0.242 11(75)	0.247(3)	0.980(12)	0.9961(4)	0.9944(15)	0.9942(22)
f_π	0.0928(6)	0.0895(7)	1.037(11)	1.0155(14)	1.0252(70)	1.0118(3)

lattices). On the smaller volume, both finite-volume corrected fits [SU(2) and SU(3)] give results for the correction factors comparable to those interpolated from Colangelo, Dürr, and Haefeli. To obtain these correction factors, we used the parameters obtained from the fits to the 24^3 data and evaluated the finite-volume corrections for $L = 16$ (instead of the original $L = 24$). The SU(2) fits resulted in $R_m^{(16c)} = 0.42(04)\%$ and $R_f^{(16c)} = 1.66(14)\%$, where the superscript is meant to indicate that this is the finite-volume correction for a spatial volume of $L^3 = 16^3$. In Table XIV we list the measured values of the meson masses and decay constants on the 24^3 and 16^3 lattices and compare their ratios to the prediction from finite-volume ChPT and the resummed Lüscher formula (interpolated from [65]). We obtain this prediction from the ratio of the finite-volume correction factor for the 16^3 spatial volume and that for the 24^3 spatial volume,

$$\frac{m_\pi^{(16c)}}{m_\pi^{(24c)}} \stackrel{?}{=} \frac{1 - R_m^{(16c)}}{1 - R_m^{(24c)}}, \qquad \frac{f_\pi^{(16c)}}{f_\pi^{(24c)}} \stackrel{?}{=} \frac{1 - R_f^{(16c)}}{1 - R_f^{(24c)}}. \tag{109}$$

The superscripts in Eq. (119) indicate the spatial volumes on which the results for m_π and f_π were obtained or for which the finite-volume corrections R_m and R_f were evaluated. The question mark reminds us that we are checking whether the measured values of the ratios are equal to the theoretical predictions for the finite-volume effects. Whereas (within the errors) the observed $(2.0 \pm 1.2)\%$ effect for the pion mass is somewhat better reproduced by the finite-volume ChPT predictions than the $(3.7 \pm 1.1)\%$ for the decay constant, in both cases all three methods tend to underestimate the observed finite-volume effects. We make the following two comments. First, the precision of finte-volume ChPT at NLO and the resummed Lüscher predictions for the finite-volume corrections are expected to improve with increasing volume. A possible reason for underestimating the difference between the results from the 16^3 and 24^3 lattices may be that the smaller volume is already borderline for the methods used here. Whereas the values for $m_\pi L$ would appear to be sufficient in both cases, on the 16^3 lattice $m_\pi L \approx 4.0$ compared to ≈ 5.8 on the 24^3 lattice, it may be that the smaller lattice does satisfy the relation $L \gg (\sqrt{2} f_\pi)^{-1} \sim 1$ fm sufficiently. The second comment is that, as has already been pointed out in Sec. IV, the errors on the measured quantities on the smaller volume in general, and on the decay constants, in particular, may be underestimated due to shorter plateaus. Furthermore, in this present paper we have obtained the decay constants using an improved ansatz (see also Sec. IV). For these reasons, we believe that the finite-volume effects on the larger lattice are well described by our approach and give a reliable estimate for the systematic error.

3. Effects of the unphysical dynamical strange quark mass

In this subsection we estimate the systematic error due to the fact that the mass of the dynamical heavy quark (m_h) turns out, *a posteriori*, to be about 15% larger than that of the physical strange quark (m_s). To perform this estimate we exploit the fact that the LECs of SU(3) ChPT are independent of the quark masses, and use the NLO conversion formulas relating SU(3) and SU(2) LECs [13] given in Eqs. (B40)–(B43), together with the results for the SU(3) LECs presented in Sec. VII A. In this way we obtain the shifts in the SU(2) LECs:

$$B(m_s) - B(m_h) = B_0 \left\{ \frac{16}{f_0^2} (2L_6^{(3)} - L_4^{(3)})(\chi_s - \chi_h) - \frac{1}{72\pi^2 f_0^2} \left(\chi_s \log \frac{2\chi_s}{3\Lambda_\chi^2} - \chi_h \log \frac{2\chi_h}{3\Lambda_\chi^2} \right) \right\}, \tag{110}$$

$$f(m_s) - f(m_h) = f_0 \left\{ \frac{8}{f_0^2} L_4^{(3)} (\chi_s - \chi_h) - \frac{1}{32\pi^2 f_0^2} \times \left(\chi_s \log \frac{\chi_s}{2\Lambda_\chi^2} - \chi_h \log \frac{\chi_h}{2\Lambda_\chi^2} \right) \right\}, \tag{111}$$

$$l_3^r(m_s) - l_3^r(m_h) = \frac{1}{576\pi^2} \log \frac{\chi_h}{\chi_s}, \tag{112}$$

$$l_4^r(m_s) - l_4^r(m_h) = \frac{1}{64\pi^2} \log \frac{\chi_h}{\chi_s}. \tag{113}$$

(Note: here one has to use B_0 to determine χ_X.) We use the shifted values of the SU(2) LECs to determine m_{ud} and f_π and again use the shift in those two quantities as the estimate of the corresponding systematic uncertainties. All these uncertainties are presented in Table XII and are small compared to the total errors. (We did not quantify the systematic error on the separate $L_i^{(2)}$, just on the $\bar{l}_{3,4}$ since these are the phenomenologically relevant observables.)

For the kaon sector the shift due to changing the dynamical heavy quark mass to its physical value can be obtained from Eqs. (B49)–(B54). We perform the conversion for fixed m_y at $m_y = 0.03$ and 0.04 separately and then in the same way as before linearly interpolate the heavy valence quark mass m_y to m_s to determine the shift in the kaon mass and the kaon decay constant. A shifted value for the physical strange quark mass is obtained by solving the following system. Find a value of m_s such that the interpolation in m_y to $m_y = m_s$ for $m_{udy}^2(m_s, m_y)$ gives the squared physical kaon mass. Here $m_{udy}^2(m_s, m_y)$ was obtained from the unitary extrapolation in the light quark mass to m_{ud} using shifted LECs. The shifted LECs are found by starting from their values at the dynamical heavy quark mass used in the simulation and changing to their values at the new value of m_s (at fixed m_y). By this method, we observe a 2% shift in $\tilde{m}_s$ and less than 0.5% shift in f_K. Therefore, conservatively we will quote the systematic error from $m_h \neq m_s$ to be 2% and 1% for $\tilde{m}_s$ and f_K, respectively.

4. Scaling errors

At present we only have data at a single value for the lattice spacing ($a = 0.11$ fm) and so cannot perform a scaling study to extrapolate our results to the continuum limit. (We are currently generating an ensemble of configurations on a finer lattice and so will soon be able to study the discretization errors directly.) We therefore take our central values and assign to them a systematic uncertainty of 4% due to the missing continuum extrapolation. The 4% is simply an estimate of $(a\Lambda_{\rm QCD})^2$ with our value of $a^{-1} = 1.73$ GeV, but we stress that it is only when we will have results at more than one value of the lattice spacing that we will be able to quantify this error reliably.

Table XII contains the 4% estimate for scaling error for the measured quantities. Again, we did not calculate this uncertainty for the (phenomenologically uninteresting) LECs $L_i^{(2)}$, but only for $\bar{l}_{3,4}$. Here one has to keep in mind that a relative error affects the universal low-energy scales

$$\Lambda_{3,4} = \Lambda_\chi \cdot \exp\left(\frac{16\pi^2}{\gamma_{3,4}} l^r_{3,4}\right) = (139\ \text{MeV}) \cdot \exp(\bar{l}_{3,4}/2), \tag{114}$$

meaning that a 4% uncertainty translates into an *absolute* error of 0.08 for $\bar{l}_{3,4}$.

D. Comparison of our results with other recent determinations

In this subsection we compare our results for the SU(2) LECs to those obtained in the continuum [66,67] and in other lattice simulations with either $N_f = 2 + 1$ [68,69] or $N_f = 2$ [70,71] dynamical fermions. We also compare the values we obtain for the quark masses with those from other recent simulations [69,72–76].

Our value for the decay constant in the SU(2) chiral limit, $f = 114.8(4.1)_{\rm stat}(8.1)_{\rm syst}$ MeV, is consistent, within our uncertainties, with the phenomenological estimates of 122.3(0.5) [66] or 121.9(0.7) [77]. For the ratio f_π/f we obtain 1.080(8) (with only the statistical error quoted, since the numerator and denominator are likely to be highly correlated), which agrees very well with the phenomenological results 1.069(4) [66] and 1.072(7) [77]. Previous lattice simulations give, e.g., $1.052(2)(^{+6}_{-3})$ [69] or 1.075 [71] for the ratio and for f the results read $f = 124.2$ MeV [69] and 121.6 MeV [71], respectively, where in Ref. [71] no estimate of the error was provided.

From MILC's results for f and the chiral condensate, $(\Sigma^{\overline{\rm MS}}(2\ \text{GeV}))^{1/3} = 278(1)_{\rm stat}(5)_{\rm ren}(^{+2}_{-3})_{\rm syst}$ MeV [69] [compare to $255(8)_{\rm stat}(8)_{\rm ren}(13)_{\rm syst}$ MeV obtained in this paper], one can via $\Sigma = f^2B/2$ deduce its result for the LO-LEC $B^{\overline{\rm MS}}(2\ \text{GeV}) = 2.79$ GeV (no estimate for the error). Comparing this number with our value of $2.52(0.11)_{\rm stat}(0.23)_{\rm ren}(0.12)_{\rm syst}$ GeV shows approximately the same relative deviation as for the decay constant in the chiral limit, f.

In Table XV we compare the values for the NLO LECs $\bar{l}_{3,4}$ [we also include the values obtained by converting the SU(3) LECs, see Sec. VII C]. Within the quoted uncertainties all these numbers agree, except the result for $\bar{l}_3$ as quoted in [78], which used the MILC SU(3) LECs as input obtained from a ''NLO plus analytic NNLO and beyond'' fit. A recent update of the MILC results finds a more consistent value for $\bar{l}_3$ obtained from a pure NLO fit. The two results in the table for $\bar{l}_4$ from the CERN Collaboration, where one was obtained by including NNLO analytic terms, not only agree with our result for the central value, but also suggest a comparable magnitude for the systematic error (as estimated from the difference between the NLO and partial NNLO fits).

Quark masses are computed in lattice simulations using a variety of actions. We end this section by making the observation that results obtained using nonperturbative renormalization (such as those in this paper) appear to be generally higher than those obtained by renormalizing the mass perturbatively (mostly using two-loops). Whether or not this is significant or merely a coincidence is still to be investigated. We illustrate this point by tabulating recent results obtained using nonperturbative renormalization [72–74] and perturbative renormalization [69,75,76] in Table XVI. Note that for the simulations in this table,

TABLE XV. Comparison of the SU(2) NLO LEC $\bar{l}_3$ and $\bar{l}_4$ [defined at a scale of 139 MeV, cf. Eq. (B44)] with results from other $N_f = 2 + 1$ and $N_f = 2$ lattice simulations [69–71] and a phenomenological estimate [67]. (Here TM-Wilson means twisted mass Wilson fermions.)

	N_f	Type	$\bar{l}_3$	$\bar{l}_4$
This work, direct SU(2) fit	2 + 1	DWF	3.13(0.33)(0.24)	4.43(0.14)(0.77)
This work, converted from SU(3)	2 + 1	DWF	2.87(0.28)(···)	4.10(0.05)(···)
MILC[a]	2 + 1	Stag.	2.85(0.07)(···)	···
MILC[b]	2 + 1	Stag.	0.6(1.2)	3.9(0.5)
ETMC [71]	2	TM-Wilson	3.44(0.08)(0.35)	4.61(0.04)(0.11)
CERN [70]	2	Impr. Wilson	3.0(0.5)(0.1)	4.1(0.1)(···)
				3.3(0.8)(···)[c]
Phenomenological estimate[67]			2.9(2.4)	4.4(0.2)

[a]Direct SU(2) fit, from [69].
[b]Converted from SU(3). See [78].
[c]First number obtained without additional NNLO term, second number from fit including NNLO term. See [70] for details.

TABLE XVI. Comparison of light physical quark masses and their ratio obtained from recent lattice simulations using various types of fermion discretizations and different renormalization techniques (nonperturbative and perturbative). (In the cases where no error is given for the quark mass ratio, no error was quoted in the cited work. Since we do not know the correlations, we could not provide the error estimate here.) (Here TM-Wilson means twisted mass Wilson fermions.)

	N_f	Type	$m_{ud}^{\overline{\rm MS}}(2\ {\rm GeV})$ [MeV]	$m_s^{\overline{\rm MS}}(2\ {\rm GeV})$ [MeV]	$m_s{:}m_{ud}$
Using nonperturbative renormalization					
This work	2 + 1	DWF	$3.72(0.16)_{\rm stat}(0.33)_{\rm ren}(0.18)_{\rm syst}$	$107.3(4.4)_{\rm stat}(9.7)_{\rm ren}(4.9)_{\rm syst}$	$28.8(0.4)_{\rm stat}(1.6)_{\rm syst}$
RBC [72]	2	DWF	$4.25(0.23)_{\rm stat}(0.26)_{\rm ren}$	$119.5(5.6)_{\rm stat}(7.4)_{\rm ren}$	$28.10(0.38)_{\rm stat}$
ETMC [73]	2	TM-Wilson	$3.85(0.12)_{\rm stat}(0.40)_{\rm syst}$	$105(3)_{\rm stat}(9)_{\rm syst}$	$27.3(0.3)_{\rm stat}(1.2)_{\rm syst}$
QCDSF [74]	2	Impr. Wilson	$4.08(0.23)_{\rm stat}(0.19)_{\rm syst}(0.23)_{\rm scale}$	$111(6)_{\rm stat}(4)_{\rm syst}(6)_{\rm scale}$	27.2(3.2)
Using perturbative renormalization					
MILC [69]	2 + 1	Stag.	$3.2(0)_{\rm stat}(0.1)_{\rm ren}(0.2)_{\rm EM}(0)_{\rm cont}$	$88(0)_{\rm stat}(3)_{\rm ren}(4)_{\rm EM}(0)_{\rm cont}$	$27.2(0.1)_{\rm stat}(0.3)_{\rm syst}$
PACS-CS [75]	2 + 1	Impr. Wilson	2.3(1.1)	69.1(2.5)	30(?)
JLQCD [76]	2 + 1	Impr. Wilson	$3.54(^{+.64}_{-.35})_{\rm total}$	$91.1(^{+14.6}_{-6.2})_{\rm total}$	25.7(?)

both different fermion actions and different numbers of dynamical fermions were used. The ratios m_s/m_{ud} are also tabulated and agree better across the different computations.

VII. FITTING MASSES AND DECAY CONSTANTS TO NLO SU(3) CHPT

In the previous section, we have fit our lattice data to NLO SU(2) ChPT formulas and found good agreement. Additionally, for quark masses where we have data, we find that for m_{ll}^2, the NLO terms are at most a 10% correction, while for f_{ll} they are less than 30%, as shown in Fig. 13. Our estimates for NNLO effects in this range are appropriately small, $<5\%$, leading to the conclusion that SU(2) ChPT converges reasonably well here. This implies that our range of light quark masses is small enough that NLO SU(2) ChPT provides more than just a useful, smooth phenomenological function to fit our data to; rather it represents the theoretically correct description of our data.

We now turn to fitting our data to SU(3) ChPT, with the following two points in mind: (1) we want to determine how well our data is fit by the NLO SU(3) ChPT formulas, and (2) if the fits agree with our data, how convincing is the convergence of the (now known) SU(3) ChPT series for the quark masses where we have data. We will see that the answer to the first point is *yes*, if we only include observables involving light quarks, and is *no* for observables including the strange quark. For the second point, even in the light quark case, we find the convergence of the series to be poor.

A. SU(3) × SU(3) chiral fits

At NLO, the 2 + 1 flavor, partially quenched chiral formulas [47] for the squared masses, m_{xy}^2, and decay constants, f_{xy}, of the light pseudoscalar mesons composed of two nondegenerate quarks with masses m_x and m_y involve six unknown LECs, which we denote as B_0, f_0, and $L_{4,5,6,8}^{(3)}$. (The complete formulas used in our chiral fits are summarized in Appendix B 1.) As f_{xy} and m_{xy}^2 share the unknown low-energy constants B_0 and f_0, we performed combined fits to both of them, using the two ensembles with dynamical light quark masses of $m_l = 0.005$ and 0.01.

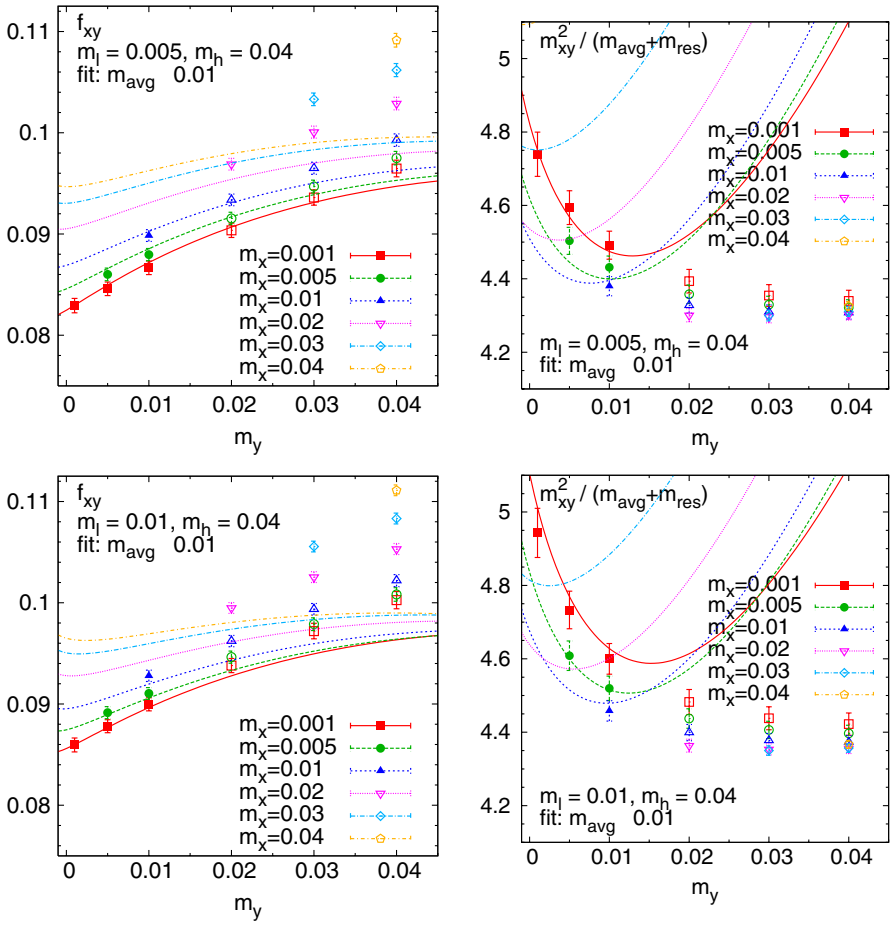

FIG. 15 (color online). Combined SU(3) × SU(3) fits for the meson decay constants (left panels) and masses (right panels) at two different values for the light sea quark mass, with valence mass cut $m_{\text{avg}} \leq 0.01$. Points marked by filled symbols were included in the fit, while those with open symbols were excluded.

A reasonable χ^2/dof of 0.7 (uncorrelated) could only be achieved by imposing a cut in the average valence quark mass of $m_{\text{avg}} \equiv (m_x + m_y)/2 \leq 0.01$, corresponding to partially quenched pion masses in the range of about 250 MeV to 420 MeV. The chiral fits with such a cut are shown in Fig. 15, and the fit parameters are given in Table XVII, where, for convenience, we quote the scale-dependent LECs at two commonly used chiral scales of $\Lambda_\chi = 770$ MeV and 1 GeV. Only statistical errors are quoted in this table, as discussed in more detail below. In these fits, the valence quark masses are all in a region where NLO SU(3) ChPT might be expected to be reasonably reliable (corresponding to masses below 420 MeV for pseudoscalar mesons made of such valence quarks), but we point out that the dynamical heavy quark mass, which is approximately 15% higher than the physical strange quark mass, lies outside of our fit region ($m_{\text{avg}} \leq 0.01$). Even the combination of our lightest valence quark mass of 0.001 with the dynamical heavy quark mass leads to a pseudoscalar mass of ≈ 554 MeV.

Extending the fit range to valence quarks satisfying $m_{\text{avg}} \equiv (m_x + m_y)/2 \leq 0.03$, or a partially quenched va-

TABLE XVII. Fitted parameters from SU(3) × SU(3) fits with a valence mass cut $m_{\text{avg}} \leq 0.01$. For convenience the LECs $L_i^{(3)}$ are quoted in units of 10^{-4} at two different chiral scales, $\Lambda_\chi = 770$ MeV and 1 GeV. The definitions of the low-energy constants are given in the appendixes. (Only statistical errors are quoted here.)

	$B_0 = 2.35(0.16)$		$f_0 = 0.0541(40)$	
Λ_χ	$L_4^{(3)}$	$L_5^{(3)}$	$(2L_6^{(3)} - L_4^{(3)})$	$(2L_8^{(3)} - L_5^{(3)})$
770 MeV	1.39(0.80)	8.72(0.99)	−0.01(0.42)	2.43(0.45)
1 GeV	−0.67(0.80)	2.51(0.99)	−0.47(0.42)	5.19(0.45)

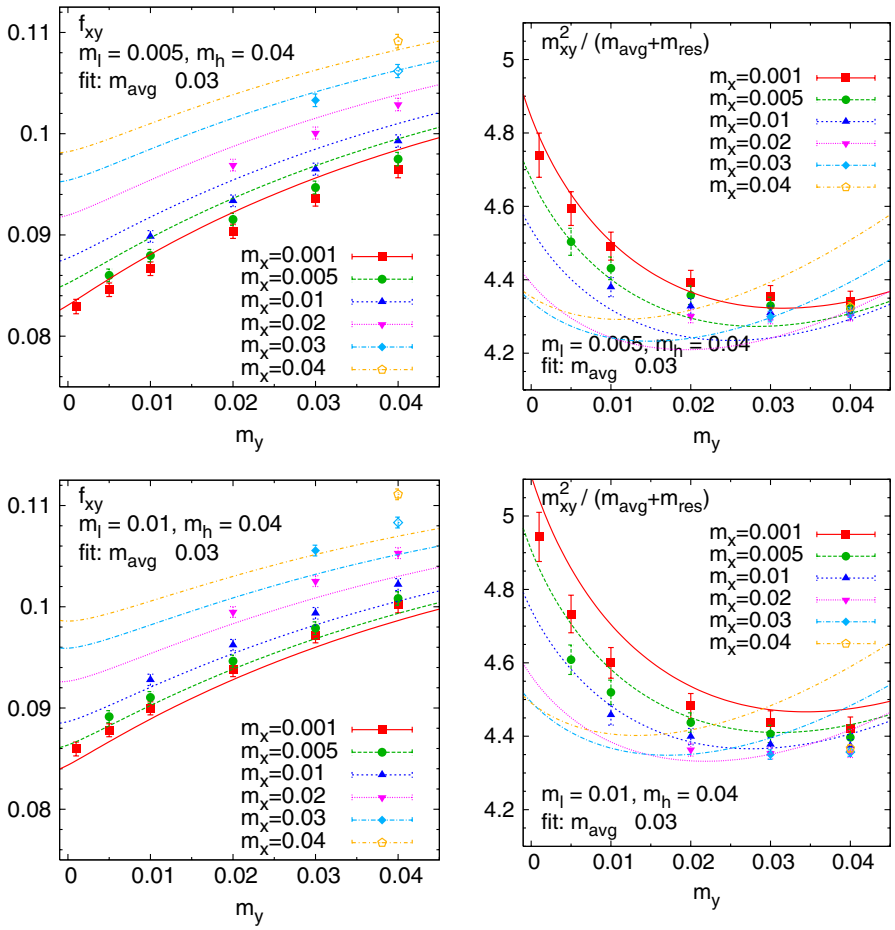

FIG. 16 (color online). Combined SU(3) × SU(3) fits for the meson decay constants (left panels) and masses (right panels) at two different values for the light sea quark mass, with valence mass cut $m_{\text{avg}} \leq 0.03$. Points marked by filled symbols were included in the fit, while those with open symbols were excluded.

lence pseudoscalar mass of up to 660 MeV, we find that the fit curves miss almost all of the data points, resulting in a poor χ^2/dof of 5.7. This is shown in Fig. 16. Similar behavior is seen for a lower mass cut of $m_{\text{avg}} \equiv (m_x + m_y)/2 \leq 0.02$, which allows the largest valence pseudoscalar masses to be just above the kaon mass, and gives an uncorrelated χ^2/dof of about 3. From these fits, we conclude that we cannot use SU(3) ChPT at NLO to obtain physical results for kaon observables, such as f_K or the physical strange quark mass from m_K, with well-controlled interpolation or extrapolation errors. For these important quantities, we have used kaon SU(2) ChPT as described in previous sections.

B. Systematic errors

For the SU(3) PQChPT results, we have to consider the same sources of systematic uncertainties (chiral extrapolation errors, finite-volume effects, and scaling errors) as in the SU(2) case, except that, in principle, the SU(3) approach allows one to directly extrapolate the dynamical heavy quark mass to the value of the physical strange quark mass.

For the chiral extrapolations, we first investigate the systematic error from the convergence of NLO ChPT. We have already seen that we cannot use NLO SU(3) ChPT for valence quarks near the physical strange quark mass, since the fits do not agree well with our data. Focusing on the results from fits to the light quark region [$m_{\text{avg}} \equiv (m_x + m_y)/2 \leq 0.01$], where our data is well represented by the NLO formula, in Fig. 17 we plot the LO and NLO contributions to the pseudoscalar decay constant f_{ll} in the unitary case. The values of f_{ll} are plotted as functions of the light quark mass parameter ($\chi_l \propto \tilde{m}_l$) and the heavy quark mass parameter ($\chi_h \propto \tilde{m}_h$) using our results from the SU(3) fit with the mass cut $m_{\text{avg}} \leq 0.01$. We see that the corrections are generally large, even for relatively small light quark masses. For example, the top left-hand panel shows that for $m_h = 0.04$ and for pseudoscalar masses in the 250–400 MeV range, i.e., in the region where we have data, the NLO correction is as large as 70% of the LO term.

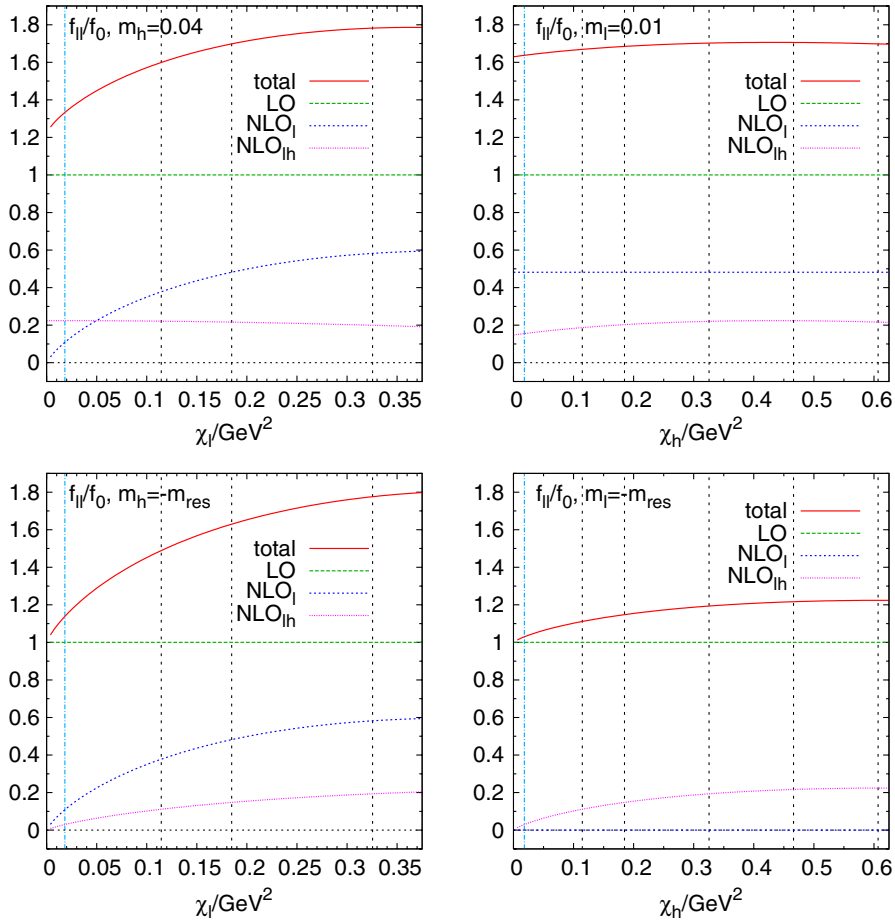

FIG. 17 (color online). LO and NLO contributions in the unitary meson decay constant fit in SU(3) PQChPT as a function of the light quark mass parameter (left panels) and the heavy quark mass parameter (right panels). In the plots in the top panels the other quark mass parameter was set to our highest value used in the fits ($m_l = 0.01$ or $m_h = 0.04$), while in those in the bottom panels the remaining quark mass parameter was set to zero (m_l or $m_h = -m_{\rm res}$). NLO$_l$ denotes the NLO contribution proportional to $\log\chi_l$, and NLO$_{lh}$ the NLO contribution proportional to $\log(\chi_l + \chi_h)/2$. The LO contribution is always normalized to one. Vertical dashed lines indicate quark masses of $m_l = m_{ud}$, 0.005, 0.01, 0.02, 0.03, and 0.04 (from left to right; left panels only show quark masses up to 0.02).

In the preceding paragraph we found that, for the unitary case with $m_\pi \approx 400$ MeV, the SU(3) ChPT expansion for the decay constant is approximately of the form $f_0(1 + 0.7 + O(p^4))$, which leads one to expect the $O(p^4)$ term to be about $(0.7)^2 \approx 0.5$. This would be a 30% correction to the sum of LO plus NLO terms. However, the NLO fits agree with our data quite well, certainly excluding corrections beyond the few percent level. From this we conclude that the agreement between our data and the SU(3) ChPT formula is not indicative of NLO SU(3) ChPT working well for these quark masses, since this would imply anomalously small $O(p^4)$ corrections. It seems that the SU(3) ChPT formulas are serving as smooth fitting functions with sufficient flexibility in the parameters to absorb the effects of higher-order terms and to match our data. We would need more data to investigate this hypothesis fully, and in particular, this data should come from ensembles with more than the single m_h we currently have. This will be done in the future and if our hypothesis is correct then, as discussed in the following section, part of the reason for the small value of f_0 is due to the fact that it absorbs some of the NNLO corrections. We now briefly discuss our limited attempts to use our current data to obtain additional information but stress that a complete analysis of the range of validity and precision of SU(3) ChPT will have to wait until we have data at more values of quark masses.

One can also try to extend the range of validity of χPT by going from NLO to NNLO. The complete continuum NNLO formulas are available in the literature [79] and we have done some preliminary fits of our data, augmented with results from an ensemble with $m_l = 0.02$ [80], to these formulas. Many more LECs are needed at NNLO [$L_i^{(3)}$ for $i = 0$ to 9 and 12 linear combinations of K_i] and it is not currently clear how stable such fits will be. We defer a discussion of these fits pending completion of the ongoing analysis.

To further probe the convergence of the series, we have dropped the additional logarithm terms that appear at

NNLO and fitted to the analytic terms, as we did for our SU(2) fits in Sec. VI A. The analytic terms for the meson masses and decay constants for SU(3) are

$$(\chi_x + \chi_y)^2, (\chi_x - \chi_y)^2, (\chi_x + \chi_y)\bar{\chi}, \bar{\chi}^2, \quad \overline{\chi^2} = (2\chi_l^2 + \chi_s^2)/3. \tag{115}$$

With our present data, limited to a single value of χ_h and to a small set of χ_l's, we were not able to include the last two terms in our NNLO phenomenological fits. The fits led, e.g., to an approximate 10% increase in the value of f_0 (for this particular case a fit range of $m_{\text{avg}} \leq 0.01$ has been used) and to even more significant changes in some of the NLO LECs. This supports our conjecture that SU(3) ChPT shows a slow convergence and NNLO terms are indeed important. On the other hand, since NNLO terms are not negligible, taking into account only (some of) the analytic NNLO terms and neglecting the logarithmic terms are not sufficient to determine the chiral behavior of observables quantitatively. It is for this reason that we choose to use SU(2) ChPT to determine our physical results and at this time we do not quote any estimates for systematic errors for quantities from our fits with SU(3) ChPT.

In spite of our reservations about the convergence of SU(3) ChPT, we have used the corresponding formulas in finite volumes to estimate finite-volume effects (see Appendix C), as we had done previously for the SU(2) case. We find similar results for the correction factors. Table XIII also contains the corrections obtained in the SU(3) case for the unitary pions; for more details see the discussion in Sec. VI C 2.

C. Comparing SU(3) × SU(3) and SU(2) × SU(2) chiral fits

In this section, we compare the results of our SU(3) ChPT fits with other results and also compare them with the results of our SU(2) fits. This serves to further probe the behavior of ChPT in the region of quark masses we are studying. We stress, however, that we believe that the convergence of the SU(3) series is relatively poor and therefore at this stage any quantitative conclusions will be limited.

To compare the SU(3) fit results with the previous ones obtained in SU(2) PQChPT (Sec. VI A), we use Eqs. (B40)–(B43) (cf. also [13,26]) to match the three flavor ChPT to the two flavor case at NLO. The results for B_0, f_0, and the low-energy constants $\bar{l}_{3,4}$ [for a definition of the low-energy constants $\bar{l}_{3,4}$ see Eq. (B44) and [13]] are shown in Table XVIII. Indeed, having a fixed dynamical heavy quark mass in the SU(3) × SU(3) theory is equivalent to having one in the SU(2) × SU(2) theory, up to terms of $O((m_l/m_s)^2)$. The remarkable agreement between the LECs obtained directly from the fit to the chiral behavior using SU(2) ChPT and those obtained by converting the SU(3) LECs using Eqs. (B40)–(B43) (see Table XVIII) is evidence that these terms of $O((m_l/m_s)^2)$ are small. Although reassuring, we stress that this in itself is insufficient to demonstrate fully the validity of the SU(3) ChPT at NLO. For example, if the m_s^2 term in the expansion for the decay constant were large, this would appear in our NLO fits as a shift in f_0 but the behavior with m_l would be equivalent to that in SU(2) ChPT [up to corrections of $O((m_l/m_s)^2)$ of course]. We suspect that this is the case and use SU(2) ChPT to obtain physical results; nevertheless, for the remainder of this section, we take our SU(3) results at face value and compare them to previous determinations of the LECs.

We first consider the ratio of the decay constants in the two and three flavor chiral limit. From our fits to SU(2) and SU(3) ChPT we obtain $f/f_0 = 1.229(59)$ (here we quote only the statistical error), showing the influence of the strange quark loops. An important observation is that the value of f_0, the pion decay constant in the SU(3) chiral limit, is much smaller than the measured pseudoscalar decay constant f_{ll} at, say, $m_l = 0.01$ and also much smaller than f_π. This is due to the large NLO correction shown in Fig. 17. The small value of f_0 may be a contributor to poor convergence, since the chiral logarithms come in with a factor of $1/f_0^2$. Of course, one can rearrange the series and expand in m_{xy}^2/f_π^2 consistently to NLO and possibly improve the convergence. We are exploring these options, but if such a rearrangement, which only affects the series at NNLO, markedly changes the convergence properties, one is still led to the conclusion that the series is not well controlled.

If we compare our result for f_0 to phenomenological estimates by Bijnens [81], our value of $f_0 = 93.5(7.3)$ MeV (statistical error only) turns out to be substantially lower than the preferred value from Bijnens, which is 124.0 MeV [NNLO, alternative fits also published there give values of 114.7 (NLO), 99.6 (NNLO), and 113.7 (NNLO) MeV]. His ratio f_π/f_0 is also different from ours [in contrast to the SU(2) case, where for the ratio f_π/f a better agreement has been achieved]: we obtain a value of 1.33(7) (statistical error only), whereas Bijnens's preferred fit suggests $f_\pi/f_0 = 1.05$. Interestingly, the $N_f = 2 + 1$

TABLE XVIII. SU(2) × SU(2) low-energy constants obtained directly from the SU(2) × SU(2) fits compared to those converted from the SU(3) × SU(3) chiral fits with a mass cut of $m_{\text{avg}} \leq 0.01$.

		B	f	$\bar{l}_3$	$\bar{l}_4$
Direct	SU(2) × SU(2)	2.414(61)	0.0665(21)	3.13(0.33)	4.43(0.14)
Converted	SU(3) × SU(3)	2.457(78)	0.0661(18)	2.87(0.28)	4.10(0.05)

TABLE XIX. Comparison of fitted SU(3) NLO LECs $L_i^{(3)}$ at $\Lambda_\chi = 770$ MeV in units of 10^{-4} to phenomenologically obtained values by Bijnens (see Table 2 in [81]) and dynamical $N_f = 2 + 1$ staggered lattice simulation (MILC), [68,69] [there, LECs were quoted at $\Lambda_\chi = m_\eta$, and conversion was done according to Eq. (B20)].

	$L_4^{(3)}$	$L_5^{(3)}$	$L_6^{(3)}$	$L_8^{(3)}$	$(2L_8^{(3)} - L_5^{(3)})$	$(2L_6^{(3)} - L_4^{(3)})$
This work[a]	$1.4(0.8)(\cdots)$	$8.7(1.0)(\cdots)$	$0.7(0.6)(\cdots)$	$5.6(0.4)(\cdots)$	$2.4(0.4)(\cdots)$	$0.0(0.4)(\cdots)$
Bijnens, NLO	$\equiv 0$	14.6	$\equiv 0$	10.0	5.4	$\equiv 0$
Bijnens, NNLO	$\equiv 0$	9.7(1.1)	$\equiv 0$	6.0(1.8)	2.3[b]	$\equiv 0$
MILC, 2007	$1.3(3.0)(^{+3.0}_{-1.0})$	$13.9(2.0)(^{+2.0}_{-1.0})$	$2.4(2.0)(^{+2.0}_{-1.0})$	7.8(1.0)(1.0)	2.6(1.0)(1.0)	$3.4(1.0)(^{+2.0}_{-3.0})$

[a]For reasons mentioned in Sec. VII B, we do not quote any systematic error for parameters obtained from the SU(3) fits.
[b]This value was derived from the quoted single values for $L_5^{(3)}$ and $L_8^{(3)}$; since we do not know the correlation between those two, we cannot provide the error estimate.

lattice simulation by MILC [68,69] also observed a higher ratio of $f_\pi/f_0 = 1.21(5)(^{+13}_{-3})$, which translates into a central value for $f_0 = 106.0$ MeV [using MILC's value for $f_\pi = 128.3(0.5)(^{+2.4}_{-3.5})$, we do not quote an error for this number, since we do not know the correlation between f_π and f_π/f_0].

For the ratio B/B_0 we obtain $B/B_0 = 1.03(05)$. The very small deviation from 1 is perhaps surprising, and indicates good agreement with the predictions of the large N_c approximation and only small Zweig-rule violations in this case. A comparison of the LO LEC B_0 is not directly possible, since this number depends on the renormalization scheme (see Sec. VI B 2). Instead, Bijnens quotes a number for the renormalization scheme independent and dimensionless ratio $2B_0 m_{ud}/m_\pi^2$ of 0.736 [from the preferred NNLO fit; alternative fits give 0.991 (NLO), 1.129 (NNLO), 0.958 (NNLO)]. From our SU(3) fit we obtain 0.995(41) (statistical error only), which agrees better with the alternative phenomenological fits than the preferred one.

The ratio of $\Sigma = f^2 B/2$, the chiral condensate in the two flavor theory, and $\Sigma_0 = f_0^2 B_0/2$, in the three flavor theory, can also be compared directly. We obtain $\Sigma/\Sigma_0 = 1.55(21)$, whereas MILC quotes a value of $1.52(17)(^{+38}_{-15})$. It should be noted, however, that we obtain slightly different values for f/f_0 and for B/B_0 than the MILC Collaboration.

In Table XIX we compare the NLO LECs to phenomenological NLO and NNLO fits [81] and the results of MILCs $N_f = 2 + 1$ dynamical lattice simulations [68,69] (all LECs in that table are quoted at the scale $\Lambda_\chi = 770$ MeV). In the fits by Bijnens, $L_4^{(3)}$ and $L_6^{(3)}$ were set to zero (at $\Lambda_\chi = 770$ MeV $\approx m_\rho$) as motivated by Zweig rule and large N_c arguments. Whereas for the latter our result agrees with this assumption within the statistical uncertainty, for $L_4^{(3)}$ we observe some discrepancy (without taking systematic errors into account). Interestingly, our NLO results for $L_5^{(3)}$ and $L_8^{(3)}$ agree very well with Bijnens's numbers from the NNLO fit, but not for his NLO fit (for which no systematic error is given however). Within the reported uncertainties, our NLO LECs agree nicely with the set of values quoted by the MILC Collaboration.

In Fig. 18 we summarize some of the results presented in this section. Here we plot our measured values for the decay constant, converted to physical units, versus the degenerate valence pseudoscalar mass squared, along with the results of fits to SU(2) and SU(3) ChPT. The

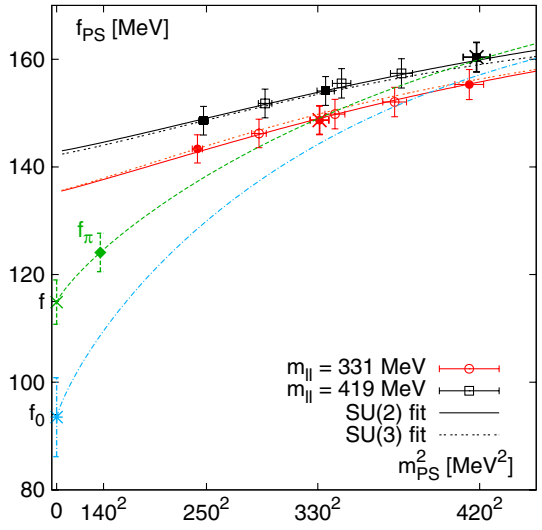

FIG. 18 (color online). A plot of our measured values for the decay constant, converted to physical units, versus the degenerate valence pseudoscalar mass squared. The data for degenerate quarks are denoted by filled symbols, and for nondegenerate quarks, open symbols are used. The graph shows that we see small effects for nondegenerate quarks. The results of SU(2) and SU(3) partially quenched ChPT fits to our data are shown, and both fits agree well with the data. The unitary SU(2) chiral extrapolation is also given, along with our value of f, and two of our data points lie on this curve, as expected. The value of f differs by $\approx 30\%$ from the decay constant measured at $m_\pi = 420$ MeV. We also plot the SU(3) chiral limit curve, for which the horizontal axis is the unitary meson mass for three degenerate mass quarks. None of our measured values must lie on this line. The large difference between f_0 and our measurements is apparent, showing the poor convergence of NLO SU(3) ChPT, with LECs as determined from our data.

data for degenerate quarks are denoted by filled symbols, and for nondegenerate quarks, open symbols are used. The graph shows that we see small effects for nondegenerate quarks. The results of SU(2) and SU(3) partially quenched ChPT fits to our data are shown, and both fits agree well with the data. From the (now determined) fit functions, we plot the unitary SU(2) chiral extrapolation. Two of our data points lie on this curve, but one sees that our measured decay constant for a pseudoscalar mass of 420 MeV is about 30% above the chiral limit value, f. We also plot the SU(3) chiral limit curve. For this curve, the horizontal axis is the unitary meson mass in the theory where all quarks are degenerate. Therefore, none of our measured values must lie on this line. Figure 18 shows graphically the large difference between f_0 and our measurements. This is graphical evidence of the poor convergence of NLO SU(3) ChPT, with LECs as determined from our data.

In summary, we have found that we can fit our data well using NLO SU(3) ChPT for average valence quark masses <0.01, corresponding to pseudoscalar masses below 420 MeV. The SU(3) LECs we determine are generally in reasonable agreement with continuum phenomenology and other lattice results (note, however, the small value of f_0 which we find). We see that the LECs from our SU(3) and SU(2) fits agree well when a conversion is performed from SU(3) to SU(2). However, since we find large corrections at NLO, we would expect significant ones also at NNLO. We are therefore not at all confident that the systematic errors in the SU(3) LECs are currently under control. In addition, the fits do not agree with our data when we extend the NLO SU(3) ChPT theory to the kaon mass scale. It is possible that with more data it will become feasible to perform NNLO SU(3) fits and to control the systematic uncertainties with sufficient precision. We will investigate this in the future but we stress that whether or not this proves to be the case, we can happily use SU(2) PQChPT to obtain predictions for physical results (including quantities in kaon physics as explained in Sec. II B). This is what we do in this paper.

VIII. B_K

A. Pseudoscalar bag parameter on the lattice

The kaon bag parameter is defined as the ratio of the neutral kaon mixing matrix element and its expectation value from the vacuum saturation approach,

$$B_K = \frac{\langle \bar{K}^0 | \mathcal{O}_{LL}^{\Delta S=2} | K^0 \rangle}{\frac{8}{3} f_K^2 m_K^2}, \tag{116}$$

where m_K is the neutral kaon mass, f_K the kaon decay constant, and

$$\mathcal{O}_{LL}^{\Delta S=2} = (\bar{s}(1-\gamma_5)\gamma_\mu d)(\bar{s}(1-\gamma_5)\gamma_\mu d) \tag{117}$$

is the local, effective four quark operator, which couples to the left-handed quarks and induces a change in strangeness by $\Delta S = 2$. In our simulations, we define the corresponding pseudoscalar bag parameter for a meson made from either valence or sea quarks with masses m_x and m_y, which we measure by fitting the ratio

$$B_{xy}(t) = \frac{3}{8} \frac{\mathcal{C}_{POP}^{WLW}(t_{\rm src}, t, t_{\rm snk})}{\mathcal{C}_{PA}^{WL}(t_{\rm src}, t)\mathcal{C}_{AP}^{LW}(t, t_{\rm snk})} \tag{118}$$

to a constant B_{xy} over some range in time t. Here, t denotes the time coordinate at which we insert the four quark operator, and $t_{\rm src}$ and $t_{\rm snk}$ are the temporal coordinates at which we insert Coulomb gauge fixed (spatial) walls of antikaon and kaon interpolating operators, respectively. The correlators using wall source and local sinks, which we construct from the WL propagators obtained with quark masses m_x and m_y, are defined as

$$\mathcal{C}_{POP}^{WLW}(t_{\rm src}, t, t_{\rm snk}) = \frac{1}{V}\sum_{y\in V} \langle q_w(t_{\rm src}) P \bar{q}_w(t_{\rm src}) \times \mathcal{O}_{LL}^{\Delta S=2}(y, t) q_w(t_{\rm snk}) P \bar{q}_w(t_{\rm snk}) \rangle, \tag{119}$$

$$\mathcal{C}_{PA}^{WL}(t_{\rm src}, t) = \frac{1}{V}\sum_{y\in V} \langle q_w(t_{\rm src}) P \bar{q}_w(t_{\rm src}) q(y, t) A \bar{q}(y, t) \rangle, \tag{120}$$

$$\mathcal{C}_{AP}^{LW}(t, t_{\rm snk}) = \frac{1}{V}\sum_{y\in V} \langle q(y, t) A \bar{q}(y, t) q_w(t_{\rm snk}) P \bar{q}_w(t_{\rm snk}) \rangle, \tag{121}$$

where $q_w(t)$ and $q(y, t)$ denote a Coulomb gauge fixed (spatial) wall smeared quark field and a local quark field, respectively. A summation over all spatial points for the local operators is performed, and a balancing volume factor $V = L^3$ included giving a spatial volume average that is statistically efficient. In addition, we average over propagators obtained with periodic and antiperiodic boundary conditions in the time direction, which results in a doubled time extent available for the plateau fit.

The values measured on the $24^3 \times 64$, $L_s = 16$ lattices are given in Table XX. There, the fit to the plateau was performed over the range $t \in [12, 52]$ using an uncorrelated fit, since, due to the large time extent, correlated fits became unstable. Previously, our collaboration also obtained the pseudoscalar bag parameter on smaller $16^3 \times 32$, $L_s = 16$ lattices with dynamical light quark masses $m_l \in \{0.01, 0.02, 0.03\}$ and $m_s = 0.04$ at the same gauge coupling [19,34,82,83]. For comparison we quote those values in Table XXI. In this case the plateau was fitted over a range $t \in [12, 22]$.

TABLE XX. Pseudoscalar B parameter B_{xy} for pseudoscalar mesons with valence masses m_x, m_y for two different values of the light sea quark mass m_l ($m_h = 0.04$) on $24^3 \times 64$ lattices, fit range 12–52 (uncorrelated fit).

		B_{xy}	
m_x	m_y	$m_l = 0.005$	$m_l = 0.01$
0.001	0.001	0.4691(83)	0.4698(53)
0.005	0.001	0.4910(66)	0.4953(41)
	0.005	0.5079(46)	0.5119(32)
0.01	0.001	0.5136(57)	0.5209(39)
	0.005	0.5267(37)	0.5312(28)
	0.01	0.5421(29)	0.5459(25)
0.02	0.001	0.5494(52)	0.5593(42)
	0.005	0.5588(31)	0.5629(26)
	0.01	0.5697(25)	0.5727(23)
	0.02	0.5911(23)	0.5935(20)
0.03	0.001	0.5777(55)	0.5886(54)
	0.005	0.5850(32)	0.5884(28)
	0.01	0.5933(26)	0.5957(22)
	0.02	0.6105(23)	0.6126(18)
	0.03	0.6267(22)	0.6287(16)
0.04	0.001	0.6012(64)	0.6131(73)
	0.005	0.6070(38)	0.6105(33)
	0.01	0.6137(30)	0.6160(24)
	0.02	0.6280(23)	0.6299(18)
	0.03	0.6418(21)	0.6435(15)
	0.04	0.6550(19)	0.6565(14)

We will have to extrapolate our measured values to the physical light and strange quark masses for which PQChPT in the SU(2) × SU(2) formulation will be used. These fits are discussed in the next part of this section; the result obtained for B_K was already published in [19], but here we provide some more details on the chiral fitting procedure. In the remainder of this section, we employ SU(3) × SU(3) PQChPT to extract the bag parameter in the chiral limit and briefly discuss the data from the 16^3 lattices.

TABLE XXI. Pseudoscalar B parameter B_{xy} for pseudoscalar mesons with valence masses m_x, m_y for three different values of the light sea quark mass m_l ($m_h = 0.04$) on $16^3 \times 32$ lattices, fit range 12–20 (uncorrelated fit).

		B_{xy}		
m_x	m_y	$m_l = 0.01$	$m_l = 0.02$	$m_l = 0.03$
0.01	0.01	0.546(8)	0.539(8)	0.527(7)
0.02	0.01	0.577(6)	0.569(6)	0.556(6)
	0.02	0.598(5)	0.589(5)	0.580(5)
0.03	0.01	0.600(6)	0.594(6)	0.579(5)
	0.02	0.617(4)	0.609(5)	0.600(4)
	0.03	0.633(4)	0.626(4)	0.618(3)
0.04	0.01	0.620(5)	0.616(6)	0.599(5)
	0.02	0.633(4)	0.627(4)	0.618(4)
	0.03	0.647(4)	0.641(4)	0.634(3)
	0.04	0.659(3)	0.655(3)	0.648(3)
0.05	0.01	0.636(5)	0.634(6)	0.616(4)
	0.02	0.648(4)	0.643(4)	0.634(3)
	0.03	0.660(3)	0.655(3)	0.648(3)
	0.04	0.671(3)	0.667(3)	0.661(3)
	0.05	0.682(3)	0.679(3)	0.673(3)

B. SU(2) × SU(2) chiral fitting procedure

For the chiral extrapolation of B_K, we use SU(2) × SU(2) ChPT for the kaon sector, as introduced in Sec. II and applied to the kaon masses and decay constants in Sec. VI A. Specifically we use Eq. (B48) to extrapolate to the physical average light quark mass m_{ud} determined in Sec. VI B 1. Here we consider the data from the 24^3 lattices at values of $m_y = 0.03$ and 0.04 for the heavier quark mass approximating the strange quark mass. Of these two values only the latter describes a truly unquenched quark and we account for possible effects of a partially quenched strange quark treatment in our discussion of systematic errors. The fits using SU(2) × SU(2) ChPT for the kaon sector are shown in Fig. 19, whereas the fitted parameters are given in Table XXII. The parameters B and f have been fixed to their values obtained in the combined SU(2) × SU(2) ChPT fits for the pseudoscalar masses and decay constants; cf. Sec. VI. We applied a cut in the light valence quark mass of $m_x \leq 0.01$. The low-energy constant $b_1(m_y)$ multiplying the dynamical light quark mass in Eq. (B48) shows almost no dependence on the heavy quark mass, whereas $b_2(m_y)$ and $B_{\mathrm{PS}}^{(K)}(m_y)$ vary by 12% and 4%, respectively, when going from $m_y = 0.03$ to 0.04. Also the value of the kaon bag parameter extrapolated to the physical average light quark mass, B_{udy}, increases by approximately 4% due to this change in m_y.

The interpolation to the physical value of the strange quark mass (obtained from the kaon mass, cf. Sec. VI B 1) is done linearly as shown in Fig. 20. Included in the plot (and also in Table XXII) is a point at $m_y = 0.02$ for information only. It was not included in the linear fit and interpolation because this supposedly heavy quark mass is likely too light to be sufficiently separated from the simulated light quark masses to enable convergent effective treatment. However, the linear interpolation does not seem to deviate much even at this point, giving us confidence that nonlinear effects in the strange quark mass region at least do not show up at the level of the numerical precision achieved. Finally, we quote for the unrenormalized physical value of the kaon bag parameter $B_K^{\mathrm{lat}} = 0.565(10)$. We will now discuss the renormalization of $\mathcal{O}_{LL}^{\Delta S=2}$ and estimate all significant contributions to the systematic error.

1. Renormalization

The renormalization of $\mathcal{O}_{LL}^{\Delta S=2}$ has been treated in [21] using the RI-MOM nonperturbative renormalization technique. Couplings to wrong chirality four quark operators

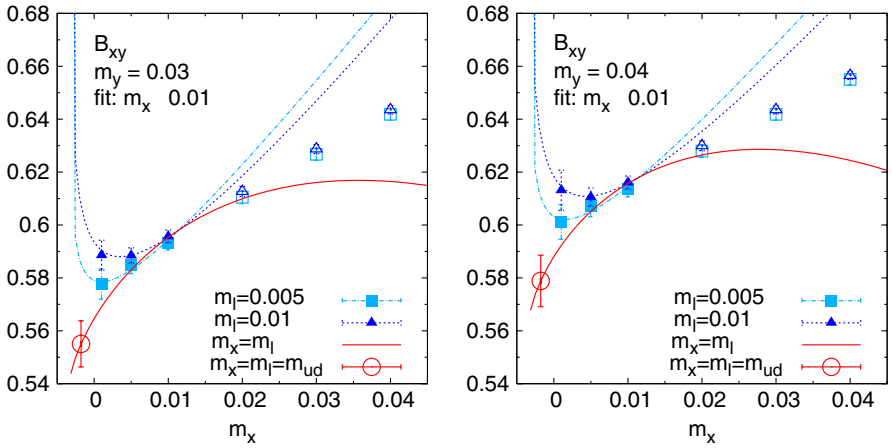

FIG. 19 (color online). Extrapolation of the pseudoscalar bag parameter B_{xy} in the light quark mass m_x to the physical point m_{ud} for $m_y = 0.03$ (left panel) and $m_y = 0.04$ (right panel). Points with filled symbols are included in the fit, while those marked by open symbols are excluded. For fit parameters see Table XXII.

are in principle admitted by the presence of a nonzero residual mass. It has been demonstrated in that paper that they are highly suppressed and small, using nonexceptional momenta to remove the spontaneous chiral symmetry breaking effects that might obscure this fact at the modest, accessible lattice momenta. Thus we only need to consider a simple, multiplicative renormalization. Here we quote the renormalization factors for the regularization-independent (RI) and the modified minimal subtraction ($\overline{\text{MS}}$) schemes both at $\mu = 2$ GeV as well as the renormalization group invariant (RGI) result:

$$Z_{B_K}^{\text{RI}}(2\text{ GeV}) = 0.910(05)_{\text{stat}}(13)_{\text{syst}},$$
$$B_K^{\text{RI}}(2\text{ GeV}) = 0.514(10)_{\text{stat}}(07)_{\text{ren}}, \quad (122)$$

$$Z_{B_K}^{\overline{\text{MS}}}(2\text{ GeV}) = 0.928(05)_{\text{stat}}(23)_{\text{syst}},$$
$$B_K^{\overline{\text{MS}}}(2\text{ GeV}) = 0.524(10)_{\text{stat}}(13)_{\text{ren}}, \quad (123)$$

$$Z_{B_K}^{\text{RGI}} = 1.275(10)_{\text{stat}}(25)_{\text{syst}},$$
$$\hat{B}_K = 0.720(13)_{\text{stat}}(14)_{\text{ren}}, \quad (124)$$

where the first error is the (combined) statistical error and the second error the systematic error from the renormalization.

TABLE XXII. Parameters and χ^2/dof for fits of B_{xy} to Eq. (B48) as shown in Fig. 19. The parameters $B = 2.414(61)$ and $f = 0.0665(21)$ were fixed from combined SU(2) × SU(2) meson masses and decay constants fits, Sec. VI; $\Lambda_\chi = 1$ GeV.

m_y	$B_{\text{PS}}^{(K)}(m_y)$	$b_1(m_y)/f^2$	$b_2(m_y)/f^2$	χ^2/dof	B_{udy}
0.02	0.513(10)	-5.2(1.6)	8.18(0.65)	0.27	0.5249(86)
0.03	0.544(10)	-5.4(1.5)	6.85(0.65)	0.20	0.5550(87)
0.04	0.568(11)	-5.4(1.7)	6.05(0.71)	0.14	0.5789(97)

2. Systematic errors

Finite-volume effects.—The spatial volume in our simulation is approximately $(2.7\text{ fm})^3$; therefore, from [84] it follows that the difference between the B_{xy} measured on the finite lattice volume and the result in infinite volume is negligible for all points except the lightest ones (both valence quarks at a mass of 0.001), where the difference may be as large as 2%. Excluding the point $m_l = 0.01$, $m_x = m_y = 0.001$ from the fit, the final result for B_K^{lat} remains almost unchanged. Comparing points with $m_l = 0.01$ from the smaller volume simulation [16^3 lattice, $\approx (1.8\text{ fm})^3$ spatial volume] from Table XXI with the corresponding ones from the 24^3 simulation (Table XX), statistically marginal differences of up to 1% are observed. See Sec. VIII D for a more detailed discussion. Conservatively, we adopt this as an estimate for finite-volume effects affecting our final number for B_K. [Note that for the lightest point in the 16^3 ensemble ($m_x = m_y = m_l$) we have

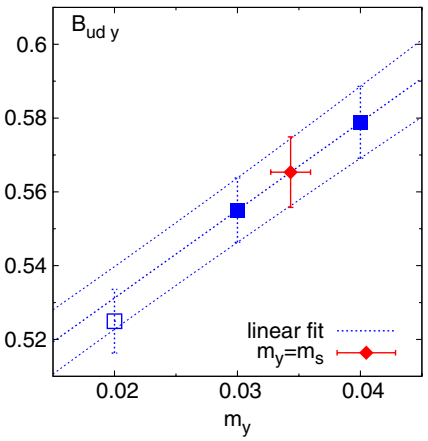

FIG. 20 (color online). Linear interpolation in m_y of the pseudoscalar bag parameter B_{udy} to the physical strange quark mass m_s (diamond). The open symbol at $m_y = 0.02$ was excluded from the interpolation.

$m_\pi L \approx 4.0$, whereas for our lightest valence pion in both 24^3 ensembles ($m_x = m_y = 0.001$, $m_l = 0.005$ or 0.01) we still have $m_\pi L \approx 3.4$, so it is reasonable to assume the finite-volume effects in those points to be comparable to the observed effect from comparing 16^3 and 24^3 lattices.]

Scaling effects.—Having only data at a single value for the lattice spacing does not allow quantifying the scaling effects affecting our data. The CP-PACS Collaboration calculated B_K in a quenched calculation using the Iwasaki gauge action with domain wall valence quarks at two different lattice scales, namely, $1/a = 1.81(4)$ and 2.81(6) GeV (determined from the ρ-meson mass) keeping the physical volume approximately fixed [85]. Extrapolating the collaboration's observed scaling violation to our coarser lattice spacing, we would expect a 3.5% scaling effect. We assume a 4% systematic error, which is in agreement with the scaling violations discussed in conjunction with the meson masses and decay constants in Sec. VI C 4.

Interpolation to the physical strange quark mass.—Currently only ensembles with a fixed value for the dynamical heavy quark mass are available. We estimate the effect of this 15% too high sea quark mass from the measurements done at the 16^3 lattices. There dynamical light quark masses of $m_l = 0.02$ and 0.03 have been simulated, which are closer to the physical value of the strange quark mass than the dynamical light quark masses available from the 24^3 data. Comparing B_{xy} for $m_x = 0.01$, $m_y = 0.04$ (lightest valence quark mass and dynamical strange quark mass) at the two aforementioned light sea quark masses, an increase of 3% is observed (Table XXI). In that case, *two* dynamical quark flavors were changed by $\Delta m = 0.01$, whereas the *single* strange quark mass only has to be changed by 0.0057. Accordingly, the systematic error has to be scaled down by 2 (from number of flavors) times ≈ 1.8 (from scaling Δm), resulting in a 1% effect. (This is an exclusive sea quark effect and should not be confused with the 4% difference discussed above, when changing the valence m_y from 0.03 to 0.04 in the kaon itself.)

Extrapolation in the light quark mass.—Including terms up to NLO in our chiral fit functions, we have to assign a systematic error to our extrapolation resulting from neglecting NNLO and higher-order terms. The linear fit to the 16^3 data gives a 6% higher value for B_K (see Sec. VIII D). Assigning this difference to the (here included) NLO terms, the size of NNLO contribution can be estimated to be 2% by scaling the observed 6% difference by $\tilde{m}_l/\tilde{m}_s \approx 0.4$ taken at the lightest value for quark mass in the linear fit, $m_l = 0.01$, and the strange quark mass at the physical point m_s.

3. Final result

Combining the 1% finite-volume, 4% scaling, 1% heavy quark mass interpolation, and 2% ChPT extrapolation systematic errors with the one from the nonperturbative renormalization (except for $B_K^{\rm lat}$, of course), our final result in the different renormalization schemes considered reads

$$B_K^{\rm lat} = 0.565(10)_{\rm stat}(27)_{\rm syst}, \tag{125}$$

$$B_K^{\rm RI}(2\ {\rm GeV}) = 0.514(10)_{\rm stat}(07)_{\rm ren}(24)_{\rm syst} = 0.514(10)_{\rm stat}(25)_{\rm comb}, \tag{126}$$

$$B_K^{\overline{\rm MS}}(2\ {\rm GeV}) = 0.524(10)_{\rm stat}(13)_{\rm ren}(25)_{\rm syst} = 0.524(10)_{\rm stat}(28)_{\rm comb}, \tag{127}$$

$$\hat{B}_K = 0.720(13)_{\rm stat}(14)_{\rm ren}(34)_{\rm syst} = 0.720(13)_{\rm stat}(37)_{\rm comb}, \tag{128}$$

where "stat" denotes the statistical error, "syst" the systematic error as discussed above, "ren" the error due to renormalization, and "comb" is the combined systematic error from the latter two.

C. Fits to SU(3) × SU(3) PQChPT

Here we apply Eq. (B22) from SU(3) × SU(3) PQChPT to fit our data. That means, we now also try to describe the dependence on the heavier (valence) quark mass by (PQ) ChPT. As discussed in Sec. II B 5, if Eq. (B22) were applied for a fixed value of the heavier valence quark mass (also fixing the heavy sea quark mass), it would naturally revert to the kaon SU(2) × SU(2) form. If we were able to describe the valence mass dependence with the SU(3) × SU(3) PQChPT form up to the strange quark mass, this form would be applicable to a determination of $B_K^{\rm lat}$. However, it is also possible that this form can be used to describe only light valence masses m_x, m_y to obtain the SU(3) × SU(3) low-energy constant $B_{\rm PS}^\chi$ representing the pseudoscalar bag parameter in the three flavor theory in the limit of all three masses being zero, which is of phenomenological interest [86]. The only remnant terms involving a large mass in such a fit of the SU(3) × SU(3) PQChPT arise from the fixed dynamical heavy quark mass m_h, and we will estimate a systematic error from this.

We observe the same behavior as for the meson masses and decay constants: a reliable fit including quark masses up to the strange quark mass is not possible with only terms of NLO included in the fit formula. In Fig. 21 fits to the 24^3 data are shown with two different ranges for the mass cut $m_{\rm avg}$. While the fit with $m_{\rm avg} \leq 0.01$ describes the data inside the fit range but badly fails at the heavier points, going to $m_{\rm avg} \leq 0.02$ already fails to describe the data at the lowest masses. The fitted parameters are given in Table XXIII. Here we fixed B_0 to its value obtained from the SU(3) × SU(3) fit for the meson masses and decay constants ($m_{\rm avg} \leq 0.01$) (cf. Sec. VII). Because of the failure to describe the data with one quark mass as heavy as the strange quark, a determination of $B_K^{\rm lat}$ is not mean-

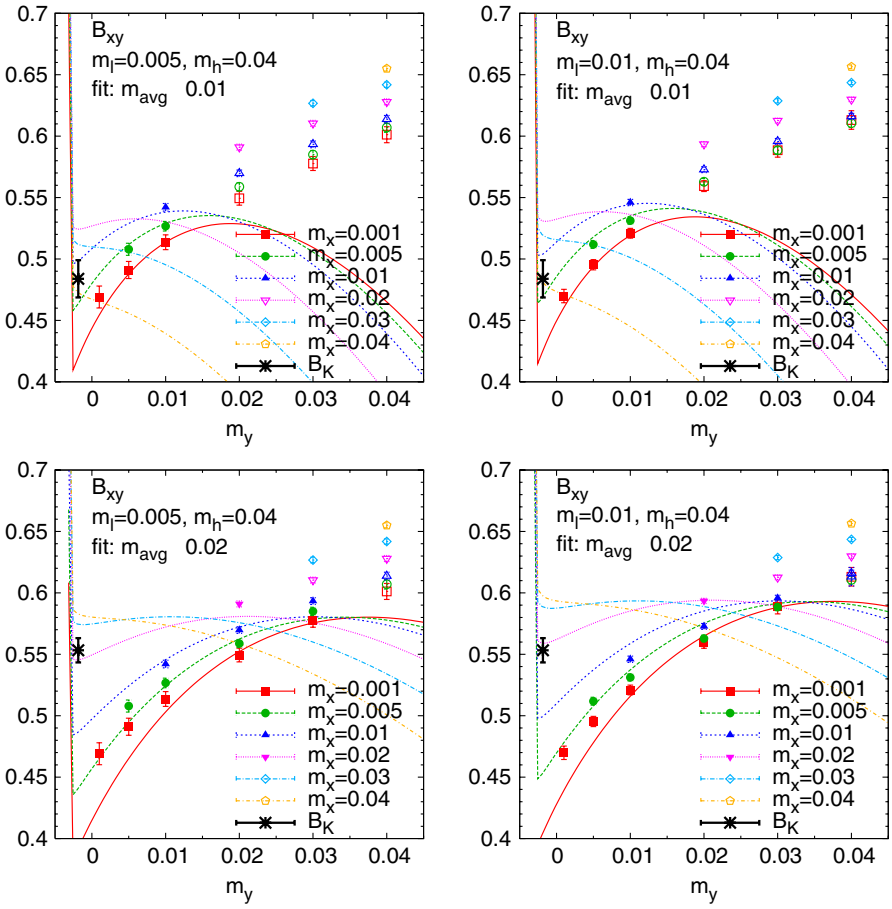

FIG. 21 (color online). Fitting the pseudoscalar bag parameter B_{xy} to the SU(3) × SU(3) χPT formulas with a cut in the average valence mass value of 0.01 (top panels) and 0.02 (bottom panels). Points marked by open symbols are excluded from the fit. The left panels are for light sea quark masses $m_l = 0.005$; the right panels for $m_l = 0.01$.

ingful using this ansatz. However, limiting the fit range to small masses, we will estimate the SU(3) × SU(3) LEC B^{χ}_{PS}. In Fig. 22 the dependence of B^{χ}_{PS} on the applied mass cut is shown. From that we conclude that at least within the statistical error the result is stable; therefore we quote (from a fit using $m_{\mathrm{avg}} \leq 0.01$)

$$B^{\chi\mathrm{lat}}_{\mathrm{PS}} = 0.266(26)_{\mathrm{stat}}, \tag{129}$$

$$B^{\chi\mathrm{RI}}_{\mathrm{PS}}(2\ \mathrm{GeV}) = 0.242(24)_{\mathrm{stat}}(03)_{\mathrm{ren}}, \tag{130}$$

$$B^{\chi\overline{\mathrm{MS}}}_{\mathrm{PS}}(2\ \mathrm{GeV}) = 0.247(24)_{\mathrm{stat}}(06)_{\mathrm{ren}}, \tag{131}$$

$$\hat{B}^{\chi}_{\mathrm{PS}} = 0.339(33)_{\mathrm{stat}}(07)_{\mathrm{ren}}, \tag{132}$$

using the same renormalization factors as in Eqs. (122)–(124) (first error statistical, second error systematics from renormalization). One has to keep in mind that this result was obtained by extrapolating $\tilde{m}_h$ from its value used in the simulation to zero (i.e., extrapolating $m_h \rightarrow -m_{\mathrm{res}}$). Considering Eq. (B22) which was used to fit the data,

TABLE XXIII. Fit parameters for fits of B_{xy} to Eq. (B22) as shown in Fig. 21. Values are quoted for different cuts m_{cut} in the average valence mass value. The parameters $B_0 = 2.35(0.16)$ and $f_0 = 0.0541(40)$ were fixed from combined SU(3) × SU(3) meson masses and decay constants fits, Sec. VII; $\Lambda_{\chi} = 1$ GeV.

m_{cut}	B^{χ}_{PS}	b	c	d	χ^2/dof	$B_K = B_{uds}$
0.01	0.266(26)	−4.5(1.6)	−0.20(0.18)	0.68(0.60)	1.8	0.484(15)
0.0125	0.249(24)	−2.5(1.5)	0.87(0.13)	0.96(0.61)	2.7	0.556(12)
0.015	0.232(22)	0.2(1.5)	0.43(0.13)	1.25(0.59)	5.4	0.546(11)
0.0175	0.223(22)	1.0(1.5)	0.94(0.12)	1.49(0.61)	6.1	0.570(12)
0.02	0.205(19)	4.2(1.4)	0.40(0.10)	1.89(0.58)	10.2	0.553(10)

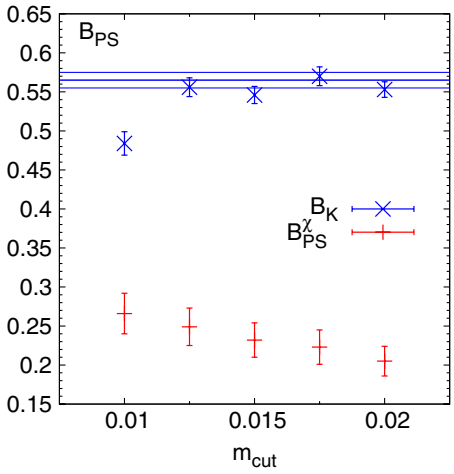

FIG. 22 (color online). Dependence of the fit parameter B^{χ}_{PS} (bars) and the extrapolated physical value of B_K (crosses) on the average valence mass cut, when fitting to the SU(3) × SU(3) fit formula. The horizontal lines indicate the result (with statistical error) for B_K obtained from the SU(2) × SU(2) fit.

one sees that—except for the analytic terms in I_{disc} where it enters via χ_η—the heavy quark mass only enters via $\bar{\chi}$, which multiplies the LEC d. By only using one dynamical heavy quark mass value, this LEC is exclusively determined by the dependence of B_{xy} on the light dynamical quark mass, a very mild dependence as can be seen by comparing the columns for $m_l = 0.005$ and 0.01 in Table XX. Two problems might arise. First, the slope with respect to variations of m_h may differ from the slope with respect to variations of m_l due to higher-order corrections. Second, with our fit procedure we might not be able to reliably determine this parameter. We assign the full size of this NLO estimate of the contribution

$$\left| B^{\chi}_{\mathrm{PS}} \frac{\chi_h}{3(4\pi f_0)^2} d \right| = \left| B^{\chi}_{\mathrm{PS}} \frac{2B_0 \tilde{m}_h}{48\pi^2 f_0^2} d \right| \tag{133}$$

to be the systematic error of our chiral extrapolation in the heavy quark mass, which is a 10% effect for the chosen cutoff, $m_{\mathrm{cut}} = 0.01$. (Going to higher values in m_{cut} the contribution increases to as much as 28% for $m_{\mathrm{cut}} = 0.02$.) The NLO contribution of the extrapolation in the light quark mass, which should be well under control by our fit procedure, we get from the difference of linearly extrapolating the measured B_{xy} values at the dynamical points with $m_l = m_x = m_y = 0.01$ and 0.005 to $m_l = m_x = m_y = -m_{\mathrm{res}}$ (i.e., $\tilde{m}_l = \tilde{m}_x = \tilde{m}_y = 0$) and the chiral extrapolation to this point ($m_h = 0.04$ is fixed in this procedure). By multiplying the resulting difference of

$$\begin{aligned} \Delta = {} & B^{\mathrm{linear}}_{ll}(\tilde{m}_l = 0, m_h = 0.04) \\ & - B^{\chi\mathrm{PT}}_{ll}(\tilde{m}_l = 0, m_h = 0.04) \approx 0.154 \end{aligned} \tag{134}$$

by $\chi_l/(4\pi f_0)^2$, we determine the uncertainty due to neglected NNLO contribution to be 8%.

For the systematic errors due to finite volume and scaling, the same applies as for the SU(2) × SU(2) analysis of B_K, so we assume them to be 1% and 4%, respectively. Eventually, with the 10% strange and 8% NNLO light quark mass extrapolation, the 1% finite volume, 4% scaling, and nonperturbative renormalization systematic error, we obtain (first error statistical, second combined systematic error)

$$B^{\chi\mathrm{lat}}_{\mathrm{PS}} = 0.266(26)_{\mathrm{stat}}(36)_{\mathrm{comb}}, \tag{135}$$

$$\begin{aligned} B^{\chi\mathrm{RI}}_{\mathrm{PS}}(2\ \mathrm{GeV}) &= 0.242(24)_{\mathrm{stat}}(03)_{\mathrm{ren}}(33)_{\mathrm{syst}} \\ &= 0.242(24)_{\mathrm{stat}}(33)_{\mathrm{comb}}, \end{aligned} \tag{136}$$

$$\begin{aligned} B^{\chi\overline{\mathrm{MS}}}_{\mathrm{PS}}(2\ \mathrm{GeV}) &= 0.247(24)_{\mathrm{stat}}(06)_{\mathrm{ren}}(33)_{\mathrm{syst}} \\ &= 0.247(24)_{\mathrm{stat}}(34)_{\mathrm{comb}}, \end{aligned} \tag{137}$$

$$\hat{B}^{\chi}_{\mathrm{PS}} = 0.339(33)_{\mathrm{stat}}(07)_{\mathrm{ren}}(46)_{\mathrm{syst}} = 0.339(33)_{\mathrm{stat}}(47)_{\mathrm{comb}}. \tag{138}$$

Our final number for $\hat{B}^{\chi}_{\mathrm{PS}}$ is in agreement with the phenomenological estimates from (i) the large N_c approximation, $\hat{B}^{\chi}_{\mathrm{PS}} = 0.38 \pm 0.15$ [86] ($\hat{B}^{\chi}_K$ in their notation), and (ii) $\hat{B}^{\chi}_{\mathrm{PS}} = 0.39 \pm 0.10$ [87] using the QCD-hadronic duality approach (which is close to the chiral limit value, see remark in [86]).

D. Results from simulations on a smaller volume

As mentioned in the beginning of this section, our collaboration first performed a study of the pseudoscalar bag parameter at a smaller volume of $(1.8\ \mathrm{fm})^3$ with higher dynamical masses $m_l \in \{0.01, 0.02, 0.03\}$ (see Table XXI). It turned out that these masses were not light enough to probe the regime of ChPT, as was revealed by comparing a simple linear fit in the light quark mass with a fit to (PQ) ChPT. The extrapolations from these fits gave similar results within the numerical uncertainty, suggesting that the chiral logarithms occurring in NLO were not represented correctly, or—in other words—the influence of the linear terms in the PQχPT formula was overestimated. Here, we just quote the result of extrapolating the three unitary points ($m_x = m_l \in \{0.01, 0.02, 0.03\}$, $m_y = m_h = 0.04$) by a linear fit to the light quark mass at the physical point m_{ud}

$$B^{16^3,\mathrm{linear}}_{udh}(m_h = 0.04) = 0.611(08), \tag{139}$$

which gives the value of the kaon bag parameter at a slightly too high strange quark mass. This has to be compared with $B_{udy} = 0.5789(97)$ at $m_y = 0.04$ from Table XXII, yielding a 6% difference between these two approaches. (More details on the fits to the 16^3 data have already been published in [83].)

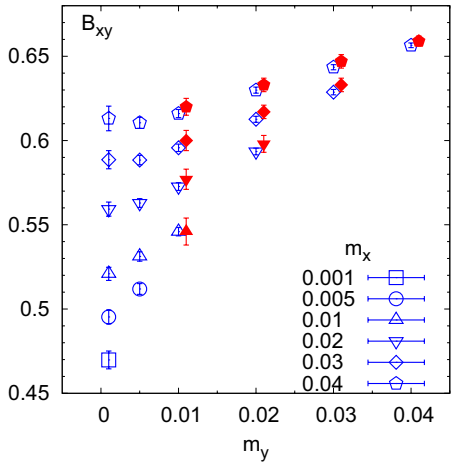

FIG. 23 (color online). Comparison of the pseudoscalar bag parameter B_{xy} for valence quark masses m_x, m_y measured on $16^3 \times 32$ (filled symbols) and $24^3 \times 64$ (open symbols) lattices at $m_l = 0.01$, $m_h = 0.04$. *(Filled symbols are slightly shifted to the right on this plot.)*

TABLE XXIV. Finite-volume comparison for the pseudoscalar bag parameter measured on 16^3 [$\approx (1.8\ \text{fm})^3$] and 24^3 ($\approx (2.7\ \text{fm})^3$] for dynamical quark masses $m_l = 0.01$, $m_h = 0.04$.

m_x	m_y	$B_{xy}^{(16^3)}$	$B_{xy}^{(24^3)}$	$\lvert B_{xy}^{(16^3)} - B_{xy}^{(24^3)}\rvert / B_{xy}^{(24^3)}$
0.01	0.01	0.546(8)	0.5459(25)	0.0(1.5)%
0.02	0.01	0.577(6)	0.5727(23)	0.8(1.1)%
	0.02	0.598(5)	0.5935(20)	0.8(0.9)%
0.03	0.01	0.600(6)	0.5957(22)	0.7(1.1)%
	0.02	0.617(4)	0.6126(18)	0.7(0.7)%
	0.03	0.633(4)	0.6287(16)	0.7(0.7)%
0.04	0.01	0.620(5)	0.6160(24)	0.6(0.9)%
	0.02	0.633(4)	0.6299(18)	0.5(0.7)%
	0.03	0.647(4)	0.6435(15)	0.5(0.7)%
	0.04	0.659(3)	0.6565(14)	0.4(0.5)%

Also this information enables us to check for possible finite-volume effects. The spatial volume increases by a factor $1.5^3 = 3.375$ when going to the 24^3 lattices. Figure 23 shows a comparison of the measured B_{xy} values at $m_l = 0.01$ for the two different volumes, revealing only small changes in the range of valence quark masses $0.01 \leq m_x, m_y \leq 0.04$, where data are available from both simulations (see also Table XXIV). The maximal deviation of 0.8% is observed for the lightest points $(m_x, m_y) = (0.01, 0.02)$ and $(0.02, 0.02)$ and decreases down to 0.4% for the heaviest point (0.04, 0.04). [Accidently, (0.01, 0.01) shows almost no (i.e., $\leq 0.1\%$) deviation in the central value.]

IX. VECTOR MESON COUPLINGS

In this section we discuss the couplings of the light vector mesons V to vector and tensor currents. These couplings f_V and f_V^T are defined through the matrix elements:

$$\langle 0|\bar{q}_2(0)\gamma^\mu q_1(0)|V(p;\lambda)\rangle = f_V m_V \varepsilon_\lambda^\mu, \tag{140}$$

$$\langle 0|\bar{q}_2(0)\sigma^{\mu\nu} q_1(0)|V(p;\lambda)\rangle = i f_V^T(\mu)(\varepsilon_\lambda^\mu p^\nu - \varepsilon_\lambda^\nu p^\mu), \tag{141}$$

where p and λ are the momentum and polarization state of the vector meson $V(p;\lambda)$ and ε_λ is the corresponding polarization vector. The tensor bilinear operator $\bar{q}_2\sigma^{\mu\nu}q_1$ [and hence $f_V^T(\mu)$] depends on the renormalization scheme and scale μ. The final results will be quoted in the $\overline{\text{MS}}$ scheme at $\mu = 2$ GeV. We have presented preliminary results for the ratios f_V^T/f_V in Ref. [88].

A. Experimental determination of f_V

The decay constants f_V can be determined experimentally. For the charged ρ and K^* mesons, one can use τ decays to deduce f_ρ and f_{K^*} as illustrated by the diagram in Fig. 24, where the curly line represents the W-boson. From the measured branching ratios one obtains the following values for the decay constants [89]:

$$\text{Br}(\tau^- \to \rho^- \nu_\tau) = (25.0 \pm 0.3)\% \Rightarrow f_{\rho^-} \simeq 208\ \text{MeV}, \tag{142}$$

$$\text{Br}(\tau^- \to K^{*-} \nu_\tau) = (1.29 \pm 0.03)\% \Rightarrow f_{K^{*-}} \simeq 217\ \text{MeV}. \tag{143}$$

One can also determine f_{ρ^0} from the width of the decay of the ρ^0 into e^+e^- which gives $f_{\rho^0} = 216(5)$ MeV. Similarly from the width of the decay $\phi \to e^+e^-$ one deduces $f_\phi \simeq 233$ MeV.

The couplings f_V^T are not known directly from experiment but are used as inputs in sum-rule calculations (see, for example, Refs. [90,91]) and other phenomenological applications to B decays (see, for example, Refs. [92–95]). Previous lattice results for the vector meson couplings are recalled below; determinations obtained using QCD sum rules are nicely reviewed in [90]. We now present our calculation and results for f_V^T/f_V, which can then be combined with the experimental values of f_V to obtain f_V^T. For the ϕ we neglect the Zweig suppressed disconnected contribution.

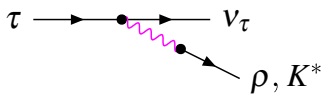

FIG. 24 (color online). The diagram illustrating how τ decays can be used to deduce f_ρ and f_{K^*}.

B. Lattice calculation of f_V^T/f_V

In order to determine f_V^T/f_V it is sufficient to calculate the following zero-momentum correlation functions for large values of the Euclidean time t:

$$C_{VV}^{s_1 s_2}(t) \equiv \sum_{\vec{x},i} \langle 0|V_i^{s_1}(t,\vec{x})V_i^{s_2}(0)|0\rangle = 3 f_V^{s_1} f_V^{s_2} m_V e^{-m_V T/2} \cosh(m_V(T/2-t)), \quad (144)$$

$$C_{TV}^{s_1 s_2}(t) \equiv \sum_{\vec{x},i} \langle 0|T_{4i}^{s_1}(t,\vec{x})V_i^{s_2}(0)|0\rangle = 3 f_V^{T s_1} f_V^{s_2} m_V e^{-m_V T/2} \sinh(m_V(T/2-t)), \quad (145)$$

where V_i and T_{4i} represent the vector and tensor currents and $i = 1, 2, 3$ is a spatial index. s_1 and s_2 label the smearing at the sink and at the source, respectively. From the ratio

$$R(t) = \frac{C_{TV}^{L s_2}}{C_{VV}^{L s_2}} = \frac{f_V^T}{f_V} \tanh(m_V(T/2-t)) \quad (146)$$

we readily obtain the ratio of (bare) couplings.

C. Results

In Table XXV we summarize our results for the vector meson masses from fits to (154) on the DEG data set (cf. Table II) and from fits to (144) and (145) on the UNI data set. In the latter case we average over various choices of the source smearing function (cf. Table IV) while always using a point sink. We restrict our study to the unitary case in which the sea and valence quarks have the same masses. The bare strange quark mass is always fixed at 0.04. On the UNI data set, again averaging over the same choices for the source and the sink, we also evaluate the ratios f_V^T/f_V. In each case Eq. (146) exhibits well pronounced plateaus which we fit to a constant.

TABLE XXV. Results for the measured vector meson masses (DEG and UNI data sets).

$m_l^{\rm sea}$	m_x	m_y	DEG	UNI
0.005	0.005	0.005	0.5053(58)	0.507(19)
	0.005	0.04		0.5591(75)
	0.04	0.04	0.6227(19)	0.6183(48)
0.01	0.01	0.01	0.5288(45)	0.527(17)
	0.01	0.04		0.5887(89)
	0.04	0.04	0.6295(18)	0.6319(48)
0.02	0.02	0.02	0.5789(55)	0.584(16)
	0.02	0.04		0.612(13)
	0.04	0.04	0.6453(33)	0.6453(84)
0.03	0.03	0.03	0.6317(33)	0.6239(76)
	0.03	0.04		0.6447(83)
	0.04	0.04	0.6622(27)	0.6609(69)

In Table XXVI we present the bare values of f_V^T/f_V. It can be seen that the measured results are obtained with excellent precision. We have also compared our results with those obtained on a $16^3 \times 32 \times 16$ lattice for $m_l = 0.01$, 0.02, and 0.03 [88] (the properties of the ensembles on the 16^3 lattice have been presented in Ref. [34]). No significant finite-volume effects were found.

From Fig. 25 it can be seen that the dependence of the bare f_V^T/f_V on the masses of the light quarks is very mild and so we restrict our chiral extrapolation to linear and quadratic functions in the quark mass as shown in the figure. For the ratio of bare couplings in the chiral limit we obtain

$$\frac{f_\rho^T}{f_\rho} = 0.619(15)(18), \qquad \frac{f_{K^*}^T}{f_{K^*}} = 0.6498(62)(60), \qquad \frac{f_\phi^T}{f_\phi} = 0.6838(32)(22), \quad (147)$$

where the central value corresponds to the linear extrapolation and the second error is the difference between the results from the linear and quadratic extrapolations.

The bare results in Eq. (147) were obtained with the notional strange quark mass of $m_h = 0.04$ rather than the physical value of $m_s = 0.0343$ (see Table XI). The values of the ratios in Eq. (147) are very similar for the ρ, K^*, and ϕ mesons and we correct for the change in m_s by linear interpolation in the valence quark mass (m_h is fixed at 0.04). Thus, for example, for the K^* meson we interpolate between the K^* and the ρ:

$$\frac{f_{K^*}^T}{f_{K^*}}(m_s = 0.0343) = \frac{f_{K^*}^T}{f_{K^*}}(m_h = 0.04) + \frac{\Delta}{(0.04 + m_{\rm res})}(0.0343 - 0.04), \quad (148)$$

where $\Delta = f_{K^*}^T/f_{K^*}(m_h = 0.04) - f_\rho^T/f_\rho$. After carrying out a similar extrapolation for f_ϕ^T/f_ϕ the corrected bare values are then

TABLE XXVI. Results for the measured of couplings f_V^T/f_V.

am_q	0.03	0.02	0.01	0.005	Physical	χ^2/dof
f_ρ^T/f_ρ	0.6806(55)	0.6646(73)	0.645(13)	0.624(21)	0.619(15)	0.17
$f_{K^*}^T/f_{K^*}$	0.6893(55)	0.6781(56)	0.6667(43)	0.6570(68)	0.6498(62)	0.11
f_ϕ^T/f_ϕ	0.6947(36)	0.6933(38)	0.6881(22)	0.6866(32)	0.6838(33)	0.10

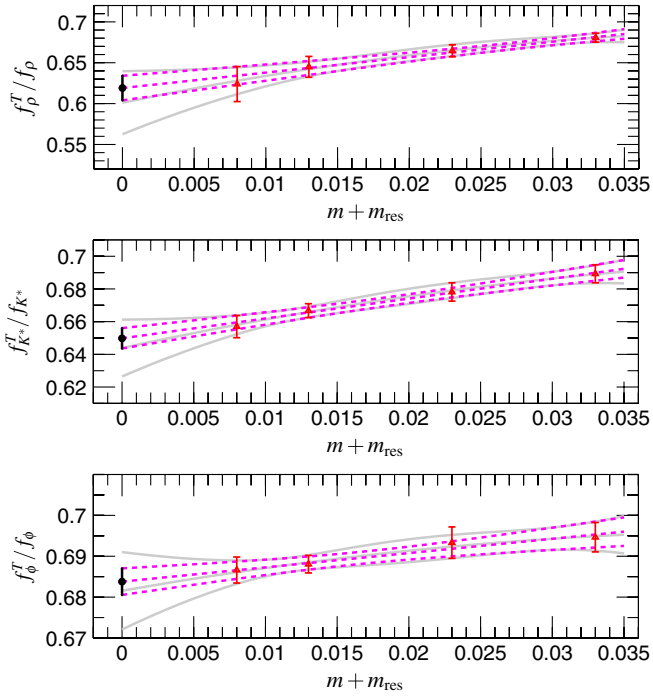

FIG. 25 (color online). Chiral extrapolations for f_ρ^T/f_ρ, $f_{K^*}^T/f_{K^*}$, and f_ϕ^T/f_ϕ, respectively. The broken lines represent a linear fit to the mass behavior, and the solid lines a quadratic fit.

$$\frac{f_\rho^T}{f_\rho} = 0.619(15)(18); \qquad \frac{f_{K^*}^T}{f_{K^*}} = 0.6457(62)(60); \qquad \frac{f_\phi^T}{f_\phi} = 0.6753(32)(22). \tag{149}$$

We determine the renormalization constants nonperturbatively using the Rome-Southampton method and run the results to 2 GeV. The results for the renormalization constants of the tensor and (local) vector currents were presented individually in Ref. [21] and for the ratio we find $Z_T/Z_A = Z_T/Z_V = 1.1101(92) \simeq 1.11(1)$, where Z_A is the renormalization constant of the local axial current. The relation between the ratios of bare and renormalized matrix elements is then

$$\frac{f_V^T(2\ \text{GeV})}{f_V} = \frac{Z_T(2\ \text{GeV}a)}{Z_V}\frac{f_V^{T\text{bare}}(a)}{f_V^{\text{bare}}} = 1.11(1)\frac{f_V^{T\text{bare}}(a)}{f_V^{\text{bare}}}. \tag{150}$$

In the $\overline{\rm MS}$ scheme with $\mu = 2$ GeV we finally obtain

$$\frac{f_\rho^T}{f_\rho} = 0.687(27); \qquad \frac{f_{K^*}^T}{f_{K^*}} = 0.717(12); \qquad \frac{f_\phi^T}{f_\phi} = 0.750(8). \tag{151}$$

These results can be compared with previous quenched lattice results which we summarize in Table XXVII. The QCDSF/UKQCD Collaboration has also presented the result $f_\rho^T = 168(3)$ MeV using an $N_f = 2$ $O(a)$ improved clover action with a range of lattice spacings ($0.07 < a < 0.11$ fm) [97]. Combining our result for the ratio from Eq. (151) together with the experimental value for f_ρ we obtain a smaller value $f_\rho^T = 143(6)$ MeV.

X. CONCLUSIONS

This paper reports the results of simulations of 2 + 1 flavor QCD with domain wall fermions at a single lattice spacing, with a larger volume than has been achieved previously. The ensembles we have generated have a length of ≈ 4000 molecular-dynamics time units, and we have seen a good distribution of global topological charge, indicative of our algorithm's ability to sample phase space. With our $(2.74\ \text{fm})^3$ spatial volume, and improvements in the RHMC algorithm, our lightest pion made of dynamical quarks has $m_\pi = 331$ MeV and our lightest valence pion has a mass of $m_\pi = 242$ MeV. For these two cases, we have $m_\pi L = 4.60$ and 3.36, respectively.

Because of the good chiral properties of domain wall fermions at nonzero lattice spacing, the only correction to continuum chiral perturbation theory at NLO order is the inclusion of the residual mass, $m_{\rm res}$, in the quark mass appearing in the ChPT formula. This means we have the same number of ChPT LECs to fit as for continuum physics, although the LECs we determine can differ from the continuum values by $O(a^2)$ terms. The small number of free parameters in our fits is a powerful advantage of working with a fermion formulation with good chiral and flavor symmetries. To have good control over our chiral extrapolations, we have developed SU(2) ChPT for kaon physics, which does not assume the kaon mass is small. We have fit our data to both SU(2) and SU(3) ChPT, at NLO, and find both approaches give good fits to our data. However, for SU(3) ChPT, the NLO corrections are very large—as much as 50% of the size of the LO term for the

TABLE XXVII. Previous quenched lattice results for the ratio of tensor and vector decay constants.

Reference	$\frac{f_\rho^T(2\ \text{GeV})}{f_\rho}$	$\frac{f_{K^*}^T(2\ \text{GeV})}{f_{K^*}}$	$\frac{f_\phi^T(2\ \text{GeV})}{f_\phi}$
Becirevic *et al.* [89]	$0.720(24)(^{+16}_{-00})$	$0.739(17)(^{+3}_{-0})$	0.759(9)(0)
Braun *et al.* [96]	0.742(14)	...	0.780(8)

pseudoscalar decay constants in the range of quark masses where we have data. This poor convergence of the series does not seem to be due to a single term, such as having the dynamical heavy quark mass close to the physical strange quark mass. Our fits have used pseudoscalar particles with mass $\lesssim 420$ MeV, where SU(3) ChPT might be expected to be more accurate than we have found it to be. We are investigating this further, making use of the full continuum NNLO expressions of [79].

For our most reliable extrapolations to the physical values for the light quark masses, we turn to SU(2) ChPT for kaons. Here we have found good fits, with the NLO corrections no larger than 35% of the LO terms for the light quark mass values we used in our simulations. This is still a somewhat large NLO contribution, but makes the dropping of NNLO terms more sensible. We have tried to estimate our systematic errors by including possible analytic NNLO terms in the fits. For our central results, we use m_Ω, m_π, and m_K to set the scale and determine $\tilde{m}_{ud}$ and $\tilde{m}_s$. For m_Ω, there are no light quark chiral logarithms and for $\tilde{m}_{ud}$ and $\tilde{m}_s$ we use the SU(2) ChPT formula to perform the extrapolation. We can then predict the decay constants, f_π, f_K and their ratio. The fits also give values for the LECs of SU(2) ChPT.

Our conclusion that SU(2) ChPT is applicable for pseudoscalar masses below 420 MeV must, of course, be viewed as a working hypothesis—one that comes from fitting the ChPT formulas to our data. Gaining a fundamental understanding of the range of masses where SU(2) ChPT is accurate is of considerable importance. Viewed from the perspective of QCD, resonances or particles that can enter loop diagrams for the quantity of interest can be expected to play a role in determining this range. Our 420 MeV value may seem large, given the physical ρ resonance at 770 MeV and the broad σ at 441 [98], but it is important to note that our quark masses are much larger than physical values and the masses of these resonances/particles are expected to increase with quark mass. In fact, for the quark masses which yield a 420 MeV pion, we find a ρ mass of 910 MeV (Table XXV). We do not know the σ mass in our calculations, but it is also likely large and the σ could be a stable particle. How the masses of these particles/resonances vary with the quark mass and enter into the convergence of ChPT is very complicated, and our demonstration that our data agree at the few percent level with the SU(2) ChPT formula in the mass range below 420 MeV is a step in probing this important question.

We have estimated our systematics through several methods. For the systematic errors from our chiral fits, we have tried varying the fit ranges and also including analytic NNLO terms, to see the effects of these changes on our results. Finite-volume effects are also estimated through ChPT and we find that the largest finite-volume effects for our measured pseudoscalar masses and decay constants are about 1.5%, which is a small enough correction that ChPT should be quite reliable. We also use ChPT to estimate the errors due to the heavy quark in our simulations being 15% heavier than the physical value. For finite lattice spacing effects, we expect them to be $O(a\Lambda_{\rm QCD})^2$ or about 4%. Scaling errors no larger than this have been seen in the quenched case [99], and since dynamical quark loop effects change the scaling at a higher order in α_S, similar scaling is expected for the full QCD case studied here. The size of this scaling error also agrees well with the deviation of our central value of $f\pi$ from the experimental results, so we have adopted a uniform 4% $O(a^2)$ error for all of our results. (Simulations are underway at a smaller lattice spacing, so that we will soon have better control over the $a \to 0$ extrapolation.)

For B_K, which has already been published [19], we have given more details about our use of SU(2) ChPT to extrapolate to the light quark limit. We have also measured the vector meson couplings for light vector mesons.

Our major results come from using SU(2) ChPT fits and are summarized below:

$$f = 114.8(4.1)_{\rm stat}(8.1)_{\rm syst}\ \text{MeV}, \tag{152}$$

$$B^{\overline{\rm MS}}(2\ \text{GeV}) = 2.52(0.11)_{\rm stat}(0.23)_{\rm ren}(0.12)_{\rm syst}\ \text{GeV}, \tag{153}$$

$$\Sigma^{\overline{\rm MS}}(2\ \text{GeV}) = (255(8)_{\rm stat}(8)_{\rm ren}(13)_{\rm syst}\ \text{MeV})^3, \tag{154}$$

$$\bar{l}_3 = 3.13(0.33)_{\rm stat}(0.24)_{\rm syst}, \tag{155}$$

$$\bar{l}_4 = 4.43(0.14)_{\rm stat}(0.77)_{\rm syst}, \tag{156}$$

$$\Lambda_3 = 666(110)_{\rm stat}(80)_{\rm syst}\ \text{MeV}, \tag{157}$$

$$\Lambda_4 = 1274(92)_{\rm stat}(490)_{\rm syst}\ \text{MeV}, \tag{158}$$

$$m_{ud}^{\overline{\rm MS}}(2\ \text{GeV}) = 3.72(0.16)_{\rm stat}(0.33)_{\rm ren}(0.18)_{\rm syst}\ \text{MeV}, \tag{159}$$

$$m_s^{\overline{\rm MS}}(2\ \text{GeV}) = 107.3(4.4)_{\rm stat}(9.7)_{\rm ren}(4.9)_{\rm syst}\ \text{MeV}, \tag{160}$$

$$\tilde{m}_{ud}{:}\tilde{m}_s = 1{:}28.8(0.4)_{\rm stat}(1.6)_{\rm syst}, \tag{161}$$

$$f_\pi = 124.1(3.6)_{\rm stat}(6.9)_{\rm syst}\ \text{MeV}, \tag{162}$$

$$f_K = 149.6(3.6)_{\rm stat}(6.3)_{\rm syst}\ \text{MeV}, \tag{163}$$

$$f_K/f_\pi = 1.205(0.018)_{\rm stat}(0.062)_{\rm syst}, \tag{164}$$

$$B_K^{\overline{\rm MS}}(2\ \text{GeV}) = 0.524(0.010)_{\rm stat}(0.013)_{\rm ren}(0.025)_{\rm syst}. \tag{165}$$

These results have total errors for the decay constants of about 6% and for the $\overline{\text{MS}}$ quark masses of about 10%. The systematic error due to $O(a^2)$ errors will be reduced by the lattices we are generating at a smaller lattice spacing ($1/a \approx 2.3$ GeV) and lighter quark masses on a similar physical volume. The errors on the quark masses are largely due to renormalization and should improve as better renormalization conditions are chosen [21].

With the expected increases in computer power over the next few years, we should be able to push to much lighter quark masses and minimize our reliance on chiral perturbation theory in the extrapolation to physical results. This is possible for domain wall fermions, since the chiral limit is decoupled from the continuum limit. With lighter quark masses, we should be able to check the convergence of the chiral perturbation theory expansion and achieve better control over the low-energy constants. Finally, the ensembles that we are generating in these basic studies of the low-energy properties of QCD are useful for a wide variety of other measurements, including heavy quark systems and hadronic weak interaction matrix elements.

ACKNOWLEDGMENTS

The calculations reported here were done on the QCDOC computers [102–104] at Columbia University, Edinburgh University, and Brookhaven National Laboratory (BNL). At BNL, the QCDOC computers of the RIKEN-BNL Research Center and the USQCD Collaboration were used. The software used includes the CPS QCD codes, http://qcdoc.phys.columbia.edu/chulwoo_index.html, supported in part by the USDOE SciDAC program; the BAGEL, http://www.ph.ed.ac.uk/~paboyle/bagel/Bagel.html, assembler kernel generator for many of the high-performance optimized kernels; and the UKHadron codes. The authors would like to acknowledge useful discussions with Heinrich Leutwyler, Jürg Gasser, Johan Bijnens, and Steve Sharpe. T. B. and T. Y. (University of Connecticut) were partially supported by the U.S. DOE under Contract No. DE-FG02-92ER40716. N. H. C., S. D. C., M. L, S. L, M. F. L., and R. D. M. (Columbia University) were partially supported by the U.S. DOE under Contract No. DE-FG02-92ER40699. C. J., E. E. S, and A. S. (BNL) were partially supported by the U.S. DOE under Contract No. DE-AC02-98CH10886. S. S (University of Tokyo) was partially supported in part by a JSPS Grant-In-Aid for Scientific Research (C) (No. 19540265). M. A. D., J. M. F., A. J., and C. T. S (University of Southampton) were partially supported by UK STFC Grant No. PP/D000211/1 and by EU Contract No. MRTN-CT-2006-035482 (Flavianet). The work of the Edinburgh authors was supported by PPARC Grants No. PP/D000238/1 and No. PP/C503154/1. The former directly supported C. M. M., J. W., J. M. Z., and P. A. B. acknowledge support from RCUK and A. H. acknowledges support from the Royal Society. The Edinburgh QCDOC system was funded by PPARC JIF Grant No. PPA/J/S/1998/00756 and operated through support from the Universities of Edinburgh, Southampton, and Wales Swansea, and from STFC Grant No. PP/E006965/1. Computations for this work were carried out in part on facilities of the USQCD Collaboration, which are funded by the Office of Science of the U.S. Department of Energy. We thank RIKEN, BNL, and the U.S. DOE for providing the facilities essential for the completion of this work.

APPENDIX A: NOTATION, CONVENTIONS

1. Quark masses

Here we discuss our notation for quark masses. In Sec. II B, where we discuss kaon ChPT, continuum notation is used and m represents the total quark mass. Throughout the rest of the paper, we need to distinguish between the input bare quark mass in the domain wall fermion formulation and the total quark mass, which includes the additive contribution to the quark mass from finite L_s.

Input (sometimes also called bare) quark masses for domain wall fermions will be denoted by the symbol m_X, where the index $X \in \{l, h, x, y, ud, s\}$ distinguishes between different types of quarks:

(i) m_l: dynamical light input quark mass (two degenerate flavors).
(ii) m_h: dynamical heavy input quark mass (one flavor).
(iii) m_x, m_y: valence input quark masses.
(iv) m_{ud}: average light input quark mass at the physical point, i.e., a meson made of two quarks of mass m_{ud} acquires the experimentally measured mass of the neutral pion [this is related to the input quark masses of the up and down quarks via $m_{ud} = (m_u + m_d)/2$].
(v) m_s: heavy input quark mass at the physical point (strange quark mass), i.e., a meson made of one quark of mass m_{ud} and one of mass m_s acquires the quadratically averaged experimentally measured mass of the neutral kaons.

The total quark mass, which has the residual mass m_{res} added, will be denoted by $\tilde{m}$,

$$\tilde{m}_X = m_X + m_{\text{res}}. \tag{A1}$$

The total renormalized quark masses at the physical point carry a superscript indicating the renormalization scheme used. For example, physical masses in the $\overline{\text{MS}}$ scheme renormalized at a scale $\mu = 2$ GeV read

$$\begin{aligned} m_{ud}^{\overline{\text{MS}}}(2\text{ GeV}) &= Z_m^{\overline{\text{MS}}}(2\text{ GeV}) \cdot (m_{ud} + m_{\text{res}}) \\ &= Z_m^{\overline{\text{MS}}}(2\text{ GeV})\tilde{m}_{ud}, \end{aligned} \tag{A2}$$

$$m_s^{\overline{\rm MS}}(2\ {\rm GeV}) = Z_m^{\overline{\rm MS}}(2\ {\rm GeV}) \cdot (m_s + m_{\rm res}) = Z_m^{\overline{\rm MS}}(2\ {\rm GeV})\tilde{m}_s, \quad \text{(A3)}$$

where $Z_m^{\overline{\rm MS}}(2\ {\rm GeV})$ is the mass renormalization constant.

2. Pseudoscalar quantities

The pseudoscalar quantities considered in this work (masses, decay constants, and bag parameters) will carry two indices, denoting the quark content. For example, the mass of a pseudoscalar made from two valence quarks with mass m_x and m_y will be labeled m_{xy}, the decay constant of a meson with one valence quark and one dynamical heavy quark is f_{xh}, and the pseudoscalar bag parameter of a meson with one quark at the physical average light quark mass and one valence quark is B_{udy}. Also we will use the obvious symbols for quantities at the physical point:

$$m_\pi = m_{udud}, \qquad m_K = m_{uds}, \qquad f_\pi = f_{udud}, \qquad f_K = f_{uds}, \qquad B_K = B_{uds}.$$

3. Low-energy constants in ChPT

The following table lists the LECs we use in the PQChPT formulas:

	LO	NLO
PQ SU(3) × SU(3)	B_0, f_0, $B_{\rm PS}^\chi$	$L_4^{(3)}$, $L_5^{(3)}$, $L_6^{(3)}$, $L_8^{(3)}$, b, c, d
PQ SU(2) × SU(2)	B, f	$L_4^{(2)}$, $L_5^{(2)}$, $L_6^{(2)}$, $L_8^{(2)}$
PQ SU(2) × SU(2) kaon	$B^{(K)}(m_h)$, $f^{(K)}(m_h)$, $B_{\rm PS}^{(K)}(m_h)$	$\lambda_1(m_h)$, $\lambda_2(m_h)$, $\lambda_3(m_h)$, $\lambda_4(m_h)$, $b_1(m_h)$, $b_2(m_h)$

The renormalization-scale-dependent NLO LECs are defined at a scale Λ_χ. For the decay constants, we use the normalization such that the experimentally measured value for the pion decay constant is $f_\pi \approx 132\ {\rm MeV} \approx \sqrt{2} \cdot 93\ {\rm MeV}$.

Further, we will use the following abbreviations for (tree-level) masses in the formulas:

$$\chi_X = 2B_0\tilde{m}_X, \qquad {\rm SU(3)} \times {\rm SU(3)}, \quad \text{(A4)}$$

$$\chi_X = 2B\tilde{m}_X, \qquad {\rm SU(2)} \times {\rm SU(2)}, \quad \text{(A5)}$$

where it should be clear from the context whether the SU(3) × SU(3) or SU(2) × SU(2) expression is to be used. In addition, we define the average dynamical mass to be

$$\bar{m} = \frac{1}{3}(2m_l + m_h), \quad \text{(A6)}$$

and the dynamical η mass

$$m_\eta = \frac{1}{3}(m_l + 2m_h). \quad \text{(A7)}$$

[Note: this is not the tree-level η mass at the physical point, which would be $(m_{ud} + 2m_s)/3$.]

APPENDIX B: PQCHPT FIT FUNCTIONS

1. SU(3) × SU(3)

The following formulas hold for $N_f = 2 + 1$ sea quark masses and two valence quarks [SU(5|3)]. The formulas for masses and decay constants were derived from [47], while the ones for the bag parameter $B_{\rm PS}$ can be found in [100].

a. Squared pseudoscalar mass

(a) *Nondegenerate* $(m_x \neq m_y)$

(i) $m_x \neq m_\eta \neq m_y$:

$$m_{xy}^2 = \frac{\chi_x + \chi_y}{2} \cdot \left\{ 1 + \frac{48}{f_0^2}(2L_6^{(3)} - L_4^{(3)})\bar{\chi} + \frac{8}{f_0^2}(2L_8^{(3)} - L_5^{(3)})(\chi_x + \chi_y) + \frac{1}{24\pi^2 f_0^2}\left[\frac{(\chi_x - \chi_l)(\chi_x - \chi_h)}{(\chi_x - \chi_y)(\chi_x - \chi_\eta)}\chi_x \log\frac{\chi_x}{\Lambda_\chi^2} + \frac{(\chi_y - \chi_l)(\chi_y - \chi_h)}{(\chi_y - \chi_x)(\chi_y - \chi_\eta)}\chi_y \log\frac{\chi_y}{\Lambda_\chi^2} + \frac{(\chi_\eta - \chi_l)(\chi_\eta - \chi_h)}{(\chi_\eta - \chi_x)(\chi_\eta - \chi_y)}\chi_\eta \log\frac{\chi_\eta}{\Lambda_\chi^2} \right] \right\}. \quad \text{(B1)}$$

(ii) $m_x \to m_\eta \neq m_y$:

$$m_{xy}^2 = \frac{\chi_x + \chi_y}{2} \cdot \Big\{ 1 + \frac{48}{f_0^2}(2L_6^{(3)} - L_4^{(3)})\bar{\chi} + \frac{8}{f_0^2}(2L_8^{(3)} - L_5^{(3)})(\chi_x + \chi_y) + \frac{1}{24\pi^2 f_0^2}\Big[\frac{(\chi_y - \chi_l)(\chi_y - \chi_h)}{(\chi_y - \chi_x)^2}\chi_y \log\frac{\chi_y}{\Lambda_\chi^2} + \frac{(\chi_x - \chi_y)[(\chi_x - \chi_h)\chi_x + (\chi_x - \chi_l)(2\chi_x - \chi_h)] - (\chi_x - \chi_l)(\chi_x - \chi_h)\chi_x}{(\chi_x - \chi_y)^2} \log\frac{\chi_x}{\Lambda_\chi^2} + \frac{(\chi_x - \chi_l)(\chi_x - \chi_h)}{\chi_x - \chi_y}\Big]\Big\}. \tag{B2}$$

(b) *Degenerate* ($m_x = m_y$)

(i) $m_x = m_y \neq m_\eta$:

$$m_{xx}^2 = \chi_x \cdot \Big\{ 1 + \frac{48}{f_0^2}(2L_6^{(3)} - L_4^{(3)})\bar{\chi} + \frac{16}{f_0^2}(2L_8^{(3)} - L_5^{(3)})\chi_x + \frac{1}{24\pi^2 f_0^2}\Big[\Big(\frac{2\chi_x - \chi_l - \chi_h}{\chi_x - \chi_\eta} - \frac{(\chi_x - \chi_l)(\chi_x - \chi_h)}{(\chi_x - \chi_\eta)^2} \Big)\chi_x \log\frac{\chi_x}{\Lambda_\chi^2} + \frac{(\chi_x - \chi_l)(\chi_x - \chi_h)}{\chi_x - \chi_\eta}\Big(1 + \log\frac{\chi_x}{\Lambda_\chi^2} \Big) + \frac{(\chi_\eta - \chi_l)(\chi_\eta - \chi_h)}{(\chi_x - \chi_\eta)^2}\chi_\eta \log\frac{\chi_\eta}{\Lambda_\chi^2}\Big]\Big\}. \tag{B3}$$

(ii) $m_x = m_y \to m_\eta$:

$$m_{xx}^2 = \chi_x \cdot \Big\{ 1 + \frac{48}{f_0^2}(2L_6^{(3)} - L_4^{(3)})\bar{\chi} + \frac{16}{f_0^2}(2L_8^{(3)} - L_5^{(3)})\chi_x + \frac{1}{24\pi^2 f_0^2}\Big[\frac{\chi_l \chi_h}{2\chi_x} + \frac{5\chi_x - 3\chi_l - 3\chi_h}{2} + (3\chi_x - \chi_l - \chi_h)\log\frac{\chi_x}{\Lambda_\chi^2}\Big]\Big\}. \tag{B4}$$

(c) *Pion and kaon masses m_π^2 and m_K^2*. From Eq. (B3) we obtain for the degenerate meson mass in unquenched QCD ($m_x = m_l$)

$$m_{ll}^2 = \chi_l \cdot \Big\{ 1 + \frac{48}{f_0^2}(2L_6^{(3)} - L_4^{(3)})\bar{\chi} + \frac{16}{f_0^2}(2L_8^{(3)} - L_5^{(3)})\chi_l + \frac{1}{24\pi^2 f_0^2}\Big[\frac{3}{2}\chi_l \log\frac{\chi_l}{\Lambda_\chi^2} - \frac{1}{2}\chi_\eta \log\frac{\chi_\eta}{\Lambda_\chi^2}\Big]\Big\}, \tag{B5}$$

and from Eq. (B1) for the kaon mass ($m_x = m_l$, $m_y = m_h$),

$$m_{lh}^2 = \frac{\chi_l + \chi_h}{2} \cdot \Big\{ 1 + \frac{48}{f_0^2}(2L_6^{(3)} - L_4^{(3)})\bar{\chi} + \frac{8}{f_0^2}(2L_8^{(3)} - L_5^{(3)})(\chi_l + \chi_h) + \frac{1}{24\pi^2 f_0^2}\chi_\eta \log\frac{\chi_\eta}{\Lambda_\chi^2}\Big\}, \tag{B6}$$

so that for $m_x = m_l = m_{ud}$ and $m_y = m_h = m_s$ we get m_π^2 and m_K^2, respectively. These expressions agree with [13]. For a "kaon" made from a light sea quark and valence quark ($m_x \neq m_l$), one obtains

(i) $m_x \neq m_\eta$:

$$m_{lx}^2 = \frac{\chi_l + \chi_x}{2} \cdot \Big\{ 1 + \frac{48}{f_0^2}(2L_6^{(3)} - L_4^{(3)})\bar{\chi} + \frac{8}{f_0^2}(2L_8^{(3)} - L_5^{(3)})(\chi_l + \chi_x) + \frac{1}{24\pi^2 f_0^2}\Big[\frac{\chi_x - \chi_h}{\chi_x - \chi_\eta}\chi_x \log\frac{\chi_x}{\Lambda_\chi^2} + \frac{\chi_\eta - \chi_h}{\chi_\eta - \chi_x}\chi_\eta \log\frac{\chi_\eta}{\Lambda_\chi^2}\Big]\Big\}. \tag{B7}$$

(ii) $m_x \to m_\eta$:

$$m_{lx}^2 = \frac{\chi_l + \chi_x}{2} \cdot \left\{ 1 + \frac{48}{f_0^2}(2L_6^{(3)} - L_4^{(3)})\bar{\chi} + \frac{8}{f_0^2}(2L_8^{(3)} - L_5^{(3)})(\chi_l + \chi_x) + \frac{1}{24\pi^2 f_0^2}\left[\chi_x - \chi_h + (2\chi_x - \chi_h)\log\frac{\chi_x}{\Lambda_\chi^2} \right] \right\}. \quad \text{(B8)}$$

Whereas for a "kaon" made from a valence quark ($m_x \neq m_h$) and a heavy sea quark, we have

(i) $m_x \neq m_\eta$:

$$m_{xh}^2 = \frac{\chi_x + \chi_h}{2} \cdot \left\{ 1 + \frac{48}{f_0^2}(2L_6^{(3)} - L_4^{(3)})\bar{\chi} + \frac{8}{f_0^2}(2L_8^{(3)} - L_5^{(3)})(\chi_x + \chi_h) + \frac{1}{24\pi^2 f_0^2}\left[\frac{\chi_x - \chi_l}{\chi_x - \chi_\eta}\chi_x \log\frac{\chi_x}{\Lambda_\chi^2} + \frac{\chi_\eta - \chi_l}{\chi_\eta - \chi_x}\chi_\eta \log\frac{\chi_\eta}{\Lambda_\chi^2} \right] \right\}. \quad \text{(B9)}$$

(ii) $m_x \to m_\eta$:

$$m_{xh}^2 = \frac{\chi_x + \chi_h}{2} \cdot \left\{ 1 + \frac{48}{f_0^2}(2L_6^{(3)} - L_4^{(3)})\bar{\chi} + \frac{8}{f_0^2}(2L_8^{(3)} - L_5^{(3)})(\chi_x + \chi_h) + \frac{1}{24\pi^2 f_0^2}\left[(2\chi_x - \chi_l)\log\frac{\chi_x}{\Lambda_\chi^2} + \chi_x - \chi_l \right] \right\}. \quad \text{(B10)}$$

b. Pseudoscalar decay constant

(a) *Nondegenerate* ($m_x \neq m_y$)

(i) $m_x \neq m_\eta \neq m_y$:

$$f_{xy} = f_0 \cdot \left\{ 1 + \frac{24}{f_0^2}L_4^{(3)}\bar{\chi} + \frac{4}{f_0^2}L_5^{(3)}(\chi_x + \chi_y) - \frac{1}{8\pi^2 f_0^2}\left[\frac{\chi_x + \chi_l}{4}\log\frac{\chi_x + \chi_l}{2\Lambda_\chi^2} + \frac{\chi_y + \chi_l}{4}\log\frac{\chi_y + \chi_l}{2\Lambda_\chi^2} \right.\right.$$
$$\left. + \frac{\chi_x + \chi_h}{8}\log\frac{\chi_x + \chi_h}{2\Lambda_\chi^2} + \frac{\chi_y + \chi_h}{8}\log\frac{\chi_y + \chi_h}{2\Lambda_\chi^2} \right] + \frac{1}{96\pi^2 f_0^2}\left[\left(\chi_x \frac{(\chi_l - \chi_x)(\chi_h - \chi_x)}{\chi_\eta - \chi_x} + \chi_y \frac{(\chi_l - \chi_y)(\chi_h - \chi_y)}{\chi_\eta - \chi_y} \right.\right.$$
$$\left. + (\chi_x - \chi_y)^2 \right) \frac{\log\frac{\chi_x}{\chi_y}}{\chi_x - \chi_y} + \chi_\eta(\chi_y - \chi_x)\frac{(\chi_\eta - \chi_l)(\chi_\eta - \chi_h)}{(\chi_\eta - \chi_x)(\chi_\eta - \chi_y)}\left(\frac{\log\frac{\chi_\eta}{\chi_x}}{\chi_x - \chi_\eta} - \frac{\log\frac{\chi_\eta}{\chi_y}}{\chi_y - \chi_\eta} \right) - \frac{(\chi_l - \chi_x)(\chi_h - \chi_x)}{\chi_\eta - \chi_x}$$
$$\left.\left. - \frac{(\chi_l - \chi_y)(\chi_h - \chi_y)}{\chi_\eta - \chi_y} \right] \right\}. \quad \text{(B11)}$$

(ii) $m_x \to m_\eta \neq m_y$:

$$f_{xy} = f_0 \cdot \left\{ 1 + \frac{24}{f_0^2}L_4^{(3)}\bar{\chi} + \frac{4}{f_0^2}L_5^{(3)}(\chi_x + \chi_y) - \frac{1}{8\pi^2 f_0^2}\left[\frac{\chi_x + \chi_l}{4}\log\frac{\chi_x + \chi_l}{2\Lambda_\chi^2} + \frac{\chi_y + \chi_l}{4}\log\frac{\chi_y + \chi_l}{2\Lambda_\chi^2} + \frac{\chi_x + \chi_h}{8} \right.\right.$$
$$\left. \times \log\frac{\chi_x + \chi_h}{2\Lambda_\chi^2} + \frac{\chi_y + \chi_h}{8}\log\frac{\chi_y + \chi_h}{2\Lambda_\chi^2} \right] + \frac{1}{96\pi^2 f_0^2}$$
$$\times \left[\frac{\chi_x^3 + \chi_x^2(\chi_l + \chi_h - 5\chi_y) + \chi_x(5\chi_y(\chi_l + \chi_h) - 5\chi_l\chi_h - 2\chi_y^2) - \chi_y\chi_l\chi_h}{2\chi_x(\chi_x - \chi_y)} \right.$$
$$\left.\left. + \frac{\chi_x(3\chi_y^2 + \chi_l\chi_h - 2\chi_y(\chi_l + \chi_h)) + \chi_y(2\chi_l\chi_h - \chi_y(\chi_l + \chi_h))}{(\chi_x - \chi_y)^2}\log\frac{\chi_x}{\chi_y} \right] \right\}. \quad \text{(B12)}$$

(b) *Degenerate* ($m_x = m_y$)

$$f_{xx} = f_0 \cdot \left\{1 + \frac{24}{f_0^2} L_4^{(3)} \bar{\chi} + \frac{8}{f_0^2} L_5^{(3)} \chi_x - \frac{1}{16\pi^2 f_0^2}\left[(\chi_x + \chi_l)\log\frac{\chi_x + \chi_l}{2\Lambda_\chi^2} + \frac{\chi_x + \chi_h}{2}\log\frac{\chi_x + \chi_h}{2\Lambda_\chi^2}\right]\right\}. \tag{B13}$$

(c) *Pion and kaon decay constants f_π and f_K.* From Eq. (B13) we obtain for the pion decay constant in unquenched QCD ($m_x = m_l$)

$$f_{ll} = f_0 \cdot \left\{1 + \frac{24}{f_0^2} L_4^{(3)} \bar{\chi} + \frac{8}{f_0^2} L_5^{(3)} \chi_l - \frac{1}{16\pi^2 f_0^2}\left[\frac{\chi_l + \chi_h}{2}\log\frac{\chi_l + \chi_h}{2\Lambda_\chi^2} + 2\chi_l \log\frac{\chi_l}{\Lambda_\chi^2}\right]\right\}, \tag{B14}$$

and from Eq. (B11) for the kaon decay constant ($m_x = m_l$, $m_y = m_h$):

$$f_{lh} = f_0 \cdot \left\{1 + \frac{24}{f_0^2} L_4^{(3)} \bar{\chi} + \frac{4}{f_0^2} L_5^{(3)} (\chi_l + \chi_h) - \frac{3}{64\pi^2 f_0^2}\left[2\frac{\chi_l + \chi_h}{2}\log\frac{\chi_l + \chi_h}{2\Lambda_\chi^2} + \chi_l \log\frac{\chi_l}{\Lambda_\chi^2} + \chi_\eta \log\frac{\chi_\eta}{\Lambda_\chi^2}\right]\right\}. \tag{B15}$$

Again, for $m_x = m_l = m_{ud}$ and $m_y = m_h = m_s$ we get f_π and f_K, respectively, and these expressions agree with [13].

For a "kaon" made from a light sea quark and valence quark ($m_x \neq m_l$), one obtains

(i) $m_x \neq m_\eta$:

$$\begin{aligned} f_{lx} = f_0 \cdot \Bigg\{1 &+ \frac{24}{f_0^2} L_4^{(3)} \bar{\chi} + \frac{4}{f_0^2} L_5^{(3)} (\chi_l + \chi_x) + \frac{1}{8\pi^2 f_0^2}\Bigg[-\frac{3}{8}\chi_l \log\frac{\chi_l}{\Lambda_\chi^2} - \frac{\chi_x + \chi_l}{4}\log\frac{\chi_x + \chi_l}{2\Lambda_\chi^2} - \frac{\chi_l + \chi_h}{8}\log\frac{\chi_l + \chi_h}{2\Lambda_\chi^2} \\ &- \frac{\chi_x + \chi_h}{8}\log\frac{\chi_x + \chi_h}{2\Lambda_\chi^2} + \frac{(\chi_x - \chi_l)^2(\chi_\eta - \chi_h)}{12(\chi_\eta - \chi_x)^2(\chi_\eta - \chi_l)}\chi_\eta \log\frac{\chi_\eta}{\Lambda_\chi^2} + \frac{\chi_x^2(\chi_h - \chi_l - \chi_\eta) - \chi_\eta\chi_l(\chi_h - 2\chi_x)}{12(\chi_\eta - \chi_x)^2} \\ &\times \log\frac{\chi_x}{\Lambda_\chi^2} - \frac{(\chi_l - \chi_x)(\chi_h - \chi_x)}{12(\chi_\eta - \chi_x)}\Bigg]\Bigg\}. \end{aligned} \tag{B16}$$

(ii) $m_x \to m_\eta$:

$$\begin{aligned} f_{lx} = f_0 \cdot \Bigg\{1 &+ \frac{24}{f_0^2} L_4^{(3)} \bar{\chi} + \frac{4}{f_0^2} L_5^{(3)} (\chi_l + \chi_x) + \frac{1}{8\pi^2 f_0^2}\Bigg[-\frac{3}{8}\chi_l \log\frac{\chi_l}{\Lambda_\chi^2} - \frac{\chi_x + \chi_l}{4}\log\frac{\chi_x + \chi_l}{2\Lambda_\chi^2} - \frac{\chi_l + \chi_h}{8}\log\frac{\chi_l + \chi_h}{2\Lambda_\chi^2} \\ &- \frac{\chi_x + \chi_h}{8}\log\frac{\chi_x + \chi_h}{2\Lambda_\chi^2} + \frac{\chi_l(\chi_h - 3\chi_x) + \chi_x(\chi_h + \chi_x)}{24\chi_x} + \frac{\chi_l(\chi_h - \chi_l)}{12(\chi_l - \chi_x)}\log\frac{\chi_x}{\Lambda_\chi^2}\Bigg]\Bigg\}. \end{aligned} \tag{B17}$$

Whereas for a "kaon" made from a valence quark ($m_x \neq m_h$) and a heavy sea quark, we have

(i) $m_x \neq m_\eta$:

$$\begin{aligned} f_{xh} = f_0 \cdot \Bigg\{1 &+ \frac{24}{f_0^2} L_4^{(3)} \bar{\chi} + \frac{4}{f_0^2} L_5^{(3)} (\chi_x + \chi_h) - \frac{1}{8\pi^2 f_0^2}\Bigg[\frac{\chi_x + \chi_l}{4}\log\frac{\chi_x + \chi_l}{2\Lambda_\chi^2} + \frac{\chi_h + \chi_l}{4}\log\frac{\chi_h + \chi_l}{2\Lambda_\chi^2} \\ &+ \frac{\chi_x + \chi_h}{8}\log\frac{\chi_x + \chi_h}{2\Lambda_\chi^2} + \frac{\chi_h}{4}\log\frac{\chi_h}{\Lambda_\chi^2}\Bigg] + \frac{1}{96\pi^2 f_0^2}\Bigg[\left(\chi_x - \chi_h - \chi_x\frac{\chi_l - \chi_x}{\chi_\eta - \chi_x}\right)\log\frac{\chi_x}{\chi_h} \\ &+ \chi_\eta(\chi_h - \chi_x)\frac{\chi_\eta - \chi_l}{\chi_\eta - \chi_x}\left(\frac{\log\frac{\chi_\eta}{\chi_x}}{\chi_x - \chi_\eta} - \frac{\log\frac{\chi_\eta}{\chi_h}}{\chi_h - \chi_\eta}\right) - \frac{(\chi_l - \chi_x)(\chi_h - \chi_x)}{\chi_\eta - \chi_x}\Bigg]\Bigg\}. \end{aligned} \tag{B18}$$

(ii) $m_x \to m_\eta$:

$$f_{xh} = f_0 \cdot \Bigg\{1 + \frac{24}{f_0^2} L_4^{(3)} \bar{\chi} + \frac{4}{f_0^2} L_5^{(3)} (\chi_x + \chi_h) - \frac{1}{8\pi^2 f_0^2} \Bigg[\frac{\chi_x + \chi_l}{4} \log \frac{\chi_x + \chi_l}{2\Lambda_\chi^2} + \frac{\chi_h + \chi_l}{4} \log \frac{\chi_h + \chi_l}{2\Lambda_\chi^2} + \frac{\chi_x + \chi_h}{8} \log \frac{\chi_x + \chi_h}{2\Lambda_\chi^2} + \frac{\chi_h}{4} \log \frac{\chi_h}{\Lambda_\chi^2} \Bigg] + \frac{1}{96\pi^2 f_0^2} \Bigg[\frac{\chi_x^3 + \chi_x^2(\chi_l - 4\chi_h) + 3\chi_x \chi_h^2 - \chi_h^2 \chi_l}{2\chi_x(\chi_x - \chi_h)} + \chi_h \frac{\chi_x(\chi_h - \chi_l) + \chi_h(\chi_l - \chi_h)}{(\chi_x - \chi_h)^2} \log \frac{\chi_x}{\chi_h} \Bigg] \Bigg\}. \tag{B19}$$

c. Scale dependence of the NLO LECs

The NLO LECs $L_i^{(3)}(\Lambda_\chi)$ at a renormalization scale Λ_χ can be converted to a different scale Λ'_χ using [13]

$$L_i^{(3)}(\Lambda'_\chi) = L_i^{(3)}(\Lambda_\chi) + \frac{\Gamma_i}{16\pi^2} \log \frac{\Lambda_\chi}{\Lambda'_\chi}, \tag{B20}$$

with

$$\Gamma_4 = \frac{1}{8}, \qquad \Gamma_5 = \frac{3}{8}, \qquad \Gamma_6 = \frac{11}{144}, \qquad \Gamma_8 = \frac{5}{48}. \tag{B21}$$

d. Pseudoscalar bag parameter

Here we follow the notation of [100] for the LECs relevant for the pseudoscalar bag parameter and denote them by b, c, and d. Also here we only work in (PQ) SU(3) chiral perturbation theory.

(a) *Nondegenerate* ($m_x \neq m_y$)

$$B_{xy} = B_{\mathrm{PS}}^\chi \Bigg\{ 1 + \frac{1}{24\pi^2 f_0^2} \Bigg[\frac{I_{\mathrm{conn}} + I_{\mathrm{disc}}}{\chi_x + \chi_y} + \frac{\chi_x + \chi_y}{4} b + \frac{(\chi_x - \chi_y)^2}{\chi_x + \chi_y} c + \frac{3}{2} \bar{\chi} d \Bigg] \Bigg\}, \tag{B22}$$

$$I_{\mathrm{conn}} = \frac{3}{2}(\chi_x + \chi_y)^2 \Bigg(-1 - \log \frac{\chi_x + \chi_y}{2\Lambda_\chi^2} \Bigg) - \frac{3}{2}(3\chi_x + \chi_y)\chi_x \log \frac{\chi_x}{\Lambda_\chi^2} - \frac{3}{2}(\chi_x + 3\chi_y)\chi_y \log \frac{\chi_y}{\Lambda_\chi^2}, \tag{B23}$$

$$I_{\mathrm{disc}} = I_x + I_y + I_\eta, \tag{B24}$$

$$I_x = \frac{(3\chi_x + \chi_y)(\chi_l - \chi_x)(\chi_h - \chi_x)}{2(\chi_\eta - \chi_x)} \Bigg(-1 - \log \frac{\chi_x}{\Lambda_\chi^2} \Bigg) - \Bigg[\frac{(3\chi_x + \chi_y)(\chi_l - \chi_x)(\chi_h - \chi_x)}{2(\chi_\eta - \chi_x)^2} + \frac{(3\chi_x + \chi_y)(\chi_l - \chi_x)(\chi_h - \chi_x)}{(\chi_y - \chi_x)(\chi_\eta - \chi_x)} + \frac{2(\chi_l - \chi_x)(\chi_h - \chi_x) - (3\chi_x + \chi_y)(\chi_h - \chi_x) - (3\chi_x + \chi_y)(\chi_l - \chi_x)}{2(\chi_\eta - \chi_x)} \Bigg] \cdot \chi_x \log \frac{\chi_x}{\Lambda_\chi^2}, \tag{B25}$$

$$I_y = I_x(x \leftrightarrow y), \tag{B26}$$

$$I_\eta = \frac{(\chi_x - \chi_y)^2(\chi_x + \chi_y + 2\chi_\eta)(\chi_l - \chi_\eta)(\chi_h - \chi_\eta)}{2(\chi_x - \chi_\eta)^2(\chi_y - \chi_\eta)^2} \chi_\eta \log \frac{\chi_\eta}{\Lambda_\chi^2}. \tag{B27}$$

For $m_x \to m_\eta$, $m_x \neq m_y$, one obtains from the disconnected diagrams

$$
\begin{aligned}
I_{\text{disc}} = & -\chi_l \frac{\chi_\eta^3 + \chi_\eta^2(7\chi_h - 16\chi_y) + \chi_\eta\chi_y(16\chi_h - 9\chi_y) + \chi_h\chi_y^2}{4\chi_\eta(\chi_\eta - \chi_y)} \\
& - \frac{-7\chi_\eta^3 - 9\chi_h\chi_y^2 + 6\chi_y^3 + \chi_\eta\chi_y(-16\chi_h + 7\chi_y) + \chi_\eta^2(\chi_h + 18\chi_y)}{4(\chi_\eta - \chi_y)} \\
& + \frac{1}{2(\chi_\eta - \chi_y)^2} \log\frac{\chi_\eta}{\Lambda_\chi^2} \cdot [2\chi_\eta^4 - 8\chi_\eta^3\chi_y - \chi_y^2(\chi_h\chi_y + \chi_l(\chi_y - 4\chi_h)) + \chi_\eta\chi_y(\chi_l(7\chi_h - 9\chi_y) \\
& + 3\chi_y(\chi_y - 3\chi_h)) + \chi_\eta^2(\chi_l(\chi_h - 2\chi_y) + \chi_y(15\chi_y - 2\chi_h))] + \frac{1}{2(\chi_\eta - \chi_y)^2} \log\frac{\chi_y}{\Lambda_\chi^2} \\
& \cdot [\chi_y(\chi_\eta^2(2\chi_h - 3\chi_y) + \chi_\eta\chi_y(9\chi_h - 11\chi_y) + \chi_y^2(\chi_h + 2\chi_y)) + \chi_l(-\chi_\eta^2(\chi_h - 2\chi_y) + \chi_y^2(\chi_y - 4\chi_h) \\
& + \chi_\eta\chi_y(9\chi_y - 7\chi_h))].
\end{aligned} \tag{B28}
$$

(b) *Degenerate* ($m_x = m_y$). In this case $I_{\text{disc}} = 0$ and therefore

$$
B_{xx} = B_{\text{PS}}^\chi \left\{ 1 + \frac{1}{24\pi^2 f_0^2} \left[-9\chi_x \log\frac{\chi_x}{\Lambda_\chi^2} + \frac{\chi_x}{2}(b - 6) + \frac{3}{2}\bar{\chi} d \right] \right\}. \tag{B29}
$$

(c) *Kaon bag parameter* B_K. From Eq. (B22) one obtains the full (unquenched) QCD result ($m_x = m_l$, $m_y = m_h$)

$$
\begin{aligned}
B_{lh} = B_{\text{PS}}^\chi \Bigg\{ 1 - \frac{1}{16\pi^2 f_0^2} \Bigg[& (\chi_l + \chi_h)\left(1 + \log\frac{\chi_l + \chi_h}{2\Lambda_\chi^2}\right) + \frac{3\chi_l + \chi_h}{2(\chi_l + \chi_h)}\chi_l \log\frac{\chi_l}{\Lambda_\chi^2} + \frac{5\chi_l + 7\chi_h}{2(\chi_l + \chi_h)}\chi_\eta \log\frac{\chi_\eta}{\Lambda_\chi^2} \\
& - b\frac{\chi_l + \chi_h}{6} - c\frac{2(\chi_l - \chi_h)^2}{3(\chi_l + \chi_h)} - d\bar{\chi} \Bigg] \Bigg\},
\end{aligned} \tag{B30}
$$

so that at the physical point ($m_l = m_{ud}$, $m_h = m_s$) we have

$$
\begin{aligned}
B_K = B_{\text{PS}}^\chi \Bigg\{ 1 - \frac{2}{(4\pi f_0)^2} \Bigg[& M_K^2\left(1 + \log\frac{M_K^2}{\Lambda_\chi^2}\right) + \frac{M_\pi^2(M_\pi^2 + M_K^2)}{4M_K^2} \log\frac{M_\pi^2}{\Lambda_\chi^2} + \frac{7M_K^2 - M_\pi^2}{4M_K^2} M_\eta^2 \log\frac{M_\eta^2}{\Lambda_\chi^2} \\
& - \frac{b}{6}M_K^2 - \frac{2c}{3}\frac{(M_\pi^2 - M_K^2)^2}{M_K^2} - \frac{d}{6}(M_\pi^2 + 2M_K^2) \Bigg] \Bigg\}.
\end{aligned} \tag{B31}
$$

Here we expressed everything in terms of meson masses: $M_\pi^2 = \chi_{ud}$, $M_K^2 = \frac{1}{2}(\chi_{ud} + \chi_s)$, $M_\eta^2 = \chi_\eta|_{m_l = m_{ud}, m_h = m_s}$. [This agrees for the nonanalytic terms with Eq. (12) of [84]; analytic terms were not considered in that reference.]

2. SU(2) × SU(2)

The following formulas hold for $N_f = 2$ (degenerate) sea quark masses (mass m_l) and two valence quarks [SU(4|2)]. The formulas for masses and decay constants were derived from [47]. Also cf. [101].

a. Squared pseudoscalar mass

(a) *Nondegenerate*

$$
\begin{aligned}
m_{xy}^2 = & \frac{\chi_x + \chi_y}{2} \cdot \Bigg\{ 1 + \frac{32}{f^2}(2L_6^{(2)} - L_4^{(2)})\chi_l \\
& + \frac{8}{f^2}(2L_8^{(2)} - L_5^{(2)})(\chi_x + \chi_y) \\
& + \frac{1}{16\pi^2 f^2} \Bigg[\frac{\chi_x - \chi_l}{\chi_x - \chi_y}\chi_x \log\frac{\chi_x}{\Lambda_\chi^2} \\
& + \frac{\chi_y - \chi_l}{\chi_y - \chi_x}\chi_y \log\frac{\chi_y}{\Lambda_\chi^2} \Bigg] \Bigg\}.
\end{aligned} \tag{B32}
$$

(b) *Degenerate*

$$m_{xx}^2 = \chi_x \cdot \Big\{1 + \frac{32}{f^2}(2L_6^{(2)} - L_4^{(2)})\chi_l + \frac{16}{f^2}(2L_8^{(2)} - L_5^{(2)})\chi_x + \frac{1}{16\pi^2 f^2}\Big[\chi_x - \chi_l + (2\chi_x - \chi_l)\log\frac{\chi_x}{\Lambda_\chi^2}\Big]\Big\}. \tag{B33}$$

(c) *Pion mass* m_π^2. From Eq. (B33) one obtains the degenerate meson mass in full (unquenched) QCD ($m_x = m_l$):

$$m_{ll}^2 = \chi_l \cdot \Big\{1 + \frac{16}{f^2}((2L_8^{(2)} - L_5^{(2)}) + 2(2L_6^{(2)} - L_4^{(2)}))\chi_l + \frac{1}{16\pi^2 f^2}\chi_l \log\frac{\chi_l}{\Lambda_\chi^2}\Big\} \tag{B34}$$

which gives for $m_x = m_l = m_{ud}$ the pion mass m_π^2 and agrees with [12]. Furthermore, we can relate the LECs $L_{4,5,6,8}^{(2)}$ from PQChPT to l_3^r in ChPT:

$$4((2L_8^{(2)} - L_5^{(2)}) + 2(2L_6^{(2)} - L_4^{(2)})) = l_3^r. \tag{B35}$$

b. Pseudoscalar decay constant

(a) *Nondegenerate*

$$f_{xy} = f \cdot \Big\{1 + \frac{16}{f^2}L_4^{(2)}\chi_l + \frac{4}{f^2}L_5^{(2)}(\chi_x + \chi_y) - \frac{1}{32\pi^2 f^2}\Big[(\chi_x + \chi_l)\log\frac{\chi_x + \chi_l}{2\Lambda_\chi^2} + (\chi_y + \chi_l)\log\frac{\chi_y + \chi_l}{2\Lambda^2}\Big] + \frac{1}{64\pi^2 f^2}\Big[\chi_x + \chi_y - 2\chi_l + \frac{2\chi_x\chi_y - \chi_l(\chi_x + \chi_y)}{\chi_y - \chi_x}\log\frac{\chi_x}{\chi_y}\Big]\Big\}. \tag{B36}$$

(b) *Degenerate*

$$f_{xx} = f \cdot \Big\{1 + \frac{16}{f^2}L_4^{(2)}\chi_l + \frac{8}{f^2}L_5^{(2)}\chi_x - \frac{\chi_x + \chi_l}{16\pi^2 f^2}\log\frac{\chi_x + \chi_l}{2\Lambda_\chi^2}\Big\}. \tag{B37}$$

(c) *Pion decay constant* f_π

$$f_{ll} = f \cdot \Big\{1 + \frac{8}{f^2}(2L_4^{(2)} + L_5^{(2)})\chi_l - \frac{\chi_l}{8\pi^2 f^2}\log\frac{\chi_l}{\Lambda_\chi^2}\Big\}. \tag{B38}$$

Again, for $m_x = m_l = m_{ud}$ this reproduces the pion decay constant f_π and agrees with [12]. Furthermore, we can relate the LECs $L_{4,5}^{(2)}$ from PQChPT to l_4^r in ChPT:

$$4(2L_4^{(2)} + L_5^{(2)}) = l_4^r. \tag{B39}$$

c. Conversion from SU(3) × SU(3) *to* SU(2) × SU(2)

The conversion from the SU(3) LECs to the SU(2) ones can be done (including terms up to NLO) following [13] (see [26] for NNLO; note the latter organizes the expansion in a slightly different way compared to the former).

$$f = f_0\Big\{1 - \frac{\chi_s}{32\pi^2 f_0^2}\log\frac{\chi_s}{2\Lambda_\chi^2} + \frac{8}{f_0^2}L_4^{(3)}\chi_s\Big\}, \tag{B40}$$

$$B = B_0\Big\{1 - \frac{\chi_s}{72\pi^2 f_0^2}\log\frac{2\chi_s}{3\Lambda_\chi^2} + \frac{16}{f_0^2}(2L_6^{(3)} - L_4^{(3)})\chi_s\Big\}, \tag{B41}$$

$$l_3^r = 4(2L_8^{(3)} - L_5^{(3)}) + 8(2L_6^{(3)} - L_4^{(3)}) - \frac{1}{576\pi^2}\Big(1 + \log\frac{2\chi_s}{3\Lambda_\chi^2}\Big), \tag{B42}$$

$$l_4^r = 8L_4^{(3)} + 4L_5^{(3)} - \frac{1}{64\pi^2}\Big(1 + \log\frac{\chi_s}{2\Lambda_\chi^2}\Big), \tag{B43}$$

where one has to use B_0 to evaluate the χ_X on the right-hand side. The relation of the SU(2) LECs in PQChPT, $L_i^{(2)}$ to the unquenched SU(2) LECs $l_{3,4}^r$ is given by Eqs. (B35) and (B39). To define them at the scale of the pion mass m_π, one has to use

$$\bar{l}_i = \frac{32\pi^2}{\gamma_i}l_i^r - \log\frac{m_\pi^2}{\Lambda_\chi^2}, \tag{B44}$$

$$\gamma_3 = -\frac{1}{2}, \qquad \gamma_4 = 2. \tag{B45}$$

3. SU(2) × SU(2) for the kaon sector

Here, we choose to denote by m_x always a light and by m_y a heavier valence quark mass. The additional low-energy constants appearing here [LO: $B^{(K)}(m_h)$, $f^{(K)}(m_h)$, $B_{\mathrm{PS}}^{(K)}(m_h)$, NLO: $\lambda_{1,2,3,4}(m_h)$, $b_{1,2}(m_h)$] are in general dependent on the dynamical heavy quark mass m_h and the valence heavy quark mass m_y. To simplify the notation the

argument m_h has to be viewed as placeholder for both of those. For more details see Sec. II.

a. Light-heavy squared pseudoscalar mass

$$m_{xy}^2 = B^{(K)}(m_h)\tilde{m}_y\left\{1 + \frac{\lambda_1(m_h)}{f^2}\chi_l + \frac{\lambda_2(m_h)}{f^2}\chi_x\right\}. \tag{B46}$$

b. Light-heavy pseudoscalar decay constant

$$f_{xy} = f^{(K)}(m_h)\left\{1 + \frac{\lambda_3(m_h)}{f^2}\chi_l + \frac{\lambda_4(m_h)}{f^2}\chi_x - \frac{1}{(4\pi f)^2} \times\left[\frac{\chi_x+\chi_l}{2}\log\frac{\chi_x+\chi_l}{2\Lambda_\chi^2} + \frac{\chi_l-2\chi_x}{4}\log\frac{\chi_x}{\Lambda_\chi^2}\right]\right\}. \tag{B47}$$

c. Light-heavy pseudoscalar bag parameter

$$B_{xy} = B_{\mathrm{PS}}^{(K)}(m_h)\left\{1 + \frac{b_1(m_h)}{f^2}\chi_l + \frac{b_2(m_h)}{f^2}\chi_x - \frac{\chi_l}{32\pi^2 f^2}\log\frac{\chi_x}{\Lambda_\chi^2}\right\}. \tag{B48}$$

d. Conversion from $\mathbf{SU}(3)\times\mathbf{SU}(3)$ to kaon $\mathbf{SU}(2)\times\mathbf{SU}(2)$

For the LECs appearing in the kaon mass and decay constant formulas [Eqs. (B46) and (B47)], we provide the relation to the SU(3) LECs as well:

$$f^{(K)}(m_h,m_y) = f_0\left\{1 + \frac{8}{f_0^2}L_4^{(3)}\chi_h + \frac{4}{f_0^2}L_5^{(3)}\chi_y + \frac{1}{32\pi^2 f_0^2}\left[\frac{\chi_y-\chi_h}{3\chi_y-2\chi_h}\chi_y - \frac{\chi_h}{2}\log\frac{\chi_h}{2\Lambda_\chi^2} - \chi_y\log\frac{\chi_y}{2\Lambda_\chi^2} + \frac{\chi_h\chi_y^2}{(3\chi_y-2\chi_h)^2}\log\frac{\chi_y}{\Lambda_\chi^2} - \frac{\chi_h\chi_y^2}{(3\chi_y-2\chi_h)^2}\log\frac{2\chi_h}{3\Lambda_\chi^2} - \frac{\chi_h+\chi_y}{2}\log\frac{\chi_h+\chi_y}{2\Lambda_\chi^2}\right]\right\}, \tag{B49}$$

$$B^{(K)}(m_h,m_y) = B_0\left\{1 + \frac{\chi_h}{f_0^2}16(2L_6^{(3)} - L_4^{(3)}) + \frac{\chi_y}{f_0^2}8(2L_8^{(3)} - L_5^{(3)}) + \frac{1}{72\pi^2 f_0^2} \times\left[9\frac{\chi_y-\chi_h}{3\chi_y-2\chi_h}\chi_y\log\frac{\chi_y}{\Lambda_\chi^2} + 2\frac{\chi_h^2}{3\chi_y-2\chi_h}\log\frac{2\chi_h}{3\Lambda_\chi^2}\right]\right\}, \tag{B50}$$

$$\lambda_1(m_h,m_y) = 32(2L_6^{(3)} - L_4^{(3)}) + \frac{1}{72\pi^2} \times\left[-\frac{18(\chi_y-\chi_h)^2}{(3\chi_y-2\chi_h)^2}\log\frac{\chi_y}{\Lambda_\chi^2} + 2\frac{5\chi_h-6\chi_y}{(3\chi_y-2\chi_h)^2}\chi_h\log\frac{2\chi_h}{3\Lambda_\chi^2} + \frac{\chi_h}{3\chi_y-2\chi_h}\right], \tag{B51}$$

$$\lambda_2(m_h,m_y) = \frac{f_0^2}{\chi_y} + 8(2L_8^{(3)} - L_5^{(3)}) + 16\frac{\chi_h}{\chi_y}(L_4^{(3)} - (2L_6^{(3)} - L_4^{(3)})) + \frac{1}{4\pi^2}\left[\frac{\chi_y-\chi_h}{2(3\chi_y-2\chi_h)}\log\frac{\chi_y}{\Lambda_\chi^2} - \frac{\chi_h}{4\chi_y}\log\frac{\chi_h}{2\Lambda_\chi^2} + \frac{\chi_h(3\chi_y-\chi_h)}{9\chi_y(3\chi_y-2\chi_h)}\log\frac{2\chi_h}{3\Lambda_\chi^2}\right], \tag{B52}$$

$$\lambda_3(m_h,m_y) = 16L_4^{(3)} + \frac{1}{16\pi^2}\left[-\frac{1}{2}\log\frac{\chi_y}{2\Lambda_\chi^2} - \frac{4\chi_h^2-11\chi_h\chi_y+8\chi_y^2}{(3\chi_y-2\chi_h)^2} + \frac{15\chi_y-14\chi_h}{4(3\chi_y-2\chi_h)^3} \times\chi_y^2\log\frac{2\chi_h}{3\Lambda_\chi^2} + \frac{(3\chi_y-\chi_h)(\chi_y-\chi_h)(\chi_y-2\chi_h)}{(3\chi_y-2\chi_h)^3}\log\frac{\chi_y}{\Lambda_\chi^2}\right], \tag{B53}$$

$$\lambda_4(m_h,m_y) = 4L_5^{(3)} + \frac{1}{16\pi^2}\left[-\frac{1}{4}\log\frac{\chi_h}{2\Lambda_\chi^2} + \frac{\chi_y-\chi_h}{3\chi_y-2\chi_h} \times\log\frac{\chi_y}{\Lambda_\chi^2} - \frac{\chi_y}{2(3\chi_y-2\chi_h)}\log\frac{2\chi_h}{3\Lambda_\chi^2}\right]. \tag{B54}$$

APPENDIX C: FINITE-VOLUME CORRECTION FOR PSEUDOSCALAR MASSES AND DECAY CONSTANTS

In the following we will provide the finite-volume corrections for the meson decay constants and squared meson masses obtained in PQChPT for $N_f = 2 + 1$ and $N_f = 2$ sea quarks (cf. [59–64]). The corrections are labeled Δ_{xy}^{Lf} and $\Delta_{xy}^{Lm^2}$, respectively, for decay constants and squared masses of mesons made of quarks with masses m_x and m_y in a finite (spatial) volume L^3. Labeling decay constants in finite-volume f_{xy}^{L} and those in infinite-volume $f_{xy}^{L\to\infty}$ we have the following relations:

$$f_{xy}^{L\to\infty} = f_{xy}^{L}(1 - \Delta_{xy}^{Lf}), \tag{C1}$$

$$= f_0(1 + \chi\mathrm{PT}_{xy}^{f}), \tag{C2}$$

$$f_{xy}^{L} = f_0(1 + \chi\mathrm{PT}_{xy}^{f})(1 + \Delta_{xy}^{Lf}), \tag{C3}$$

$$= f_0(1 + \chi\mathrm{PT}_{xy}^{f} + \Delta_{xy}^{Lf}), \tag{C4}$$

and similar for squared meson masses. Here we denote the NLO contribution in infinite-volume (PQ)ChPT (as given in the previous section) by $\chi\mathrm{PT}_{xy}^{f}$. (These equalities hold up to terms of NLO; higher-order terms are neglected.) Note further that in the case of SU(2) × SU(2) the f_0 has to be replaced by f.

The Bessel functions of imaginary argument (modified Bessel functions of the 2nd kind) $K_n(x)$ enter the expressions for the finite-volume corrections via

$$\delta_1(x) = \frac{4}{x}\sum_{\vec{r}\neq 0}\frac{K_1(rx)}{r}, \tag{C5}$$

$$\delta_3(x) = 2\sum_{\vec{r}\neq 0}K_0(rx), \tag{C6}$$

$$\delta_5(x) = -\sum_{\vec{r}\neq 0}\frac{r}{x}K_1(rx), \tag{C7}$$

where the argument is typically $x = \sqrt{\chi_X}L$. For the numerical implementation, we made use of the multiplicities $m(n)$ and rewrite the sum as

$$\sum_{\vec{r}\neq 0} f(r) = \sum_{n>0} m(n) f(\sqrt{n}), \tag{C8}$$

where the sum is evaluated until the relative change is less than the required precision ϵ or a maximum number N for n is reached. (Typically, we use $\epsilon = 5 \times 10^{-4}$ and $N = 100$, but checked that going to $\epsilon = 5 \times 10^{-6}$, $N = 1000$ does not change the result.) The multiplicities for $n \leq 20$ can, e.g., be found in [65]. Here we list $m(n)$ for $n = 1, \ldots, 100$:

6, 12, 8, 6, 24, 24, 0, 12, 30, 24, 24, 8, 24, 48, 0, 6, 48, 36, 24, 24, 48, 24, 0, 24, 30, 72, 32, 0, 72, 48, 0, 12, 48, 48, 48, 30, 24, 72, 0, 24, 96, 48, 24, 24, 72, 48, 0, 8, 54, 84, 48, 24, 72, 96, 0, 48, 48, 24, 72, 0, 72, 96, 0, 6, 96, 96, 24, 48, 96, 48, 0, 36, 48, 120, 56, 24, 96, 48, 0, 24, 102, 48, 72, 48, 48, 120, 0, 24, 144, 120, 48, 0, 48, 96, 0, 24, 48, 108, 72, 30. (C9)

Note that we have the following relations involving the δ_i:

$$\frac{\mathrm{d}}{\mathrm{d}\chi}\chi\delta_1(\sqrt{\chi}L) = -\delta_3(\sqrt{\chi}L), \tag{C10}$$

$$\frac{\mathrm{d}}{\mathrm{d}\chi}\delta_3(\sqrt{\chi}L) = L^2\delta_5(\sqrt{\chi}L). \tag{C11}$$

Furthermore, by doing the substitutions in the finite-volume correction part Δ_{xy}^{L}

$$\delta_1(\sqrt{\chi_X}L) \to \log\frac{\chi_X}{\Lambda_\chi^2}, \tag{C12}$$

$$\delta_3(\sqrt{\chi_X}L) \to -\left(1 + \log\frac{\chi_X}{\Lambda_\chi^2}\right), \tag{C13}$$

$$L^2\delta_5(\sqrt{\chi_X}L) \to -\frac{1}{\chi_X}, \tag{C14}$$

one obtains at NLO the nonanalytic part of the corresponding $\chi\mathrm{PT}_{xy}$ (i.e., without the analytic terms multiplying the LECs).

1. SU(3) × SU(3)

a. Finite-volume correction for the squared pseudoscalar mass

(a) *Nondegenerate* ($m_x \neq m_y$)

(i) $m_x \neq m_\eta \neq m_y$:

$$\begin{aligned}\Delta_{xy}^{Lm^2} = \frac{1}{24\pi^2 f_0^2} &\times\left[\frac{(\chi_\eta - \chi_l)(\chi_\eta - \chi_h)}{(\chi_\eta - \chi_x)(\chi_\eta - \chi_y)}\chi_\eta\delta_1(\sqrt{\chi_\eta}L)\right.\\ &+\frac{(\chi_x - \chi_l)(\chi_x - \chi_h)}{(\chi_x - \chi_y)(\chi_x - \chi_\eta)}\chi_x\delta_1(\sqrt{\chi_x}L)\\ &\left.+\frac{(\chi_y - \chi_l)(\chi_y - \chi_h)}{(\chi_y - \chi_x)(\chi_y - \chi_\eta)}\chi_y\delta_1(\sqrt{\chi_y}L)\right].\end{aligned} \tag{C15}$$

(ii) $m_x \to m_\eta$ ($m_y \neq m_\eta$):

$$\Delta_{xy}^{Lm^2} = \frac{1}{24\pi^2 f_0^2}\Bigg[-\frac{(\chi_x-\chi_l)(\chi_x-\chi_h)}{\chi_x-\chi_y}\delta_3(\sqrt{\chi_x}L) + \frac{(2\chi_x-\chi_l-\chi_h)(\chi_x-\chi_y)-(\chi_x-\chi_l)(\chi_x-\chi_h)}{(\chi_x-\chi_y)^2}\chi_x\delta_1(\sqrt{\chi_x}L) + \frac{(\chi_y-\chi_l)(\chi_y-\chi_h)}{(\chi_x-\chi_y)^2}\chi_y\delta_1(\sqrt{\chi_y}L)\Bigg]. \tag{C16}$$

(b) *Degenerate*
(i) $m_x \neq m_\eta$:

$$\Delta_{xx}^{Lm^2} = \frac{1}{24\pi^2 f_0^2}\Bigg[\frac{(\chi_\eta-\chi_l)(\chi_\eta-\chi_h)}{(\chi_\eta-\chi_x)^2}\chi_\eta\delta_1(\sqrt{\chi_\eta}L) + \frac{(\chi_x-\chi_\eta)(2\chi_x-\chi_h-\chi_l)-(\chi_x-\chi_l)(\chi_x-\chi_h)}{(\chi_x-\chi_\eta)^2}\chi_x\delta_1(\sqrt{\chi_x}L) - \frac{(\chi_x-\chi_l)(\chi_x-\chi_h)}{\chi_x-\chi_\eta}\delta_3(\sqrt{\chi_x}L)\Bigg]. \tag{C17}$$

(ii) $m_x \to m_\eta$:

$$\Delta_{xx}^{Lm^2} = \frac{1}{24\pi^2 f_0^2}\Bigg[\chi_x\delta_1(\sqrt{\chi_x}L) - (2\chi_x-\chi_l-\chi_h)\delta_3(\sqrt{\chi_x}L) - \frac{(\chi_x-\chi_l)(\chi_x-\chi_h)}{2}L^2\delta_5(\sqrt{\chi_x}L)\Bigg]. \tag{C18}$$

b. Finite-volume correction for the pseudoscalar decay constant

(a) *Nondegenerate* $m_x \neq m_y$
(i) $m_x \neq m_\eta \neq m_y$:

$$\begin{aligned}\Delta_{xy}^{Lf} = &-\frac{1}{8\pi^2 f_0^2}\Bigg[\frac{\chi_x+\chi_l}{4}\delta_1\Bigg(\sqrt{\frac{\chi_x+\chi_l}{2}}L\Bigg) + \frac{\chi_y+\chi_l}{4}\delta_1\Bigg(\sqrt{\frac{\chi_y+\chi_l}{2}}L\Bigg) + \frac{\chi_x+\chi_h}{8}\delta_1\Bigg(\sqrt{\frac{\chi_x+\chi_h}{2}}L\Bigg) \\ &+ \frac{\chi_y+\chi_h}{8}\delta_1\Bigg(\sqrt{\frac{\chi_y+\chi_h}{2}}L\Bigg)\Bigg] + \frac{1}{96\pi^2 f_0^2}\Bigg[-\frac{(\chi_l-\chi_x)(\chi_h-\chi_x)}{\chi_x-\chi_\eta}\delta_3(\sqrt{\chi_x}L) - \frac{(\chi_l-\chi_y)(\chi_h-\chi_y)}{\chi_y-\chi_\eta}\delta_3(\sqrt{\chi_y}L) \\ &+ \Bigg(\frac{(\chi_l-\chi_\eta)(\chi_h-\chi_\eta)}{(\chi_x-\chi_\eta)^2} + \frac{(\chi_l-\chi_\eta)(\chi_h-\chi_\eta)}{(\chi_y-\chi_\eta)^2} - 2\frac{(\chi_l-\chi_\eta)(\chi_h-\chi_\eta)}{(\chi_x-\chi_\eta)(\chi_y-\chi_\eta)}\Bigg)\chi_\eta\delta_1(\sqrt{\chi_\eta}L) \\ &+ \Bigg(\frac{\chi_h+\chi_l-2\chi_x}{\chi_\eta-\chi_x} - \frac{(\chi_l-\chi_x)(\chi_h-\chi_x)}{(\chi_\eta-\chi_x)^2} - 2\frac{(\chi_l-\chi_x)(\chi_h-\chi_x)}{(\chi_\eta-\chi_x)(\chi_y-\chi_x)}\Bigg)\chi_x\delta_1(\sqrt{\chi_x}L) \\ &+ \Bigg(\frac{\chi_h+\chi_l-2\chi_y}{\chi_\eta-\chi_y} - \frac{(\chi_l-\chi_y)(\chi_h-\chi_y)}{(\chi_\eta-\chi_y)^2} - 2\frac{(\chi_l-\chi_y)(\chi_h-\chi_y)}{(\chi_\eta-\chi_y)(\chi_x-\chi_y)}\Bigg)\chi_y\delta_1(\sqrt{\chi_y}L)\Bigg].\end{aligned} \tag{C19}$$

(ii) $m_x \to m_\eta$, $m_y \neq m_\eta$:

$$\Delta_{xy}^{Lf} = -\frac{1}{8\pi^2 f_0^2}\Big[\frac{\chi_x+\chi_l}{4}\delta_1\Big(\sqrt{\frac{\chi_x+\chi_l}{2}}L\Big) + \frac{\chi_y+\chi_l}{4}\delta_1\Big(\sqrt{\frac{\chi_y+\chi_l}{2}}L\Big) + \frac{\chi_x+\chi_h}{8}\delta_1\Big(\sqrt{\frac{\chi_x+\chi_h}{2}}L\Big)$$
$$+ \frac{\chi_y+\chi_h}{8}\delta_1\Big(\sqrt{\frac{\chi_y+\chi_h}{2}}L\Big)\Big] + \frac{1}{96\pi^2 f_0^2}\Big[-\frac{1}{2}(\chi_l-\chi_x)(\chi_h-\chi_x)L^2\delta_5(\sqrt{\chi_x}L)$$
$$- \frac{(\chi_l-\chi_y)(\chi_h-\chi_y)}{\chi_y-\chi_x}\delta_3(\sqrt{\chi_y}L) + \Big(1-2\frac{2\chi_x-\chi_l-\chi_h}{\chi_x-\chi_y}+3\frac{(\chi_l-\chi_x)(\chi_h-\chi_x)}{(\chi_x-\chi_y)^2}\Big)\chi_x\delta_1(\sqrt{\chi_x}L)$$
$$- \Big(2\chi_x-\chi_l-\chi_h-2\frac{(\chi_l-\chi_x)(\chi_h-\chi_x)}{\chi_x-\chi_y}\Big)\delta_3(\sqrt{\chi_x}L) + \Big(\frac{\chi_h+\chi_l-2\chi_y}{\chi_x-\chi_y} - \frac{(\chi_l-\chi_y)(\chi_h-\chi_y)}{(\chi_x-\chi_y)^2}$$
$$- 2\frac{(\chi_l-\chi_y)(\chi_h-\chi_y)}{(\chi_x-\chi_y)^2}\Big)\chi_y\delta_1(\sqrt{\chi_y}L)\Big]. \tag{C20}$$

(b) *Degenerate*, $m_x = m_y$

$$\Delta_{xx}^{Lf} = -\frac{1}{8\pi^2 f_0^2}\Big[\frac{\chi_x+\chi_l}{2}\delta_1\Big(\sqrt{\frac{\chi_x+\chi_l}{2}}L\Big) + \frac{\chi_x+\chi_h}{4}\delta_1\Big(\sqrt{\frac{\chi_x+\chi_h}{2}}L\Big)\Big]. \tag{C21}$$

2. SU(2) × SU(2)

a. Finite-volume correction for the squared pseudoscalar mass

(a) *Nondegenerate* ($m_x \neq m_y$)

$$\Delta_{xy}^{Lm^2} = \frac{1}{16\pi^2 f^2}\Big[\frac{\chi_x-\chi_l}{\chi_x-\chi_y}\chi_x\delta_1(\sqrt{\chi_x}L) + \frac{\chi_y-\chi_l}{\chi_y-\chi_x}\chi_y\delta_1(\sqrt{\chi_y}L)\Big]. \tag{C22}$$

(b) *Degenerate* ($m_x = m_y$)

$$\Delta_{xx}^{Lm^2} = \frac{1}{16\pi^2 f^2}[\chi_x\delta_1(\sqrt{\chi_x}L) - (\chi_x-\chi_l)\delta_3(\sqrt{\chi_x}L)]. \tag{C23}$$

b. Finite-volume correction for the pseudoscalar decay constant

(a) *Nondegenerate* ($m_x \neq m_y$)

$$\Delta_{xy}^{Lf} = -\frac{1}{32\pi^2 f^2}\Big[(\chi_x+\chi_l)\delta_1\Big(\sqrt{\frac{\chi_x+\chi_l}{2}}L\Big) + (\chi_y+\chi_l)\delta_1\Big(\sqrt{\frac{\chi_y+\chi_l}{2}}L\Big)\Big]$$
$$+ \frac{1}{64\pi^2 f^2}\Big[-(\chi_x-\chi_l)\delta_3(\sqrt{\chi_x}L) - (\chi_y-\chi_l)\delta_3(\sqrt{\chi_y}L) + \frac{\chi_x+\chi_y-2\chi_l}{\chi_y-\chi_x}$$
$$\times\chi_x\delta_1(\sqrt{\chi_x}L) + \frac{\chi_y+\chi_x-2\chi_l}{\chi_x-\chi_y}\times\chi_y\delta_1(\sqrt{\chi_y}L)\Big]. \tag{C24}$$

(b) *Degenerate* ($m_x = m_y$)

$$\Delta_{xx}^{Lf} = -\frac{1}{16\pi^2 f^2}(\chi_x+\chi_l)\delta_1\Big(\sqrt{\frac{\chi_x+\chi_l}{2}}L\Big). \tag{C25}$$

[1] K. Symanzik, Nucl. Phys. **B226**, 187 (1983).
[2] M. Bochicchio, L. Maiani, G. Martinelli, G. C. Rossi, and M. Testa, Nucl. Phys. **B262**, 331 (1985).
[3] R. Sommer, arXiv:hep-lat/0611020.
[4] T. Blum *et al.* (RBC Collaboration), Phys. Rev. D **68**, 114506 (2003).
[5] D. B. Kaplan, Phys. Lett. B **288**, 342 (1992).
[6] Y. Shamir, Nucl. Phys. **B406**, 90 (1993).
[7] V. Furman and Y. Shamir, Nucl. Phys. **B439**, 54 (1995).
[8] R. Narayanan and H. Neuberger, Phys. Lett. B **302**, 62 (1993).
[9] H. Neuberger, Phys. Lett. B **417**, 141 (1998).

[10] P. Hasenfratz, V. Laliena, and F. Niedermayer, Phys. Lett. B **427**, 125 (1998).
[11] R. Frezzotti, P. A. Grassi, S. Sint, and P. Weisz (Alpha Collaboration), J. High Energy Phys. 08 (2001) 058.
[12] J. Gasser and H. Leutwyler, Ann. Phys. (N.Y.) **158**, 142 (1984).
[13] J. Gasser and H. Leutwyler, Nucl. Phys. **B250**, 465 (1985).
[14] T. Blum, Nucl. Phys. B, Proc. Suppl. **73**, 167 (1999).
[15] Y. Aoki *et al.*, Phys. Rev. D **72**, 114505 (2005).
[16] D. J. Antonio *et al.* (RBC and UKQCD Collaborations), Phys. Rev. D **75**, 114501 (2007).
[17] D. J. Antonio *et al.* (RBC and UKQCD Collaborations), Phys. Rev. D **77**, 014509 (2008).
[18] P. A. Boyle *et al.*, Phys. Rev. Lett. **100**, 141601 (2008).
[19] D. J. Antonio *et al.* (RBC Collaboration), Phys. Rev. Lett. **100**, 032001 (2008).
[20] P. Boyle (RBC and QCD Collaborations), Proc. Sci. LAT2007 (2007) 005 [arXiv:0710.5880].
[21] Y. Aoki *et al.*, Phys. Rev. D **78**, 054510 (2008).
[22] S. R. Sharpe, arXiv:0706.0218.
[23] T. Blum *et al.*, Phys. Rev. D **66**, 014504 (2002).
[24] T. Blum *et al.*, Phys. Rev. D **69**, 074502 (2004).
[25] O. Bar, G. Rupak, and N. Shoresh, Phys. Rev. D **70**, 034508 (2004).
[26] J. Gasser, C. Haefeli, M. A. Ivanov, and M. Schmid, Phys. Lett. B **652**, 21 (2007).
[27] A. Roessl, Nucl. Phys. **B555**, 507 (1999).
[28] C. W. Bernard and M. F. L. Golterman, Phys. Rev. D **46**, 853 (1992).
[29] C. W. Bernard and M. F. L. Golterman, Phys. Rev. D **49**, 486 (1994).
[30] A. Morel, J. Phys. II (France) **48**, 1111 (1987).
[31] S. R. Sharpe, arXiv:hep-lat/0607016.
[32] S. R. Sharpe and Y. Zhang, Phys. Rev. D **53**, 5125 (1996).
[33] B. Grinstein, E. E. Jenkins, A. V. Manohar, M. J. Savage, and M. B. Wise, Nucl. Phys. **B380**, 369 (1992).
[34] C. Allton *et al.* (RBC and UKQCD Collaborations), Phys. Rev. D **76**, 014504 (2007).
[35] M. A. Clark and A. D. Kennedy, Phys. Rev. Lett. **98**, 051601 (2007).
[36] A. D. Kennedy, I. Horvath, and S. Sint, Nucl. Phys. B, Proc. Suppl. **73**, 834 (1999).
[37] C. Urbach, K. Jansen, A. Shindler, and U. Wenger, Comput. Phys. Commun. **174**, 87 (2006).
[38] M. Hasenbusch and K. Jansen, Nucl. Phys. **B659**, 299 (2003).
[39] M. A. Clark, Proc. Sci., LAT2006 (2006) 004 [arXiv:hep-lat/0610048].
[40] P. de Forcrand, M. Garcia Perez, and I.-O. Stamatescu, Nucl. Phys. **B499**, 409 (1997).
[41] P. Boyle (UKQCD Collaboration), J. Comput. Phys. **179**, 349 (2002).
[42] M. Lin and E. E. Scholz (RBC and UKQCD Collaborations), Proc. Sci., LATTICE2007 (2007) 120 [arXiv:0710.0536].
[43] D. Toussaint and C. T. H. Davies, Nucl. Phys. B, Proc. Suppl. **140**, 234 (2005).
[44] B. C. Tiburzi and A. Walker-Loud, Nucl. Phys. **A748**, 513 (2005).
[45] S. Eidelman *et al.* (Particle Data Group Collaboration), Phys. Lett. B **592**, 1 (2004).
[46] K. Sasaki and S. Sasaki, Phys. Rev. D **72**, 034502 (2005).
[47] S. R. Sharpe and N. Shoresh, Phys. Rev. D **62**, 094503 (2000).
[48] F. Farchioni, C. Gebert, I. Montvay, E. Scholz, and L. Scorzato (qq + q Collaboration), Phys. Lett. B **561**, 102 (2003).
[49] M. J. Booth, Phys. Rev. D **51**, 2338 (1995).
[50] H.-W. Lin and N. Christ, Phys. Rev. D **76**, 074506 (2007).
[51] N. H. Christ, M. Li, and H.-W. Lin, Phys. Rev. D **76**, 074505 (2007).
[52] M. Li and H.-W. Lin, Proc. Sci. LAT2007 (2007) 117 [arXiv:0710.0910].
[53] G. Martinelli, C. Pittori, C. T. Sachrajda, M. Testa, and A. Vladikas, Nucl. Phys. **B445**, 81 (1995).
[54] W. M. Yao *et al.* (Particle Data Group Collaboration), J. Phys. G **33**, 1 (2006).
[55] In a recent publication [56] an updated measurement of the CKM matrix element $V_{ud} = 0.974\,18(26)$ [57] from superallowed nuclear β decays has been used to determine $f_K/f_\pi = 1.192(07)$ and $f_\pi = 130.5(0.1)$ MeV resulting in $f_K = 155.6(0.9)$ MeV. (In [56] $1 = V_{ud}^2 + V_{us}^2$ has been assumed, resulting in $V_{us} = 0.2258(11)$.)
[56] V. Bernard and E. Passemar, Phys. Lett. B **661**, 95 (2008).
[57] I. S. Towner and J. C. Hardy, Phys. Rev. C **77** 025501 (2008).
[58] W. J. Marciano, Phys. Rev. Lett. **93**, 231803 (2004).
[59] J. Gasser and H. Leutwyler, Phys. Lett. B **184**, 83 (1987).
[60] J. Gasser and H. Leutwyler, Phys. Lett. B **188**, 477 (1987).
[61] J. Gasser and H. Leutwyler, Nucl. Phys. **B307**, 763 (1988).
[62] C. Bernard (MILC Collaboration), Phys. Rev. D **65**, 054031 (2002).
[63] C. Aubin and C. Bernard, Phys. Rev. D **68**, 034014 (2003).
[64] C. Aubin and C. Bernard, Phys. Rev. D **68**, 074011 (2003).
[65] G. Colangelo, S. Durr, and C. Haefeli, Nucl. Phys. **B721**, 136 (2005).
[66] J. Bijnens, G. Colangelo, and P. Talavera, J. High Energy Phys. 05 (1998) 014.
[67] G. Colangelo, J. Gasser, and H. Leutwyler, Nucl. Phys. **B603**, 125 (2001).
[68] C. Aubin *et al.* (MILC Collaboration), Phys. Rev. D **70**, 114501 (2004).
[69] C. Bernard *et al.*, Proc. Sci. LAT2007 (2007) 090.
[70] L. Del Debbio, L. Giusti, M. Luscher, R. Petronzio, and N. Tantalo, J. High Energy Phys. 02 (2007) 056.
[71] C. Urbach, Proc. Sci. LAT2007 (2007) 022.
[72] T. Blum, T. Doi, M. Hayakawa, T. Izubuchi, and N. Yamada, Phys. Rev. D **76**, 114508 (2007).
[73] B. Blossier *et al.* (European Twisted Mass Collaboration), J. High Energy Phys. 04 (2008) 020.
[74] M. Gockeler *et al.*, Phys. Rev. D **73**, 054508 (2006).
[75] N. Ukita *et al.* (PACS-CS Collaboration), Proc. Sci. LAT2007 (2007) 138.
[76] T. Ishikawa *et al.* (CP-PACS and JLQCD Collaborations), Phys. Rev. D **78**, 011502 (2008).
[77] G. Colangelo and S. Durr, Eur. Phys. J. C **33**, 543 (2004).
[78] H. Leutwyler, arXiv:0706.3138.
[79] J. Bijnens, N. Danielsson, and T. A. Lahde, Phys. Rev. D **73**, 074509 (2006).
[80] M. Lin, Ph.D. thesis, Columbia University, 2007.
[81] J. Bijnens, Proc. Sci. LAT2007 (2007) 004 [arXiv: 0708.1377].

[82] S. D. Cohen and J. Noaki (RBC and UKQCD Collaborations), Proc. Sci., LAT2006 (2006) 080.
[83] S. D. Cohen and D. J. Antonio (RBC and UKQCD Collaborations), Proc. Sci., LATTICE2007 (2007) 347.
[84] D. Becirevicand G. Villadoro, Phys. Rev. D **69**, 054010 (2004).
[85] A. Ali Khan *et al.* (CP-PACS Collaboration), Phys. Rev. D **64**, 114506 (2001).
[86] J. Bijnens, E. Gamiz, and J. Prades, J. High Energy Phys. 03 (2006) 048.
[87] J. Prades, C. A. Dominguez, J. A. Penarrocha, A. Pich, and E. de Rafael, Z. Phys. C **51**, 287 (1991).
[88] D. Antonio *et al.*, Proc. Sci. LAT2007 (2007) 369 [arXiv:0710.0869].
[89] D. Becirevic, V. Lubicz, F. Mescia, and C. Tarantino, J. High Energy Phys. 05 (2003) 007.
[90] P. Ball, G. W. Jones, and R. Zwicky, Phys. Rev. D **75**, 054004 (2007).
[91] P. Ball and R. Zwicky, Phys. Rev. D **71**, 014015 (2005).
[92] M. Beneke, T. Feldmann, and D. Seidel, Nucl. Phys. **B612**, 25 (2001).
[93] S. W. Bosch and G. Buchalla, Nucl. Phys. **B621**, 459 (2002).
[94] A. Ali, B. D. Pecjak, and C. Greub, Eur. Phys. J. C **55**, 577 (2008).
[95] M. Beneke and M. Neubert, Nucl. Phys. **B675**, 333 (2003).
[96] V. M. Braun *et al.*, Phys. Rev. D **68**, 054501 (2003).
[97] M. Göckeler *et al.*, Proc. Sci., LAT2005 (2006) 063 [arXiv:hep-lat/0509196].
[98] I. Caprini, G. Colangelo, and H. Leutwyler, Phys. Rev. Lett. **96**, 132001 (2006).
[99] A. Ali Khan *et al.* (CP-PACS Collaboration), Phys. Rev. D **64**, 114506 (2001).
[100] R. S. Van de Water and S. R. Sharpe, Phys. Rev. D **73**, 014003 (2006).
[101] S. R. Sharpe, Phys. Rev. D **56**, 7052 (1997); **62**, 099901(E) (2000).
[102] P. Boyle *et al.*, IBM J. Res. Dev. **49**, No. 2/3, 351 (2005).
[103] P. A. Boyle, C. Jung, and T. Wettig (QCDOC Collaboration), arXiv:hep-lat/0306023.
[104] P. A. Boyle *et al.*, J. Phys. Conf. Ser. **16**, 129 (2005).